

Automating Virtual Calculations in Supersymmetric Theories



Gavin Cullen

A thesis submitted in fulfilment of the requirements
for the degree of Doctor of Philosophy
to the
University of Edinburgh
August 2011



For Thomas Binoth

Abstract

The LHC has begun collecting data and the first results have now been published. This is truly an exciting time in the field as we wait for the experimental data to exclude or verify new physics beyond the Standard Model. In order to make a precise prediction for the LHC one must go beyond the leading order of our perturbation series. In this thesis I present the extension of tools for the automation of one loop calculations for supersymmetric models. The second part of the thesis contains the application of these tools to neutralino pair production in the Minimal Supersymmetric Model.

Declaration

All work herein is my own except where clearly referenced. The work presented here has not been submitted for any other degree or professional qualification.

Chapter 3 contains work that is published in [1] that was completed in collaboration with T. Reiter. Chapter 4 contains work that was completed with T. Binoth, G. Heinrich and J. Ph. Guillet as part of the Golem collaboration and is published in [2]. The calculation in Chapter 5 was completed in collaboration with G. Heinrich, T. Reiter and N. Greiner.

This research was funded by a grant awarded by the Science and Technology Funding Council (STFC).

G. Cullen
August 2011

Acknowledgements

I am deeply grateful to Gudrun Heinrich for performing the role of my supervisor. Your help, advice and hands-on guidance has been invaluable and I really could not have completed this without you. Thank you.

I would also like to thank Thomas Reiter for his constant and incredibly useful help in physics and the computational side of the project. Likewise, I want to acknowledge my collaborator Jean-Philippe Guillet for the work we completed on the triangle integrals and also Nicolas Greiner for the work we completed for the neutralino pair production calculation.

I would like to thank Nikhef for their hospitality during my short stay there. Similarly, I would like to thank the MPI in Munich for their warm hospitality when I spent a week there earlier this year.

This thesis was brought to you by the letters STFC.

In Edinburgh I would like to thank all my fellow PhD students past and present for their help and support. Sadly, there are too many names to list you all here but I would like to thank in particular my old basement inmates: Claudia, Erik, Eoin, Liam and Sam. Additionally I would like to show my appreciation to Ioan, George and Samuel for useful discussions.

On the administrative side I would like to thank Jane Paterson for being incredibly helpful from start to finish.

I would also like to thank my family for their patience, love and support.

And Anna, thank you.

Contents

Abstract	ii
Declaration	v
Acknowledgements	vii
Contents	ix
List of figures	xiii
List of tables	xv
1 Introduction	1
1.1 The Standard Model	1
1.1.1 Introduction	1
1.1.2 Experimental tests of the SM	2
1.1.3 Experimental issues with the Standard Model	2
1.1.4 Theoretical issues with the SM	2
1.1.5 The Hierarchy Problem	3
1.1.6 Outline of Thesis	5
2 Higgs bosons and Supersymmetry	7
2.1 Introduction	7
2.2 The Standard Model Higgs Sector	7
2.2.1 Spontaneous Symmetry Breaking and the Higgs Mechanism	7
2.2.2 Abelian Higgs Toy Model	8
2.2.3 Gauge Boson Interactions	11
2.2.4 Higgs Mass bounds	17
2.2.5 The Hunt for the Higgs	19
2.3 Supersymmetry	20
2.3.1 Introduction	20
2.3.2 The MSSM Higgs Sector	22
2.3.3 Sfermion Sector	25
2.3.4 Neutralino Sector	26
2.3.5 The Search for Supersymmetry	28
3 Details of Next to Leading Order Calculations	31
3.1 Set up of Calculation	31
3.2 Hadronic Observables and Scale Dependence at Next to Leading Order	32
3.3 Color	33
3.3.1 Color Basis	34

3.3.2	Color Insertion Operators	35
3.3.3	Example: Neutralino Pair Production	35
3.3.4	Example: Neutralino Pair Production plus One Jet	38
3.4	Spinor Helicity Formalism	39
3.4.1	Definitions	39
3.4.2	Chisholm Identities	46
3.5	Majorana Fermions	47
3.5.1	Working with Majorana Spinors	48
3.6	Tests of Implementation	50
3.7	Regularisation Scheme	50
3.7.1	The 't Hooft Veltman Scheme	52
3.7.2	Regularisation scheme dependence	53
3.7.3	Examples	54
3.7.4	Boson quark quark vertex	54
3.7.5	Chiral Coupling	55
4	Loop Integrals	57
4.1	Reduction Scheme	57
4.1.1	Overview	57
4.1.2	Form Factor Representation	58
4.1.3	Tensor Reduction	61
4.1.4	Subtraction for Scalar Integrals	63
4.1.5	Subtraction for Tensor integrals	65
4.1.6	Landau conditions	67
4.2	Evaluation of 3-point functions	67
4.2.1	Triangles with no internal mass	69
4.2.2	Triangles with one internal mass	72
4.2.3	Triangles with two internal masses	77
4.3	Evaluation of 2-point functions	79
4.3.1	Bubbles with no internal mass	81
4.3.2	Bubbles with one internal mass	82
4.3.3	Bubbles with two internal masses	85
4.4	Derivatives of Bubbles	86
4.5	Tadpole Integral	89
4.6	Evaluation of Three Point Tensor Integrals	89
4.6.1	Explicit results for $I_3^n(s_1, s_2, 0; m_1^2, 0, 0)$	90
4.6.2	Numerical Results	90
5	Neutralino Pair Production at Next to Leading Order	91
5.1	Outline	91
5.2	Renormalization	91
5.2.1	Self Energies	92
5.2.2	Renormalization Conditions	94
5.2.3	Mixing Squark Renormalization	96
5.2.4	Finite Squark Quark Neutralino Coupling	97
5.3	Results for $pp \rightarrow \chi_1^0 \chi_1^0$	97
5.3.1	Comparison to the Literature	97
5.3.2	Details of our Calculation	99
5.4	Details of Checks	101
5.5	Observables	101

6	Conclusions and Outlook	109
6.1	Conclusions	109
6.2	Outlook	110
A	Feynman Rules	111
A.1	Supersymmetric QCD	111
A.2	Neutralino Sector	112
B	Breaking SUSY by choice of Regularisation Scheme	119
B.1	Verifying the invariance of the SUSY Yang Mills Lagrangian	119
B.1.1	\mathcal{L}_1	120
B.1.2	\mathcal{L}_2	120
B.2	Finite Scheme Dependent Differences	122
B.2.1	Squark Self Energy	122
C	Loop Integrals	125
C.1	Derivation of loop integral formula	125
C.2	Derivation in dimension splitting	129
D	Miscellaneous comments	135
D.1	Loop Integral conventions	135
D.1.1	The Integral $\int_0^1 dz \frac{1}{z^{1+2\epsilon}}$	135
D.1.2	Combining complex logarithms	135
D.1.3	Notes on the integral $I_3^n(m_1^2, s_2, 0, m_1^2, 0, 0)$	136
D.1.4	Functions arising in results	136
D.1.5	Dilogarithm Identities	137
D.1.6	r_Γ	137
D.1.7	s	137
E	Outline of Code	139
E.1	Generation of the Virtual matrix elements	139
E.2	Majorana fermion issues	140
E.2.1	On the Relative Sign of Feynman Graphs	140
E.2.2	Majorana Exchange	141
F	Numerical Results for Three Point Tensor Integrals	143
	Bibliography	150

List of Figures

2.1	A picture of the Higgs potential.	9
2.2	Plot of the triviality and the vacuum stability bounds on the Higgs boson mass. . .	18
2.3	The $\Delta\chi^2$ electroweak analysis.	19
2.4	Contributions to Higgs mass corrections.	21
2.5	A plot of the excluded region in the mSUGRA breaking scenario.	28
2.6	A plot of the excluded region in the mSUGRA/CMSSM breaking scenario. . . .	29
2.7	The χ^2 plots for m_h in two SUSY breaking scenarios.	30
3.1	The born, real correction and virtual correction to the process $e^-e^+ \rightarrow 2$ jets at NLO.	31
3.2	Feynman rules for the computation of color factors in the gauge group $SU(N_c)$. . .	36
3.3	Diagrammatic representation of the inversion of the Lie algebra (3.10).	36
3.4	Diagrammatic representation of identity of the Lie algebra (3.11).	36
3.5	Diagrammatic representation of the Fierz identity (3.12).	37
3.6	The Casimirs written in diagrammatic form.	37
3.7	Diagrammatic representation of identity (3.15).	37
3.8	Diagrammatic representation of identity (3.16).	38
3.9	Feynman graph of the process $(ff \rightarrow VV)$ mediated by the exchange of a Majorana fermion (χ).	49
3.10	Comparison of our implementation of flipping rules with [3].	51
4.1	Generic N -point loop graph.	59
4.2	Kinematics for triangles integrals.	68
4.3	The set of infrared divergent integrals.	70
4.4	Graphs of the real and imaginary part of the ϵ^0 term of $I_3^n(s_1, s_2, 0, m_1^2, 0, 0)$ against s_2 with fixed $m_1^2 = 5.0$ and $s_1 = -5.0$	73
4.5	Graphs of the real and imaginary part of the ϵ^0 term of $I_3^n(m_1^2, s_2, 0, m_1^2, 0, 0)$ against s_2 with fixed $m_1^2 = 5.0$ and $s_1 = -5.0$	74
4.6	Graphs of the real part and imaginary part of the ϵ^0 term of $I_3^n(s_1, s_1, 0, m_1^2, 0, 0)$ against s_1 with fixed $m_1^2 = 5.0$	76
4.7	Graphs of the real part and imaginary part of the ϵ^0 term of $I_3^n(m_1^2, s_2, m_2^2, m_1^2, m_2^2, 0)$ against s_2 with fixed $m_1^2 = 9.0$ and $m_2^2 = 3.0$	78
4.8	Graphs of the real part and imaginary part of the ϵ^0 term of $I_3^n(m_1^2, s_2, m_1^2, m_1^2, m_1^2, 0)$ against s_2 with fixed $m_1^2 = 5.0$	80
4.9	Kinematics for bubble integrals.	80
4.10	Comparison of the real part and imaginary part of the ϵ^0 term of $I_2^n(s; m^2, 0)$. . .	83
4.11	Comparison of the real part and imaginary part of the ϵ^0 term of $I_2^n(m^2; m^2, 0)$. .	84
4.12	Comparison of the real part and imaginary part of the ϵ^0 term of $I_2^n(s, m_1^2, m_2^2)$. .	86
4.13	Comparison of the real part and imaginary part of the ϵ^0 term of $I_2^n(s, m^2, m^2)$. .	87

5.1	Quark self energy contributions.	92
5.2	Squark self energy contributions.	93
5.3	The subset of diagrams corresponding to Figure 5.4.	98
5.4	Numerical check of finite counter terms.	98
5.5	Diagrams for the process $pp \rightarrow \chi_1^0 \chi_1^0$. They are drawn using the Feynman rules defined in Appendix A.	100
5.6	Comparison of the NLO and LO $m_{\chi_1^0 \chi_1^0}$ distributions for the process $pp \rightarrow \chi_1^0 \chi_1^0$	103
5.7	Contributions to the NLO $m_{\chi_1^0 \chi_1^0}$ distributions for the process $pp \rightarrow \chi_1^0 \chi_1^0$	104
5.8	Contributions to the real emission differential cross section.	105
5.9	Effect of jet veto on the contributions to the real emission differential cross section.	106
5.10	Comparison of the NLO and LO $m_{\chi_1^0 \chi_1^0}$ distributions for the process $pp \rightarrow \chi_1^0 \chi_1^0$ with a jet veto.	107
A.1	Diagrammatic representation of particles.	113
A.2	QCD feynman rules.	114
A.3	Supersymmetric QCD feynman rules	115
A.4	Four scalar interactions in Supersymmetric QCD.	116
A.5	Squark-Gauge boson-gluon vertices with squark mixing.	116
A.6	Squark-Gauge boson gluon vertices without squark mixing.	117
A.7	Neutralino Feynman Rules.	118
C.1	The complex plane in the Wick rotation.	127
E.1	Schematic diagram of the code.	140

List of Tables

3.1	Summary of the differences in the choice of regularisation scheme.	52
4.1	Basis integrals of our reduction scheme.	58
4.2	Kinematic points for $I_3^n(s_1, s_2, 0, m_1^2, 0, 0)$	72
4.3	Kinematic points for $I_3^n(m_1^2, s_2, 0, m_1^2, 0, 0)$	74
4.4	Kinematic points for $I_3^n(s_1, s_1, 0, m_1^2, 0, 0)$	75
4.5	Kinematic points for $I_3^n(m_1^2, s_2, m_2^2, m_1^2, m_2^2, 0)$	77
4.6	Kinematic points for $I_3^n(m_1^2, s_2, m_1^2, m_1^2, m_2^2, 0)$	79
4.7	Kinematic points for $I_2^n(s; 0, 0)$	82
4.8	Kinematic points for $I_2^n(s; m^2, 0)$	82
4.9	Kinematic points for $I_2^n(m^2; m^2, 0)$	83
4.10	Kinematic points for $I_2^n(0; m^2, 0)$	85
4.11	Kinematic points for $I_2^n(s, m^2, m^2)$	87
F.1	Kinematic points for $I_3^n(s_1, s_2, 0, m_1^2, 0, 0)$	145
F.2	Kinematic points for $I_3^n(m_1^2, s_2, 0, m_1^2, 0, 0)$	146
F.3	Kinematic points for $I_3^n(s_1, s_1, 0, m_1^2, 0, 0)$	147
F.4	Kinematic points for $I_3^n(m_1^2, s_2, m_2^2, m_1^2, m_2^2, 0)$	149
F.5	Kinematic points for $I_3^n(m_1^2, s_2, m_1^2, m_1^2, m_2^2, 0)$	150

Chapter 1

Introduction

1.1 The Standard Model

1.1.1 Introduction

The *Standard Model* of particle physics began emerging in the 1970's as a framework for the fundamental constituents of the world. Over the last four decades it has provided a platform on which to make experimental predictions for a variety of phenomena to a high precision. Furthermore, it explains physics on a vast range of energy scales from an electron volt to 100 GeV and is currently being tested at the *Large Hadron Collider* (LHC) at the TeV scale. Thus far it has been remarkably successful.

It is based on the idea that we can reduce the matter content of our world into fundamental particles: quarks, leptons and gauge bosons. The simplicity of the model is apparent when one writes it down in one line:

$$\mathcal{L}_{\text{SM}} = \sum_j i\bar{q}_j \not{D} q_j - \frac{1}{2} \text{tr} G^{\mu\nu} G_{\mu\nu} + \sum_k i\bar{\psi}_k \not{D} \psi_k - \frac{1}{4} F_{\mu\nu}^j F^{j\mu\nu} - \frac{1}{4} B^{\mu\nu} B_{\mu\nu} + \mathcal{L}_{\text{Higgs}}. \quad (1.1)$$

The Standard Model incorporates the electromagnetic force, the weak nuclear force and the *strong* nuclear force into a renormalizable quantum field theory. The strong force is described by Quantum Chromodynamics [4, 5, 6] and provides a very rich and diverse area of physics research. A major success in the development of the Standard Model was the unification of the electromagnetic and weak forces into the *electroweak* theory of Glashow, Salam and Weinberg [7, 8, 9, 10, 11]. This unified symmetry is broken at low energies and the breaking was confirmed with the discovery of the massive W and Z gauge bosons. When brought together the Standard Model is a non-abelian Yang Mills theory based on the gauge group $SU(3)_c \times SU(2)_L \times U(1)_Y$ with $SU(2)_L \times U(1)_Y$ spontaneously broken to $U(1)_{\text{em}}$.

The cornerstone of the Standard Model is the Higgs mechanism that offers an explanation as to how electroweak symmetry is broken. The minimal version of the Higgs mechanism postulates a massive scalar field: the Higgs boson. The inclusion of the Higgs mechanism in the Standard Model is a contentious issue, as no experimental evidence for the Higgs boson has

been found. How electroweak symmetry is broken is an open question in current research in *Beyond the Standard Model* (BSM) physics.

1.1.2 Experimental tests of the SM

The Standard Model has been verified experimentally to a high degree of precision. Generally, the development of particle physics has been driven by the increasing power of particle accelerators allowing matter to be probed at ever decreasing distances. The development of QCD began with the quark model introduced by Murray Gell-Mann as a mathematical explanation behind the *particle zoo*, an explosion in the discovery of different species of hadrons. Initially quarks were not thought of as physical particles and it wasn't until 1968, when Bjorken scaling was discovered at SLAC confirming that protons were made up of partons, that quarks were thought of as real confined physical particles. This discovery followed on from the accelerator passing a physical boundary 1 GeV that allowed the substructure of the proton to be resolved for the first time. In 1976 the τ lepton was discovered at SLAC; this was a completely unexpected discovery and was the first observation of a third generation particle. Later, in 1983, striking evidence for electroweak symmetry breaking was found as the W and Z bosons were discovered at CERN. In 1995 the predicted top quark was found at the CDF and D0 experiments at the Tevatron collider with a mass of about 175 GeV.

This brief historical review teaches us that progress in theoretical particle physics has been achieved by using theoretical models as guiding principles in the search for new physics, and refining these models with the advent of new experimental evidence. Pertinently, at this time, we observe that for every increase in energy at particle accelerators *new physics* has been found, whether or not it was predicted by the accepted model of the time.

1.1.3 Experimental issues with the Standard Model

Despite the success of the Standard Model, there are good experimental and theoretical reasons to believe that it is incomplete. We list some of the experimental reasons below:

- In 1998 it was confirmed that neutrinos are not in fact massless as is assumed in the Standard Model and do, in fact, have a small mass.
- The WMAP experiment conclusively confirmed the existence of cold dark matter in the Universe which has no explanation in the Standard Model.
- Current direct searches for the Higgs boson have been inconclusive and indirect searches have set exclusion limits on the mass range.

1.1.4 Theoretical issues with the SM

Alongside the reasons outlined above there are many theoretical issues with the Standard Model. These issues are:

- There is no underlying explanation to the pattern of masses and mixing parameters observed. Questions of this type include, for example, “Why are there 3 generations?” and “Why is the top quark so heavy compared to the other quarks?”.
- Why do the fundamental particles lie in the representations they do and is there a reason the world is described by these gauge groups?
- The Higgs potential behind electroweak symmetry breaking is completely ad-hoc and is chosen because it is the simplest potential that breaks electroweak symmetry.
- Gravity is not included in the framework of the Standard Model.
- Finally, the hierarchy problem provides a convincing argument as to why a fundamental scalar needs to be protected by some symmetry at a higher energy scale, and therefore why the Standard Model is not complete. We examine this in more detail in Section 1.1.5.

The first two are mostly philosophical questions. One can adopt a pragmatic viewpoint and accept that we have free parameters and there is no underlying reason behind them. The third point is an issue that can be illuminated by further experiment. It is certainly hoped that the LHC will shed light on the nature of electroweak symmetry breaking and, if it is caused by a scalar potential, the form of the potential can be uncovered. The fourth problem is certainly one that questions how natural and complete the Standard Model is and we shall outline it in the next section. In fact, it can be rephrased to point to the scale of *new physics* (see, for example, [12]).

1.1.5 The Hierarchy Problem

The most compelling theoretical argument concerns the notion of *naturalness* in the electroweak symmetry breaking sector. If one considers the Standard Model as a low energy effective theory then one must introduce a scale, an ultraviolet cut off, into the picture at which physics outside the Standard Model ceases to become negligible. Gravity is not included in the Standard Model therefore one could choose this cut off to be the Planck scale. However, we have no reason to assume that the Standard Model is valid all the way up to the Planck scale and it is more common to introduce a generic scale Λ for *new physics*, the Planck scale being an upper bound on its value. In perturbative calculations one way to regulate ultraviolet divergences arising from the integral over the unresolved loop momenta is to use Λ as a ultraviolet momentum cut-off. Symbolically

$$\int dk \rightarrow \int^{\Lambda} dk. \quad (1.2)$$

Our perturbative calculations to any given loop order will therefore have dependence on this scale. If we focus on corrections to particle masses, then the corrections to the scalar particle mass are the most problematic to appear as these are quadratic divergences. One can contrast this with the corrections to the fermion mass which are milder due to chiral symmetry and gauge

boson masses are protected by gauge invariance (one must use a gauge invariant regulator to see this, such as dimensional regularisation). The problem is that the mass term for the scalar field has the form

$$m^2 = m_0^2 + c\Lambda^2 \tag{1.3}$$

and we see that the scalar mass correction is driven to the scale Λ . If this scale is large then we have a problem in keeping the m^2 as small as indicated by theoretical and experimental constraints. We need to “fine-tune” the parameter in the bare Lagrangian m_0 to cancel with the large contribution Λ^2 [13]. This will need to be repeated at each order in perturbation theory.

We are led to the following tension [14]: precision electroweak physics show no compelling evidence for physics beyond the Standard Model, and we have no signal for a Higgs boson. And as of now there has been no indication of any new particles being produced. This seems to point that the scale of new physics is quite high above 1 TeV leading to fine-tuning.

1.1.5.1 Solutions

How does one solve the hierarchy problem? We present four possible solutions below. Firstly, one could simply be happy with the fine tuning, after all this quadratic divergence is no longer manifest when we use dimensional regularisation. However, by adopting this viewpoint, we lose contact with the interpretation of the cut-off being a scale of new physics which is what we wish to investigate.

The second solution could be that fundamental scalars do not exist and that composite objects play the role of the Higgs boson. These ideas go by the name *Technicolor* (for a recent review see [15]) and consist of new *technipions* that are bound together by a new color-like force that becomes strong at the TeV scale. The idea that the electroweak sector is simply QCD at a higher scale is attractive but due to constraints on flavour changing neutral currents the original models are incompatible with experimental results. However, new research in the field of walking technicolor [16] look promising as a way of avoiding experimental constraints.

Thirdly, we can embed our gauge group into a larger one and use *collective symmetry breaking* in order to solve the problem at the one-loop level. This is exactly what happens in *little higgs* models (for a comprehensive review see [12]).

The final solution we present is that of *supersymmetry* where we work on the observation that loop diagrams containing fermions and bosons come with the opposite sign; one can arrange a cancellation of the quadratic divergences between diagrams containing fermions and bosons at the multiloop level if there is a suitable relation between the two couplings. The implications of this symmetry is that each Standard Model particle has a superpartner with the same quantum number except spin, where a fermion has a boson for a partner and vice versa. An equivalent way to describe this solution is that the unrenormalized theory is free of quadratic divergences [17] and therefore provides a natural solution to the hierarchy problem before renormalization. We will talk more about this theory in the next chapter.

1.1.6 Outline of Thesis

In this thesis we present the development and implementation of an automated approach to Next to Leading Order (NLO) calculations within the context of the Minimal Supersymmetric Standard Model (MSSM), specifically focusing on the virtual contribution.

In Chapter 2 of this thesis we examine the theory of the Higgs mechanism and explore the current experimental status of the search for the Higgs boson. We then proceed to motivate Supersymmetry as a solution to the Hierarchy problem. After a discussion of different sectors of the MSSM we discuss the current experimental searches for this theory.

In Chapter 3 we discuss details of NLO calculations, namely how one deals with the color and spinor degrees of freedom. We present an algebraic method of reducing our amplitude to an expression involving spinor products suitable for a numerical evaluation. We also consider how one defines a regularisation scheme and how to deal with fermionic objects specific to beyond the Standard Model theories.

In Chapter 4 we investigate the computation of virtual diagrams and, in particular, how we reduce the integrals to a suitable basis. We introduce a reduction scheme that avoids potential artificial singularities in certain kinematic regions. The end point of this reduction requires the analytic evaluation of the basis set of massive infra red divergent triangles and we present our results for these. Furthermore, we look at the end point of our reduction process for the corresponding tensor integrals.

Our implementation of these ideas into an automated code is tested in Chapter 5 where we present the full NLO results for neutralino pair production for the LHC in the MSSM. This includes the presentation of the relevant counter terms needed for our renormalization procedure and a discussion of the checks that we performed.

The conclusions reached are presented in Chapter 6.

Chapter 2

Higgs bosons and Supersymmetry

2.1 Introduction

In this chapter we examine the Higgs mechanism. Firstly we look at its representation in the Standard Model, the so called minimal Higgs mechanism and its experimental and theoretical constraints within the Standard Model. Then we move on to a popular extension of this implementation, the two Higgs doublet model in the context of the Minimal Supersymmetric Standard Model (MSSM). Finally, we discuss other aspects of the MSSM and its experimental status.

2.2 The Standard Model Higgs Sector

In this section we examine the Standard Model Higgs sector, what is known as the *minimal* Higgs sector. Although electroweak symmetry breaking is concerned with a larger gauge group, the main features of the Higgs mechanism are present in the $U(1)$ group, so we begin with this case and move on to the Standard Model gauge group.

2.2.1 Spontaneous Symmetry Breaking and the Higgs Mechanism

The solutions of an equation of motion generally do not possess the same symmetries as the equation of motion. If we act on these solutions with a symmetry transformation of the equation of motion we will obtain other solutions with the same total energy. However, *if* the solution is invariant under the symmetry transformations we cannot generate new solutions this way; we have a unique solution to our equation of motion.

In the following chapter we consider the case that the ground state of the system is not invariant under the original symmetry therefore we can generate other solutions by acting on a given ground state with the symmetries of the Lagrangian. Therefore the ground state is

degenerate. One must choose between these (infinite, in our case of a continuous symmetry) equivalent ground states. Once the choice has been made, and we re-express the ground state in terms of this choice the original symmetry of the Lagrangian is hidden or is said to be *spontaneously broken*. The *Higgs mechanism* is the general idea that describes the process by which the Goldstone bosons that are associated with a spontaneously broken gauge symmetry are absorbed when the symmetry is gauged to become the longitudinal components of a massive gauge field.

The simplest way to break the gauge symmetry is through a scalar potential. This can lead to *Higgs bosons*. These are fundamental scalar particles of the original gauge multiplet from which the Goldstone bosons came from. They are degrees of freedom that can not be absorbed/gauged away and are therefore observable particles.

2.2.2 Abelian Higgs Toy Model

We choose the simplest example to demonstrate the main features of the Higgs mechanism. We will see that most of the ideas that go into this case are simply repeated for larger gauge groups. We consider the abelian $U(1)$ group. The field content is a complex scalar field $\phi = \frac{1}{\sqrt{2}}(\phi_1 + i\phi_2)$ and a gauge field A^μ . The Lagrangian is written as

$$\mathcal{L} = -\frac{1}{4}F_{\mu\nu}F^{\mu\nu} + (D^\mu\phi)^*(D_\mu\phi) - V(\phi^*\phi). \quad (2.1)$$

where the covariant derivative is $D^\mu = \partial^\mu + igA^\mu$ and the field strength tensor is $F^{\mu\nu} = \partial^\mu A^\nu - \partial^\nu A^\mu$. This is gauge invariant under the gauge transformations

$$A^\mu \rightarrow UA^\mu U^\dagger - \frac{i}{g}U\partial^\mu U^\dagger \quad (2.2)$$

$$\phi \rightarrow U\phi \quad (2.3)$$

where the gauge transformation is

$$U = \exp\left[i\frac{\theta(x)}{v}\right] \quad (2.4)$$

and θ is a local gauge parameter. We *choose* the potential to be of the form

$$V(\phi^*\phi) = \lambda(\phi^*\phi)^2 - \mu^2(\phi^*\phi) \quad (2.5)$$

with $\lambda > 0, \mu^2 > 0$. This potential has a local maximum at the point $(\phi_1, \phi_2) = (0, 0)$ and has a circle of degenerate minima at radius (see Figure 2.1)

$$|\phi|^2 = \frac{\mu^2}{2\lambda} = \frac{v^2}{2}. \quad (2.6)$$

This circle comprises of an infinite number of degenerate ground states. If we act on this ground state with the $U(1)$ transformation, a symmetry of the Lagrangian, we obtain another

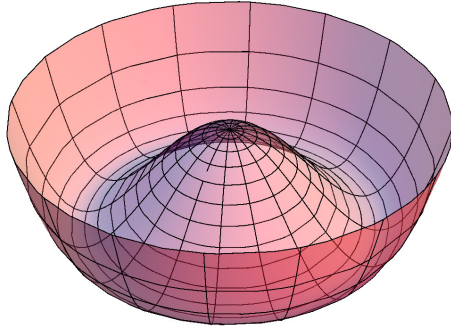


Figure 2.1: A picture of the Higgs potential.

ground state. However, we can only have one ground state, therefore we must choose one point on this circle. Once we make this choice the symmetry is hidden or is said to be *spontaneously broken*. Goldstone's theorem tells us that for each broken generator of the symmetry we have a massless field, and the *Higgs mechanism* is the process of a massless gauge boson absorbing this degree of freedom. This means that, in this case, we have broken the $U(1)$ symmetry so we expect one massless Goldstone field to be absorbed by the gauge boson. We must choose a gauge to really examine what happens to the degrees of freedom after breaking. We look at the unitary gauge and then the 't Hooft gauge.

2.2.2.1 The Unitary Gauge

We start our discussion by reparameterizing the field. We expand ϕ about one of the ground states giving:

$$\phi = \frac{v + h(x)}{\sqrt{2}} \exp i(\theta(x) + \alpha). \quad (2.7)$$

We *break* the gauge symmetry by choosing a particular value for α (i.e. we choose a point on the circle of degenerate minima, $\alpha = 0$). Because the model is gauged the field $\theta(x)$ can be considered as a parameter of the local gauge transformation (2.4) i.e. it has no physical significance. With this parameterization we have

$$\phi^\dagger \phi = \frac{1}{2}(v + h)^2 \quad (2.8)$$

i.e. we are at the vacuum expectation value only where the field $h = 0$. This fixes the gauge to be the *unitary* gauge; in this gauge we have removed the unphysical degree of freedom θ . We

have

$$\begin{aligned}
 D^\mu U^\dagger \phi &= \frac{1}{\sqrt{2}} (\partial^\mu + igA^\mu) U^\dagger (h + v) \\
 &= \frac{1}{\sqrt{2}} U^\dagger \left[\partial^\mu + ig \left(A^\mu - \frac{1}{g} \partial_\mu \theta \right) \right] (h + v) \\
 &= \frac{1}{\sqrt{2}} U^\dagger [\partial^\mu + igA^\mu] (h + v) = U^\dagger D^\mu \phi
 \end{aligned} \tag{2.9}$$

as we expect from the covariant derivative. Upon expanding out the Lagrangian we see that there are bilinear terms mixing the h field and the A_μ field. The A_μ field now has a mass $M = gv$ and the h field also has a mass. We have 4-point and 3-point h interactions coming from the scalar potential and interactions between the A and h fields from the gauged kinetic part. The field θ that links the two fields, has completely disappeared and the degree of freedom associated with it has been absorbed by the gauge boson for it to become massive.

2.2.2.2 The 't Hooft Gauge

While the unitary gauge is very convenient it is instructive to look also at another choice. We begin with a reparameterization of our complex field

$$\phi = \frac{1}{\sqrt{2}} (v + h(x) + i\chi(x)) \tag{2.10}$$

so our new fields, h and χ have zero vacuum expectation value. Our fields are defined relative to the point on $v + i0$ on the complex plane. In the new coordinates, $\phi^\dagger \phi = \frac{v^2}{2}$ only at the point $\chi = h = 0$. Our covariant derivative is now:

$$D_\mu \phi = \frac{1}{\sqrt{2}} [\partial_\mu h + i(\partial_\mu \chi + gvA_\mu) + igA_\mu (h + i\chi)]. \tag{2.11}$$

Because of the spontaneous symmetry breaking the gauge field is now mixed with the Goldstone mode χ . We see this by examining the gauged kinetic term for the scalars:

$$\begin{aligned}
 (D^\mu \phi)^* (D_\mu \phi) &= \frac{1}{2} [\partial_\mu h \partial^\mu h + \partial_\mu \chi \partial^\mu \chi + M^2 A_\mu A^\mu + g^2 h^2 A_\mu A^\mu - g^2 A_\mu^2 \chi^2] \\
 &\quad + MA_\mu (\partial^\mu \chi) - g(\partial_\mu \chi) h A^\mu - gMhA_\mu A^\mu.
 \end{aligned} \tag{2.12}$$

where, as before, we are led to $M = gv$. The scalar potential looks like

$$V(h, \chi) = \frac{\lambda}{4} \chi^4 + \frac{\lambda}{2} h^2 \chi^2 + \frac{\lambda}{4} h^4 + v\lambda \chi^2 h + \mu^2 h^2 + v\lambda h^3 - \frac{\lambda}{4} v^4 \tag{2.13}$$

i.e. as expected we have a mass term for the h field and the χ field remains massless. This is not the whole story here as our term $MA_\mu (\partial^\mu \chi)$ mixes our gauge field and the χ field; this is the usual problem of not being able to write down a gauge boson propagator without fixing a gauge. We now outline a procedure in which the gauge is fixed and in doing so the two fields

are disentangled. We add a 't Hooft gauge fixing term to the Lagrangian

$$\begin{aligned}\mathcal{L}_{\text{fix}} &\equiv -\frac{1}{2\xi} (\partial^\mu A_\mu - \xi M\chi)^2 \\ &= -\frac{1}{2\xi} (\partial_\mu A^\mu)^2 - MA_\mu(\partial^\mu\chi) - \frac{1}{2}\xi M^2\chi^2.\end{aligned}\tag{2.14}$$

This term un-mixes the fields A^μ and χ and gives the field χ a mass $\sqrt{\xi}M$. In this gauge the χ field has the usual scalar propagator

$$\frac{i}{k^2 - \xi M^2 + i\epsilon}\tag{2.15}$$

and the gauge field has the propagator

$$D^{\mu\nu} = \frac{i}{k^2 - M^2} \left(-g^{\mu\nu} + \frac{k^\mu k^\nu}{k^2} \right) - \frac{i\xi}{k^2} \left(\frac{k^\mu k^\nu}{k^2 - \xi M^2} \right).\tag{2.16}$$

where we decompose it into transverse and longitudinal components. We see that the ξ dependence of the propagator lies in the longitudinal part of the propagator i.e. the mixing between the fields χ and A^μ is between the field χ and the longitudinal part of A^μ . If we wish to recover the physical ‘unitary’ gauge we take the limit $\xi \rightarrow \infty$. In this limit the χ propagator vanishes and the longitudinal part of the gauge boson propagator tends to the usual massive case

$$\begin{aligned}\lim_{\xi \rightarrow \infty} D^{\mu\nu} &= \frac{i}{k^2 - M^2} \left(-g^{\mu\nu} + \frac{k^\mu k^\nu}{k^2} \right) + i \frac{k^\mu k^\nu}{k^2 M^2} \\ &= \frac{i}{k^2 - M^2} \left(-g^{\mu\nu} + \frac{k^\mu k^\nu}{M^2} \right).\end{aligned}\tag{2.17}$$

Thus our field content is the same as in the unitary gauge where the unphysical Goldstone boson χ is gauged away. Before taking this limit the longitudinal degree of freedom of the gauge boson and the Goldstone boson mix through the parameter ξ . The two degrees of freedom correspond to only one physical degree of freedom which is obtained when we take the limit $\xi \rightarrow \infty$. In the Higgs mechanism this limit corresponds precisely to, what is referred to as, the gauge boson ‘eating’ the Goldstone boson. The Higgs mechanism is much more tangible with this gauge choice, whereas the unitary gauge somewhat hides the mechanism. Now it is understood, it is certainly more convenient to choose the unitary gauge for the discussion of the Standard Model Higgs sector as is far simpler algebraically.

2.2.3 Gauge Boson Interactions

We extend the above analysis to the Standard Model electroweak gauge group $SU(2)_L \times U(1)_Y$, where we have three massless bosons associated with the gauge group $SU(2)$: W^i ($i = 1, 2, 3$) and one massless boson B associated with the abelian $U(1)$ gauge group. We follow the procedure

presented in [18]. The kinetic part of the Lagrangian is

$$\mathcal{L}_{\text{kin}} = -\frac{1}{4}W_{\mu\nu}^i W_{\mu\nu}^i - \frac{1}{4}B_{\mu\nu}B^{\mu\nu} \quad (2.18)$$

with the field strength tensors defined as

$$W_{\mu\nu}^i = \partial_\mu W_\nu^i - \partial_\nu W_\mu^i - g\epsilon^{ijk}W^jW^k \quad (2.19)$$

$$B^{\mu\nu} = \partial_\mu B_\nu - \partial_\nu B_\mu \quad (2.20)$$

where g is the $SU(2)$ gauge coupling. One couples gauge fields to matter by introducing the covariant derivative

$$D_{ij}^\mu = \delta_{ij}\partial^\mu + ig(T \cdot W^\mu)_{ij} + iY\delta_{ij}g' B^\mu \quad (2.21)$$

where g' is the $U(1)$ coupling. The matrices T are a representation of the $SU(2)$ algebra and the matrix $Y\delta_{ij}$ is a representation of the $U(1)$ algebra. We are free to choose a representation for the matter fields. We choose $T^i = \tau^i/2$ where τ are the usual Pauli matrices

$$[T^i, T^j] = i\epsilon^{ijk}T^k \quad (2.22)$$

and we choose $Y = 1/2$. With this choice we can rewrite

$$D_\mu = \partial^\mu + ig[W_\mu^1 \cdot T^1 + W_\mu^2 \cdot T^2] + i\left[\frac{g'}{2}B_\mu + gT^3W_\mu^3\right] \quad (2.23)$$

Under the field redefinitions:

$$W_\mu^\pm = \frac{W_\mu^1 \mp iW_\mu^2}{\sqrt{2}} \quad (2.24)$$

and rewriting the $SU(2)$ generators as raising and lowering operators:

$$T^\pm = T^1 \pm iT^2 \quad (2.25)$$

this becomes

$$D_\mu = \partial^\mu + ig\frac{[T^+W_\mu^+ + T^-W_\mu^-]}{\sqrt{2}} + i\left[\frac{g'}{2}B_\mu + gT^3W_\mu^3\right]. \quad (2.26)$$

With the explicit choice for generators of $SU(2)$ specified above we have

$$T^3 = \frac{1}{2} \begin{pmatrix} 1 & 0 \\ 0 & -1 \end{pmatrix} \quad T^+ = \begin{pmatrix} 0 & 1 \\ 0 & 0 \end{pmatrix} \quad T^- = \begin{pmatrix} 0 & 0 \\ 1 & 0 \end{pmatrix}. \quad (2.27)$$

Our Lagrangian describes four massless vector bosons that form a singlet B and a triplet W^\pm, W^3 under the gauge group. Physically, this is unsatisfactory. To describe the electroweak

interaction one needs to introduce a Higgs sector that provides the theory with the following particle content: three massive gauge bosons (to describe the weak interaction) and one massless gauge boson (the photon). The minimal choice to achieve this is a scalar doublet with four degrees of freedom. We break $SU(2) \times U(1)$ down to $U(1)_{em}$ as above. Goldstone's theorem tells us that we have 3 massless Goldstone bosons corresponding to the three broken generators in this breaking. Because of the gauge symmetry, one can consider these Goldstone bosons as parameters of the gauge transformation. Therefore, one can gauge away these unphysical degrees of freedom. The most convenient choice of gauge is, as above, the unitary gauge. We parametrise our $SU(2)$ doublet as

$$\phi = \frac{1}{\sqrt{2}} U^\dagger \begin{pmatrix} 0 \\ h + v \end{pmatrix} = \frac{1}{\sqrt{2}} \exp \left[-\frac{i}{v} T \cdot \theta(x) \right] \begin{pmatrix} 0 \\ h + v \end{pmatrix} \quad (2.28)$$

with U belonging to our gauge group. This parameterisation allows us to manipulate the covariant derivative

$$\begin{aligned} D^\mu &= (\partial^\mu + igT \cdot W^\mu + ig' Y B^\mu) \\ &= (\partial^\mu + igT \cdot W^\mu + ig' Y B^\mu) \frac{1}{\sqrt{2}} U^\dagger (h + v) \alpha \\ &= U^\dagger \left(\partial^\mu + igUT \cdot W^\mu U^\dagger + ig' Y B^\mu + U \partial^\mu U^\dagger \right) \frac{1}{\sqrt{2}} (h + v) \alpha \\ &= U^\dagger \left(\partial^\mu + ig(UT \cdot W^\mu U^\dagger - \frac{i}{g} U \partial^\mu U^\dagger) + ig' Y B^\mu + U \partial^\mu U^\dagger \right) \frac{1}{\sqrt{2}} (h + v) \alpha \\ &= U^\dagger \left(\partial^\mu + igT \cdot W'^\mu + ig' Y B^\mu \right) \frac{1}{\sqrt{2}} (h + v) \alpha \\ &= U^\dagger D'^\mu \frac{1}{\sqrt{2}} (h + v) \alpha \end{aligned} \quad (2.29)$$

where α is the unit vector $(0, 1)^T$. So under the gauge transformation U we have

$$D^\mu \phi \rightarrow U D^\mu \phi = D'^\mu \frac{1}{\sqrt{2}} (h + v) \alpha. \quad (2.30)$$

Using this result alongside (2.23) we can easily write out our Lagrangian. Focusing on the part that is quadratic in the gauge fields we have

$$\begin{aligned} \mathcal{L} &\supset (D^\mu \phi)^\dagger (D_\mu \phi) \\ &= \frac{1}{2} \left[\alpha^T \left(\partial^\mu - igT \cdot W^\mu - ig' Y B^\mu \right) (h + v) \left(\partial^\mu + igT \cdot W^\mu + ig' Y B^\mu \right) (h + v) \alpha \right] \\ &= \frac{1}{2} \partial_\mu h \partial^\mu h + \frac{(v + h)^2}{2} \alpha^T \left[gT \cdot W^\mu + g' Y B^\mu \right] \left[gT \cdot W^\mu + g' Y B^\mu \right] \alpha. \end{aligned} \quad (2.31)$$

This gives two terms quadratic in the gauge boson fields. The first is simply

$$\mathcal{L} \supset \frac{(v + h)^2}{4} g^2 W^+ W^- \quad (2.32)$$

and the second is

$$\mathcal{L} \supset \frac{(v+h)^2}{2} \left(g' B_\mu - g W_\mu^3 \right) \left(g' B^\mu - g W^{3\mu} \right). \quad (2.33)$$

These terms include interactions between the Higgs field h and the gauge fields and also mass terms for the bosons. There is a slight complication in the second expression- we have mixing terms between the gauge fields B, W^3 meaning we cannot write down two separate propagators for these fields. We diagonalise the mass matrix for these two fields to the basis Z and A . The mixing is

$$\begin{pmatrix} Z^\mu & A^\mu \end{pmatrix} = \begin{pmatrix} \cos \theta & \sin \theta \\ -\sin \theta & \cos \theta \end{pmatrix} \begin{pmatrix} W^{3\mu} \\ A^\mu \end{pmatrix} \quad (2.34)$$

where

$$\sin \theta = \frac{g'}{\sqrt{g^2 + g'^2}}. \quad (2.35)$$

The observed value of $\sin^2 \theta$ is about 0.23, therefore we see that the Z field is dominated by the W^3 component and the photon by the B field. This is reflected in the mass spectrum of the theory where

$$m_W = \frac{vg}{2} \quad (2.36)$$

and

$$m_Z = \frac{m_W}{\cos \theta} \quad (2.37)$$

so the Z boson mass is pushed slightly higher than the W boson mass.

2.2.3.1 Yukawa Sector

As we have just seen, the Higgs mechanism allows one to construct a mass term in the Lagrangian in a gauge invariant way for gauge bosons. In addition to this the Higgs mechanism also allows one to write gauge invariant mass terms for the fermions. This is provided in the Yukawa sector. Now we outline how this works. For one generation of quarks and leptons our Lagrangian is [19]

$$\mathcal{L}_{\text{yukawa}} = \lambda_e \bar{e}_R \phi^\dagger \begin{pmatrix} \nu_e \\ e \end{pmatrix}_L + \lambda_d \bar{d}_R \phi^\dagger \begin{pmatrix} u \\ d \end{pmatrix}_L + \lambda_u \bar{u}_R \phi^T (i\sigma_2) \begin{pmatrix} u \\ d \end{pmatrix}_L + \text{h.c.} \quad (2.38)$$

which is invariant under $SU(2)_L \times U(1)_Y$ with the correct assignments of the quantum numbers Y . What's interesting to note here, for reasons later, is the different structure of the up-type and down-type quark terms. We will see this structure reappearing when we consider supersymmetric theories. As before, we expand the field around its vacuum expectation value

and pick the unitary gauge, again for convenience,

$$\begin{aligned}
 \mathcal{L}_{\text{yukawa}} &= \lambda_e \frac{v}{\sqrt{2}} (\bar{e}_R e_L + \bar{e}_L e_R) + \lambda_d \frac{v}{\sqrt{2}} (\bar{d}_R d_L + \bar{d}_L d_R) + \lambda_u \frac{v}{\sqrt{2}} (\bar{u}_R e_L + \bar{u}_L e_R) \\
 &+ \lambda_e \frac{h}{\sqrt{2}} (\bar{e}_R e_L + \bar{e}_L e_R) + \lambda_d \frac{h}{\sqrt{2}} (\bar{d}_R d_L + \bar{d}_L d_R) + \lambda_u \frac{h}{\sqrt{2}} (\bar{u}_R u_L + \bar{u}_L u_R) \\
 &= m_e \bar{e}e + m_u \bar{u}u + m_d \bar{d}d \\
 &+ \lambda_e \frac{h}{\sqrt{2}} \bar{e}e + \lambda_d \frac{h}{\sqrt{2}} \bar{d}d + \lambda_u \frac{h}{\sqrt{2}} \bar{u}u
 \end{aligned} \tag{2.39}$$

where, explicitly, we have substituted

$$\phi \rightarrow \frac{1}{\sqrt{2}} \begin{pmatrix} 0 \\ v + h \end{pmatrix}. \tag{2.40}$$

We have managed to write mass terms for the fermions in a gauge invariant way. To do so we had to introduce interactions between the fermions and the Higgs. It is non-trivial to extend this example to accommodate three generations as experiments shows that the matrices cannot be diagonal (or universal) in flavour space. We need to accommodate this into our Yukawa sector. To do this we introduce three 3 by 3 complex matrices. These are non-diagonal matrices in flavour space, explicitly,

$$\begin{aligned}
 \mathcal{L}_{\text{yukawa}} &= -(\bar{e}_R, \bar{\mu}_R, \bar{\tau}_R) C_l \begin{pmatrix} \phi^\dagger \cdot \begin{pmatrix} \nu_e \\ e \end{pmatrix}_L \\ \phi^\dagger \cdot \begin{pmatrix} \nu_\mu \\ \mu \end{pmatrix}_L \\ \phi^\dagger \cdot \begin{pmatrix} \tau_e \\ \tau \end{pmatrix}_L \end{pmatrix} \\
 &+ (\bar{d}'_R, \bar{s}'_R, \bar{b}'_R) C_q \begin{pmatrix} \phi^\dagger \cdot \begin{pmatrix} u \\ d' \end{pmatrix}_L \\ \phi^\dagger \cdot \begin{pmatrix} c \\ s' \end{pmatrix}_L \\ \phi^\dagger \cdot \begin{pmatrix} t \\ b' \end{pmatrix}_L \end{pmatrix} + (\bar{u}_R, \bar{c}_R, \bar{t}_R) C'_q \begin{pmatrix} \phi^T \cdot i\sigma_2 \cdot \begin{pmatrix} u \\ d' \end{pmatrix}_L \\ \phi^T \cdot i\sigma_2 \cdot \begin{pmatrix} c \\ s' \end{pmatrix}_L \\ \phi^T \cdot i\sigma_2 \cdot \begin{pmatrix} t \\ b' \end{pmatrix}_L \end{pmatrix} \\
 &+ \text{h.c.}
 \end{aligned} \tag{2.41}$$

where the set of C matrices are 3×3 complex matrices. Above we have five distinct “vectors” in flavour space. We can therefore define 5 distinct basis changes, one for each “vector”:

$$\begin{pmatrix} e_R \\ \mu_R \\ \tau_R \end{pmatrix} \rightarrow U_1 \begin{pmatrix} e_R \\ \mu_R \\ \tau_R \end{pmatrix}, \begin{pmatrix} u_R \\ c_R \\ t_R \end{pmatrix} \rightarrow U_2 \begin{pmatrix} u_R \\ c_R \\ t_R \end{pmatrix}, \begin{pmatrix} d'_R \\ s'_R \\ b'_R \end{pmatrix} \rightarrow U_3 \begin{pmatrix} d'_R \\ s'_R \\ b'_R \end{pmatrix} \quad (2.42)$$

$$\begin{pmatrix} \begin{pmatrix} e \\ \nu_e \end{pmatrix}_L \\ \begin{pmatrix} \mu \\ \nu_\mu \end{pmatrix}_L \\ \begin{pmatrix} \tau \\ \nu_\tau \end{pmatrix}_L \end{pmatrix} \rightarrow V_1 \begin{pmatrix} \begin{pmatrix} e \\ \nu_e \end{pmatrix}_L \\ \begin{pmatrix} \mu \\ \nu_\mu \end{pmatrix}_L \\ \begin{pmatrix} \tau \\ \nu_\tau \end{pmatrix}_L \end{pmatrix}, \begin{pmatrix} \begin{pmatrix} u \\ d' \end{pmatrix}_L \\ \begin{pmatrix} c \\ s' \end{pmatrix}_L \\ \begin{pmatrix} t \\ b' \end{pmatrix}_L \end{pmatrix} \rightarrow V_2 \begin{pmatrix} \begin{pmatrix} u \\ d' \end{pmatrix}_L \\ \begin{pmatrix} c \\ s' \end{pmatrix}_L \\ \begin{pmatrix} t \\ b' \end{pmatrix}_L \end{pmatrix}. \quad (2.43)$$

where $U_i, V_j \in U(3)$ for $i = 1, 2, 3$ and $j = 1, 2$.

These transformations give the mass eigenstates. Without going into details we are able to choose U_1 and V_1 such that the combination appearing in the leptonic Yukawa interaction is diagonal: i.e. $C^l \rightarrow U_1^\dagger C^l V_1 = D$, where D is a diagonal matrix with its entries as the coupling $\lambda_e, \lambda_\mu, \lambda_\tau$. We can do this because $C^l C^{l\dagger}$ is a positive, semi-definite Hermitian matrix that can be diagonalised.

We can carry out the same procedure for the quark cases: we are free to choose U_2, V_2 to give us $C^{q'} \rightarrow U_2^\dagger C^{q'} V_2 = D_2$ where D_2 is a diagonal matrix with entries of λ_u, λ_c and λ_t . We have already used our free choice for U_2 and V_2 so we transform

$$C_q \rightarrow U_3^\dagger C_q V_2 = U_3^\dagger V_3 V_3^\dagger V_2 = U_3^\dagger C_q V_3 V^\dagger = V V^\dagger U_3^\dagger C_q V_3 V^\dagger = V (U_3 V)^\dagger C_q V_3 V^\dagger \quad (2.44)$$

which allows us to choose V_3 and U_3 to give us

$$C_q \rightarrow V D_3 V^\dagger \quad (2.45)$$

where D_3 is a diagonal matrix with eigenvalues λ_d, λ_s and λ_b . We have already used our free choice for U_2 and V_2 to diagonalise C'_q so we are unable to fully diagonalise C'_q at the same time. Hence we are left with a unitary rotation that acts on the d, s, b quarks. This is $V (= V_2 V_3^\dagger)$ and is known as the CKM matrix. The entries of this matrix occur in charged W boson, flavour changing, interactions. We have a 3×3 unitary matrix therefore we have 9 parameters. We have 3 rotation angles (i.e. $O(3)$ rotation) and 6 phases. We can make phase rotations on all 6 quarks to get rid of these phases but we still have an overall phase. Therefore, the CKM matrix has 4 physical parameters: 3 rotation angles and a complex phase. The complex phase is responsible for all the CP -violation that occurs in the Standard Model. A review of the experimental measurements of this matrix and the current values can be found in [20].

2.2.4 Higgs Mass bounds

The Higgs boson enters the Standard Model with the free parameter: its mass m_h . We outline a few arguments here that give limits on the mass in the minimal model outlined above. They are derived from considerations of triviality, vacuum stability and unitarity.

2.2.4.1 Triviality

We consider the simplest case of a pure scalar theory defined by (2.5). We relate the coupling to the mass by

$$\lambda = \frac{m_h^2}{2v^2}. \quad (2.46)$$

The renormalization group equation gives [21]

$$\frac{d\lambda}{dt} = \frac{3\lambda^2}{4\pi^2} + \mathcal{O}(\lambda^3) \quad (2.47)$$

where $t = \log(Q^2/Q_0^2)$ and Q_0 is some reference scale. We solve this to get

$$\frac{1}{\lambda(Q_0)} - \frac{1}{\lambda(Q)} = \frac{3}{4\pi^2} \log\left(\frac{Q^2}{Q_0^2}\right). \quad (2.48)$$

where we have evolved from a large scale Q to a lower scale Q_0 (typically we would choose this as the electroweak scale). If we keep our coupling at the higher scale fixed $\lambda(Q) > 0$ and then take the limit $Q \rightarrow \infty$ then $\lambda(Q_0) \rightarrow 0$. The theory is *trivial* as, at low energy, the theory is no longer interacting; we have a free scalar propagator only.

Alternatively, we could solve (2.47) to give:

$$\lambda(Q) = \frac{\lambda(Q_0)}{\left[1 - \frac{3\lambda(Q_0)}{4\pi^2} \log\left(\frac{Q^2}{Q_0^2}\right)\right]}. \quad (2.49)$$

We have a Landau pole as $Q \rightarrow \Lambda$ only if (2.47) remains correct up to a high scale. We can obtain a bound on the Higgs mass by essentially demanding that the above behaviour does not happen i.e. that the quartic coupling be finite as $Q \rightarrow \infty$:

$$\frac{1}{\lambda(\Lambda)} > 0 \quad (2.50)$$

where Λ is the scale of new physics. Letting $Q_0 = v$ gives the following upper bound on the Higgs mass:

$$m_h^2 < \frac{8\pi^2 v^2}{3 \log\left(\frac{\Lambda^2}{v^2}\right)}. \quad (2.51)$$

This is known as the *triviality* or *perturbativity* bound. Decreasing the scale of new physics pushes up this bound. In the Standard Model the relation (2.47) changes as we now have

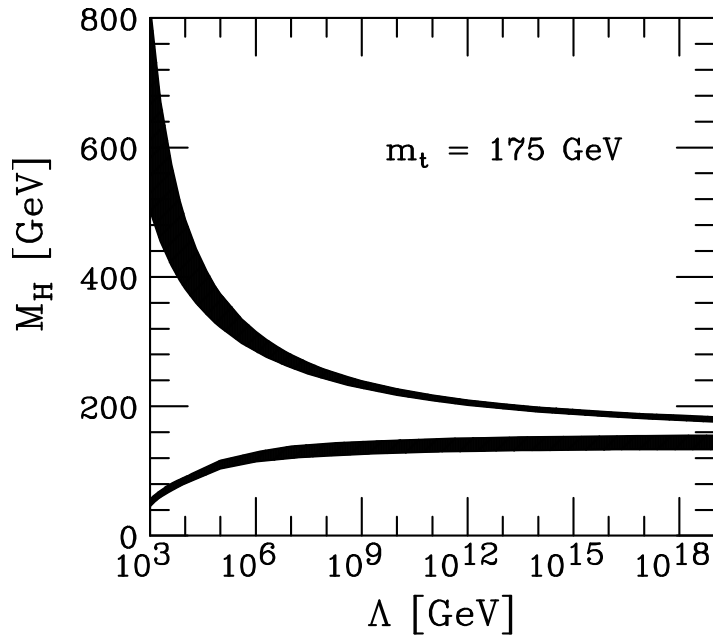


Figure 2.2: A plot of the perturbativity (or triviality) bound and the vacuum stability bound [23].

fermions and gauge bosons for the Higgs boson to couple to. As we are interested in the upper bound we look at the region where the Higgs is heavy therefore the quartic coupling is dominant and we can use the same bound we arrived at above.

2.2.4.2 Vacuum Stability

A lower bound on the Higgs mass can be derived from the allowed shape of the potential. If λ becomes negative at some scale Λ the potential has no state of minimum energy and spontaneous symmetry breaking cannot occur. We arrive at the bound [22]

$$m_h^2 > \frac{3y_t^4 v^2}{8\pi^2} \log\left(\frac{\Lambda^2}{v^2}\right) \quad (2.52)$$

where $y_t = \frac{m_t}{v}$, the coupling of the Higgs to the top quark (in this regime, this is the dominant contribution). This is known as the *stability* bound.

A more detailed study of both bounds was carried out in [23] and we show the result in Figure 2.2. They use the full two loop renormalization group evolution equations to extrapolate the effective Higgs potential to high scales. We can conclude from this picture that, if the Higgs mass is large enough, the quartic coupling will blow up entailing some new non-perturbative dynamics or, if the Higgs mass is small enough, the vacuum may be unstable. In summary the Standard Model could be perturbative all the way up to the Planck scale for values of the Higgs mass between 160 GeV and 170 GeV but for all other masses new physics must set in below the Planck scale.

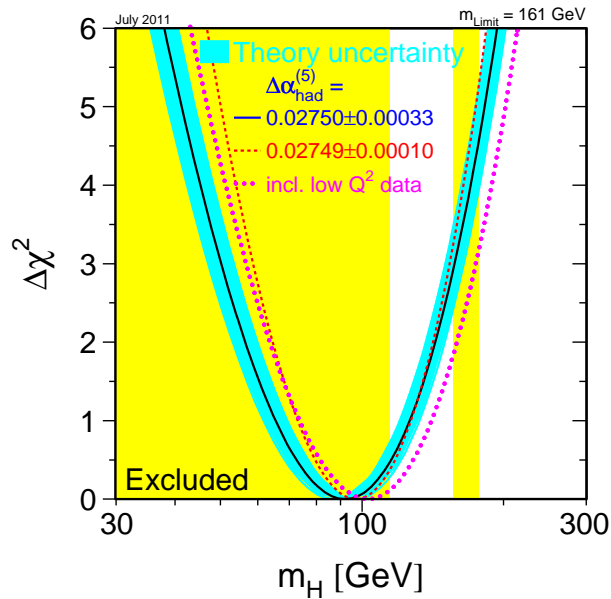


Figure 2.3: The $\Delta\chi^2$ electroweak analysis. The plot is an update of the plot in [25]

2.2.4.3 Unitarity

The amplitude for $WW \rightarrow WW$ scattering is proportional to its centre of mass energy if we do not include the Higgs boson channel. The Higgs boson regulates this unsatisfactory high energy behaviour and prevents unitarity violation. This is because the theory is renormalizable with the Higgs boson. One can derive a bound on the Higgs boson by demanding that unitarity is not violated [24]

$$m_h^2 \leq \frac{4\pi\sqrt{2}}{3G_F} \sim (700 \text{ GeV})^2. \quad (2.53)$$

This a bound from the tree-level amplitude: in the large Higgs mass regime the Higgs self coupling is becoming strong so one cannot reliably ask if the higher order corrections will restore unitarity above this bound. The bound is the highest Higgs boson mass that allows WW scattering to be perturbative at all energies. The LHC can study $WW \rightarrow WW$ up to a centre of mass energy of 1 TeV so unitarity will be violated in this channel if the Higgs, and/or some new strongly interacting sector is not seen.

2.2.5 The Hunt for the Higgs

The theoretical bounds narrow down the m_h search window significantly. Direct experimental searches have failed to find the Higgs boson: these lead to stringent exclusion ranges in the mass range. Furthermore, we can use indirect searches to get an idea of favourable mass ranges from

precision electroweak data. These arise from examining the effect that Higgs boson quantum corrections have on electroweak observables. We show the χ^2 electroweak analysis in Figure 2.3 [25]. If one combines all the present electroweak data (a total of 17 high energy observables) we see that the preferred value of the mass (the minimum of the curve) lies at 92 GeV with an experimental uncertainty of +34 GeV and -26 GeV at the 0.68 confidence level, where the theoretical uncertainty of the blue band is not taken into account, nor the low Q^2 observables. On this plot we can also see the direct search exclusions in the yellow band. These are indicated on the plot but not used in the determination of $\Delta\chi^2$. LEP excluded the Higgs mass up to 114.4 GeV and Tevatron excluded the mass from 156 to 177 GeV. In making these fits one is assuming that the Standard Model is true and we have previously outlined theoretical arguments and experimental hints why this assumption may not be true.

Presently the LHC is reporting some exciting updates to the excluded direct search region. At the 0.95 confidence level, the ATLAS experiment excludes the range 146 to 232, 256 to 282 and 296 to 466 for a Standard Model Higgs [26]. Likewise, CMS excludes the ranges 145 to 216, 226 to 288 and 310 to 340 [27]. The hunt for the Higgs boson at the LHC continues.

2.3 Supersymmetry

2.3.1 Introduction

One of the most popular extensions to the Standard Model of particle physics is the theory of Supersymmetry. The origins of supersymmetry lies in two independent branches. Around 1971 Golfand and Likhtman [28] wrote down an extension of the Poincaré algebra and constructed a version of supersymmetric scalar QED with a charged Dirac spinor and two charged scalars. Subsequently Akulov and Volkov [29] tried to associate the massless fermion that appeared due to spontaneous symmetry breaking with the neutrino. This idea was used in supergravity: a spin 3/2 gravitino becomes massive upon eating this Goldstino. Concurrent to the development of these ideas Wess and Zumino [30] formulated a supersymmetric gauge theory. The roots of this idea came from work in the area of dual resonance models of strong interactions [31, 32, 33]. Although both branches were developed independently they were both theory driven as opposed to data driven; they were not developed to explain experimental evidence. Since then, supersymmetry has become a large area of research but no experimental evidence for its existence has been discovered. It is widely believed that the LHC will either provide evidence to support supersymmetry as a theory or rule it out in most regions of parameter space. Many comprehensive reviews of Supersymmetry exist including [34] and [35].

2.3.1.1 How supersymmetry solves the Hierarchy problem

Although not the original source of the Hierarchy problem one may introduce and motivate supersymmetry by showing that it provides a solution to it. Let's elaborate on the discussion started in Section 1.1.5 by considering the following example [36].

We consider the one-loop corrections to the Higgs mass from a massive fermion. There is

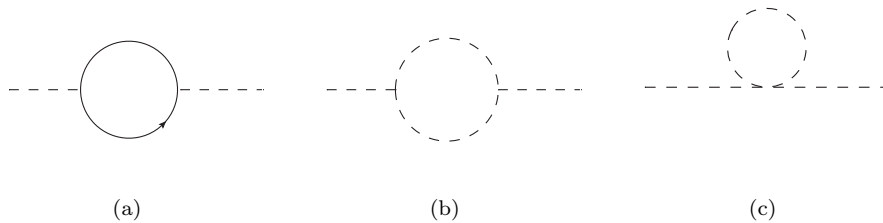


Figure 2.4: Contributions to the Higgs mass correction. The fermionic line is a generic quark of which we have N_f flavours and the internal scalar line is a generic scalar with N_s flavours.

Yukawa type coupling between the massive fermion and the Higgs $\lambda_f = \sqrt{2}m_f/v$. The one loop fermionic contribution, as in Figure 2.4(a), gives the following correction to the Higgs mass:

$$\delta m_h^2 = N_f \frac{\lambda_f^2}{8\pi^2} \left[-\Lambda^2 + 6m_f^2 \log \frac{\Lambda}{m_f} - 2m_f^2 \right] + \mathcal{O}(1/\Lambda^2) \quad (2.54)$$

where N_f is the number of fermions with mass m_f . The mass correction for a scalar particle is driven to the cut-off scale as we discussed in Section 1.1.5 and we have the fine-tuning problem. We assume that in this same theory we have N_s scalars with masses m_s and 3-point and 4-point interactions with the Higgs boson (their couplings are $v\lambda_s$ and λ_s). We can compute the scalar correction to the Higgs mass, as in Figure 2.4(b) and Figure 2.4(c) and obtain

$$\delta m_h^2 = \frac{\lambda_s N_s}{16\pi^2} \left[-\Lambda^2 + 2m_s^2 \log \left(\frac{\Lambda}{m_s} \right) \right] - \frac{\lambda_s^2 N_s}{16\pi^2} v^2 \left[-1 + 2 \log \left(\frac{\Lambda}{m_s} \right) \right] + \mathcal{O} \left(\frac{1}{\Lambda^2} \right). \quad (2.55)$$

The crucial observation is that the dangerous quadratic divergences are present in this result also, but come with the opposite sign to (2.54). If we impose the constraint that

$$\lambda_f^2 = -\lambda_s \quad (2.56)$$

and $N_s = 2N_f$ then we have the total contribution

$$\delta m_h^2 = \frac{\lambda_f^2 N_f}{4\pi^2} \left[(m_f^2 - m_s^2) \log \left(\frac{\Lambda}{m_s} \right) + 3m_f^2 \log \left(\frac{m_s}{m_f} \right) \right] + \mathcal{O} \left(\frac{1}{\Lambda^2} \right). \quad (2.57)$$

Our quadratic divergences can be made to cancel by imposing a symmetry between the two couplings. Therefore our solution to the Hierarchy problem is that for every Standard Model particle we have a supersymmetric partner and we adjust the couplings such that the quadratic divergences are cancelled. The result (2.57) shows us that if the masses of the superpartners are not exactly the same we can have soft-breaking of supersymmetry. We know that supersymmetry must be softly-broken by the mass differences between the Standard Model particles and their superpartners; we have not observed equal mass superpartners. To avoid a reintroduction of fine-tuning problems the mass difference should be small; the new particles should be around the TeV scale. The details of the breaking of supersymmetry are not known, and are not discussed here but comprehensive reviews can be found in the literature (for example

in [35]).

2.3.2 The MSSM Higgs Sector

As we touched upon previously, the choice of the Standard Model Higgs potential is *ad hoc*. We simply chose the simplest representation. The supersymmetric Higgs sector is a two Higgs doublet model. Two constraints on extensions of the minimal Higgs lead us to consider the two Higgs doublet model. The first is the experimental fact the parameter

$$\rho = \frac{m_W^2}{m_Z^2 \cos^2 \theta_W} \quad (2.58)$$

is measured to be very close to 1. The second is that experimentally there are very strong limits on the (non)existence of flavour changing neutral currents (FCNCs). In the minimal Higgs model considered above these are absent. For higher representations of the Higgs one can evade these limits by either pushing up the Higgs masses (to the unacceptably large 1 TeV) so that the tree level FCNCs are suppressed sufficiently or one follows the theorem in [37]. This states that tree-level FCNCs will be absent if all fermions of a given electric charge couple to no more than one Higgs doublet. Therefore, for the MSSM one introduces two Higgs doublets; one couples to up type quarks and the other to down type quarks. This idea is also reinforced because supersymmetry imposes structure on what Higgs multiplets are allowed in the potential. The interactions of Higgs bosons and fermions arise from the superpotential [17]:

$$W_F = w_{ij} \left[f \hat{H}_1^i \hat{L}^j \hat{R} + f_1 \hat{H}_1^i \hat{Q}^j \hat{D} + f_2 \hat{H}_2^j \hat{Q}^i \hat{U} \right]. \quad (2.59)$$

and supersymmetry prevents the inclusion of H_1^* and H_2^* ; the superpotential must be an analytic function of left chiral superfields. The simplest way to think of this is that supersymmetry imposes that the superpotential be an analytic function of the superfields, but the Higgs mechanism wants a term of the form $\phi^\dagger \phi$. Therefore we must introduce two superfields to allow for this type of term.

2.3.2.1 Two Higgs Doublet Model

The next to minimal Higgs sector contains two Higgs doublets which we call ϕ_1, ϕ_2 with hypercharge $Y = 1$. The scalar potential which spontaneously breaks $SU(2)_L \times U(1)_Y$ down

to $U(1)_{em}$ is [17]:

$$\begin{aligned}
 \mathcal{V}(\phi_1, \phi_2) &= \lambda_1(\phi_1^\dagger\phi_1 - v_1^2)^2 + \lambda_2(\phi_2^\dagger\phi_2 - v_2^2)^2 \\
 &+ \lambda_3 \left[(\phi_1^\dagger\phi_1 - v_1^2) + (\phi_2^\dagger\phi_2 - v_2^2) \right]^2 \\
 &+ \lambda_4 \left[(\phi_1^\dagger\phi_1)(\phi_2^\dagger\phi_2) - (\phi_1^\dagger\phi_2)(\phi_2^\dagger\phi_1) \right] \\
 &+ \lambda_5 \left[\text{Re}(\phi_1^\dagger\phi_2) - v_1v_2 \cos \xi \right]^2 \\
 &+ \lambda_6 \left[\text{Im}(\phi_1^\dagger\phi_2) - v_1v_2 \sin \xi \right]^2.
 \end{aligned} \tag{2.60}$$

where the parameters λ_i are real. The minimum of this potential can be written as

$$\langle \phi_1 \rangle = \begin{pmatrix} 0 \\ v_1 \end{pmatrix} \quad \langle \phi_2 \rangle = \begin{pmatrix} 0 \\ v_2 e^{i\xi} \end{pmatrix}. \tag{2.61}$$

Supersymmetry imposes the condition that $\lambda_5 = \lambda_6$ and therefore can redefine one of the fields by rotating away the phase ξ . Thus our vacuum expectation values for the potential can be chosen to be real and positive. Therefore, from here on we set $\xi = 0$. This is the most general CP-invariant two-Higgs doublet model.

2.3.2.2 Higgs Potential in the MSSM

We carry out the same analysis as in the Standard Model case except we start from the vector boson kinetic term where now g_1, g_2 are the $SU(2), U(1)$ gauge couplings. :

$$D_\mu \mathcal{H}_1 = \left(\partial_\mu + ig_1 T \cdot W_\mu + i\frac{g_2}{2} B_\mu \right) \mathcal{H}_1 \tag{2.62}$$

$$D_\mu \mathcal{H}_2 = \left(\partial_\mu - ig_1 T^* \cdot W_\mu - i\frac{g_2}{2} B_\mu \right) \mathcal{H}_2. \tag{2.63}$$

We now have two vevs which modify our gauge boson mass relations as:

$$m_W^2 = \frac{g_2^2}{2}(v_1^2 + v_2^2) \tag{2.64}$$

$$m_Z^2 = \frac{g_1^2 + g_2^2}{2}(v_1^2 + v_2^2). \tag{2.65}$$

The new vevs are related to the Standard Model one by the relation:

$$v = \sqrt{v_1^2 + v_2^2}. \tag{2.66}$$

The Higgs potential is [38]

$$\mathcal{V} = m_1^2 |\mathcal{H}_1|^2 + m_2^2 |\mathcal{H}_2|^2 - m_{12}^2 (\epsilon_{ab} \mathcal{H}_1^a \mathcal{H}_2^b + \text{h.c.}) \tag{2.67}$$

$$+ \frac{1}{8}(g_1^2 + g_2^2) [|\mathcal{H}_1|^2 - |\mathcal{H}_2|^2]^2 + \frac{1}{2}g_2^2 |\mathcal{H}_1^\dagger \mathcal{H}_2|^2 \tag{2.68}$$

where m_1, m_2, m_{12} are soft SUSY breaking parameters. We rewrite this in terms of component fields, where the decomposition is

$$\mathcal{H}_1 = \begin{pmatrix} \mathcal{H}_1^0 \\ \mathcal{H}_1^- \end{pmatrix} = \begin{pmatrix} v_1 + \frac{1}{\sqrt{2}}(\phi_1^0 + i\chi_1^0) \\ -\phi_1^- \end{pmatrix} \quad (2.69)$$

$$\mathcal{H}_2 = \begin{pmatrix} \mathcal{H}_2^+ \\ \mathcal{H}_2^0 \end{pmatrix} = \begin{pmatrix} \phi_2^+ \\ v_2 + \frac{1}{\sqrt{2}}(\phi_2^0 + i\chi_2^0) \end{pmatrix}. \quad (2.70)$$

Both Higgs doublets develop a vev. We can use the $SU(2)_L$ symmetry to rotate the vev of $\langle \mathcal{H}_1 \rangle = v_1$ to its upper component and likewise $\langle \mathcal{H}_2 \rangle = v_2$ to its lower component. The vevs are neutral forcing $\langle \phi_1^- \rangle = 0$ and $\langle \phi_2^+ \rangle = 0$. Furthermore, the Higgs potential has been constructed to be CP-invariant therefore the ϕ and χ fields decouple. Also, conservation of electric charge on its own forbids mixing between the charged scalars and the neutral scalars.

Minimizing the potential, and evaluating it at the above vevs gives the following constraints

$$m_1^2 = -m_{12} \tan \beta + \frac{1}{4}(g_1 + g_2)(v_2^2 - v_1^2) \quad (2.71)$$

$$m_2^2 = -m_{12} \tan \beta + \frac{1}{4}(g_1 + g_2)(v_1^2 - v_2^2).$$

where we have defined the useful parameter:

$$\tan \beta = \frac{v_2}{v_1}. \quad (2.72)$$

Therefore, one expects that large $\tan \beta$ gives an enhancement to up-type quark couplings and, conversely small $\tan \beta$ enhances down-type quark couplings. We use the relations (2.71) to extract the physical particles from the potential. The physical masses are

$$m_A^2 = -m_{12}(\cot \beta + \tan \beta) \quad (2.73)$$

$$m_G^0 = 0 \quad (2.74)$$

$$m_{H,h} = \frac{1}{2} \left[(m_A^2 + m_Z^2) \pm \sqrt{(m_A^2 + m_Z^2)^2 - 4m_A^2 m_Z^2 \cos^2 2\beta} \right] \quad (2.75)$$

$$m_H^\pm = -m_{12}(\cot \beta + \tan \beta) + m_W^2 \quad (2.76)$$

$$m_G^\pm = 0 \quad (2.77)$$

and are obtained by rotating the gauge eigenstates using the following representation:

$$\begin{pmatrix} H \\ h \end{pmatrix} = \begin{pmatrix} \cos \alpha & \sin \alpha \\ -\sin \alpha & \cos \alpha \end{pmatrix} \begin{pmatrix} \phi_1^0 \\ \phi_2^0 \end{pmatrix} \quad (2.78)$$

$$\begin{pmatrix} G^0 \\ A^0 \end{pmatrix} = \begin{pmatrix} \cos \beta & \sin \beta \\ -\sin \beta & \cos \beta \end{pmatrix} \begin{pmatrix} \chi_1^0 \\ \chi_2^0 \end{pmatrix} \quad (2.79)$$

$$\begin{pmatrix} G^\pm \\ H^\pm \end{pmatrix} = \begin{pmatrix} \cos \beta & \sin \beta \\ -\sin \beta & \cos \beta \end{pmatrix} \begin{pmatrix} \phi_1^\pm \\ \phi_2^\pm \end{pmatrix} \quad (2.80)$$

where

$$\tan \alpha = \frac{-(m_A^2 + m_Z^2) \sin \beta \cos \beta}{m_Z^2 \cos^2 \beta + m_A^2 \sin^2 \beta - m_h^2}, \quad -\frac{\pi}{2} < \alpha < 0. \quad (2.81)$$

To summarize we have the following Higgs spectrum:

- h, H : 2 neutral CP even bosons
- A : 1 neutral CP odd boson
- H^\pm : 2 charged bosons
- G^0, G^+, G^- : 3 unphysical Goldstone bosons.

For certain regions of parameter space, α and β can enhance the couplings of the charged Higgs bosons to quarks. This could have new phenomenological consequences.

We are now in a position to piece together the mass spectrum; we expect $m_H^\pm \geq m_W$, $m_H \geq m_Z$, $m_A \geq m_h$. The lowest mass neutral Higgs is the h boson. There is interesting result in the limit of $m_A^2 > m_Z^2$, at fixed $\tan \beta$: we have the constraint

$$m_h^2 \leq m_Z^2 \cos^2 2\beta. \quad (2.82)$$

and the interactions of h are equivalent to the interactions of the Standard Model Higgs [17]. So in this case we have a very strict upper bound where we expect a SM-like Higgs to be lighter than the Higgs boson. Direct experimental searches at LEP2 for such a SM-like Higgs completely rule out this mass range. The MSSM is saved by including radiative corrections which push the expected mass up. One can conclude that, when looking at the MSSM electroweak breaking sector, including one-loop corrections is necessary to avoid experimental constraints.

2.3.3 Sfermion Sector

We analyse the mixing in the Squark sector. Because in high energy physics the light quark masses can be taken to be massless a usual approximation to take is that only the superpartners of the top quark (the stop) mix but the squarks corresponding to the light quarks do not. This is because the mixing matrix has a dependence on the mass of the quark. The squark mass matrix is written as [38, 39]:

$$\mathcal{L}_m = -\frac{1}{2}(\tilde{f}_L^\dagger, \tilde{f}_R^\dagger) Z \begin{pmatrix} \tilde{f}_L \\ \tilde{f}_R \end{pmatrix} \quad (2.83)$$

where

$$Z = \begin{pmatrix} M_{\tilde{f}}^{LL} + m_{\tilde{f}}^2 & m_f (M_f^{LR})^* \\ m_f M_f^{LR} & M_{\tilde{f}}^{RR} + m_{\tilde{f}}^2 \end{pmatrix} \quad (2.84)$$

where

$$M_f^{LL} = m_Z^2 (I_3^f - Q_f \sin \theta_w) \cos 2\beta + \begin{cases} M_Q^2 & \text{for left handed squarks} \\ M_L^2 & \text{for left handed sleptons} \end{cases} \quad (2.85)$$

$$M_f^{LR} = A_f - \mu^* \begin{cases} \cot \beta & \text{for } u\text{-type sfermions} \\ \tan \beta & \text{for } d\text{-type sfermions} \end{cases} \quad (2.86)$$

$$M_f^{RR} = m_Z^2 (Q_f \sin^2 \theta_w) \cos 2\beta + \begin{cases} M_U^2 & \text{for right handed } u\text{-type squarks} \\ M_D^2 & \text{for right handed } d\text{-type squarks} \\ M_L^2 & \text{for right handed sleptons} \end{cases} \quad (2.87)$$

The parameters A_f are the entries in the Yukawa matrix in the superpotential and are present in the couplings between sfermions and Higgs bosons. The parameter μ is also present in our superpotential. We diagonalize this matrix to obtain the physical mass eigenstates via the unitary matrix S :

$$S^f Z S^{f\dagger} = \begin{pmatrix} m_{\tilde{f}_1}^2 & 0 \\ 0 & m_{\tilde{f}_2}^2 \end{pmatrix}. \quad (2.88)$$

and the masses are

$$m_{\tilde{f}}^2 = m_f^2 + \frac{1}{2} \left(M_f^{LL} + M_f^{RR} \mp \sqrt{(M_f^{LL} - M_f^{RR})^2 + 4m_f^2 |M_f^{LR}|^2} \right). \quad (2.89)$$

2.3.4 Neutralino Sector

Supersymmetry adds an extra layer of complexity to the electroweak sector. In the MSSM the 4 physical Higgs bosons have fermionic superpartners called Higgsinos and the electroweak gauge bosons have fermionic partners also, namely the wino, zino and photino. Due to electroweak symmetry breaking, in analogy to the mixing of the B and W^3 bosons in the Standard Model, any particle with the same charge, color and spin will mix. So the physical states of this sector are two Charginos (a mixing of the charged Higgs and winos) and 4 Neutralinos (a mixing of the neutral Higgsinos and the zino and photino). Here we look at the mixing of the Neutralino sector in detail in order to clarify the parameters that enter our result.

There are three sources of mass terms in this sector [40]. Firstly, we have quadratic terms in the superpotential W that, when the derivative is taken, give bilinear terms. Secondly, electroweak symmetry breaking gives mass terms to the gauginos when the Higgs bosons acquire a vev (in analogy to the Standard Model case). Finally, there are soft supersymmetry breaking gaugino masses.

We write the fermionic superpartners, in what is known as the Wino-Bino-Higgsino basis, as

$$\psi_j^0 = \left(\tilde{B}^0, \tilde{W}^0, \tilde{H}_2^0, \tilde{H}_1^0 \right). \quad (2.90)$$

Explicitly, all the contributions mentioned above, give the mass term in this basis as [17] :

$$\mathcal{L}_m = -\frac{1}{2}(\psi^0)^T Y \psi^0 + \text{h.c.} \quad (2.91)$$

where Y is in general a complex symmetric matrix given by

$$Y = \begin{pmatrix} M_1 & 0 & -m_Z \sin \theta_W \cos \beta & m_Z \sin \theta_w \sin \beta \\ 0 & M_2 & m_Z \cos \theta_W \cos \beta & -m_Z \cos \theta_w \sin \beta \\ -m_Z \sin \theta_W \cos \beta & m_Z \cos \theta_W \cos \beta & 0 & -\mu \\ m_Z \sin \theta_W \sin \beta & -m_Z \cos \theta_W \sin \beta & -\mu & 0 \end{pmatrix} \quad (2.92)$$

with M_1 the Majorana mass term for the bino, M_2 is the Majorana mass term for the wino. All the other parameters have been defined previously. We define the two component mass eigenstates as

$$\chi_i^0 = N_{ij} \psi_j^0 \quad (2.93)$$

where i, j run from 1 to 4. N is a unitary matrix that diagonalises the mass matrix Y :

$$N^* Y N^{-1} = N_D. \quad (2.94)$$

One can choose N such that the components of N_D are real and non-negative. We can then write our physical, 4-component, Majorana fermions as

$$\tilde{\chi}_i^0 = \begin{pmatrix} \chi_i^0 \\ \bar{\chi}_i \end{pmatrix} \quad (2.95)$$

where again, i runs from 1 to 4.

It is sometimes useful to use the photino, zino, higgsino basis i.e.

$$\psi_j^{\prime 0} = \left(\tilde{A}^0, \tilde{Z}^0, \tilde{H}_2^0, \tilde{H}_1^0 \right) \quad (2.96)$$

and $\chi_i^0 = N'_{ij} \psi_j^{\prime 0}$. We can relate the two mixing matrices by

$$N_{i1} = \cos \theta_w N'_{i1} - \sin \theta_w N'_{i2} \quad (2.97)$$

$$N_{i2} = \sin \theta_w N'_{i1} + \cos \theta_w N'_{i2} \quad (2.98)$$

$$N_{i3} = N'_{i3} \quad (2.99)$$

$$N_{i4} = N'_{i4}. \quad (2.100)$$

i.e. the wino and bino components of the mixing matrices mix in the same manner as the W^3, B gauge bosons.

The diagonalisation of the matrix Y can be computed analytically but it is simple, for a

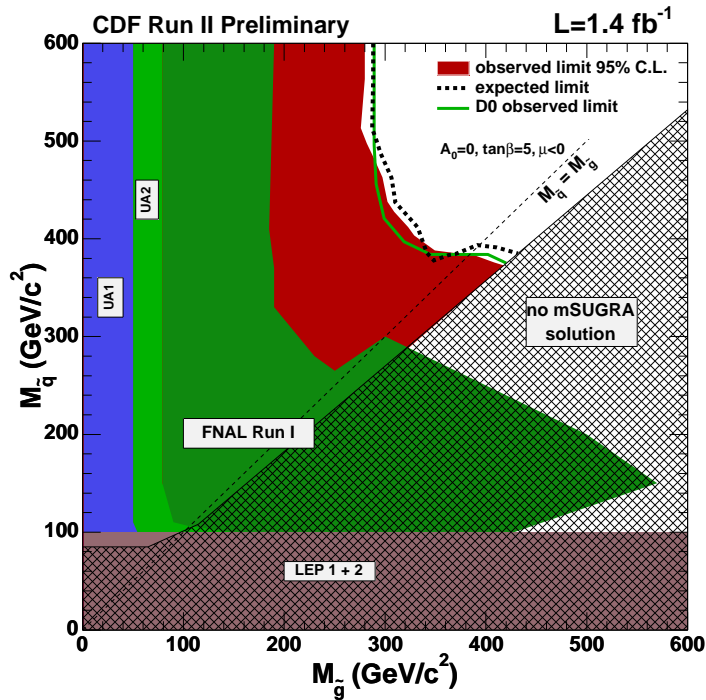


Figure 2.5: A plot of the excluded region in the mSUGRA breaking scenario [43] .

given point in parameter space, to compute it numerically.

2.3.5 The Search for Supersymmetry

The search for supersymmetry is entering a critical stage, as new data from the LHC is analyzed. In analogy to the search for the Higgs boson, one could expect deviations from the Standard Model in low energy experiments that could point towards new physics. Obviously we want to establish what this new physics is so we need a collider with energy at or beyond the energy scale of the new physics. In this section we highlight the status of experimental searches for supersymmetry through both the direct and indirect searches.

Due to the vast number of parameters present in the MSSM it is useful to introduce certain benchmark points for experimental and theoretical comparison. These are based on specific SUSY breaking scenarios [41]. The experimental strategy is to search for generic SUSY signatures and then, from the determined couplings and masses, determine the nature of supersymmetry breaking. A review of these search strategies can be found in [42].

2.3.5.1 Direct Searches

The lack of any direct evidence for super partners has led to lower bounds on their masses, however, these negative results are often model dependent. An example of such a result can be found in [43] and we present it in Figure 2.5. They look at a very generic SUSY signature, that

of large missing transverse energy and multiple jets. One can look at this search channel in the context of the mSUGRA (minimal supergravity) scenario where supersymmetry breaking is mediated by gravitation interactions, thus, reducing the SUSY parameter space to only 5 parameters : the common scalar mass m_0 , the common gaugino mass $m_{1/2}$, the common soft trilinear SUSY breaking parameters A_0 , the ratio of the Higgs vevs $\tan\beta$ and the sign of the Higgsino mass term μ . In this analysis mSUGRA parameters are chosen to be $A_0 = 0$, $\tan\beta = 5$ and $\mu < 0$. Then there are two parameters to vary (m_0 and $m_{1/2}$). The gluino and squark masses are a function of these two free parameters and shown in the plot are 95% C.L. exclusion regions.

More recent results from the LHC have also shown negative results in the search for superpartners. As of writing, the ATLAS [44] and CMS collaboration [45] have released similar plots to the previous one. The ATLAS result is shown in Figure 2.6. This plot contains a lot of information, and again, it is model dependent. What is interesting about this plot, is the difference between the exclusion regions between 2010 and 2011. At this rate supersymmetry, if it exists, should be in the reach of the LHC within the next year. The collaboration exclude gluino masses below 500 GeV at the 95 % confidence level for these given parameter points.

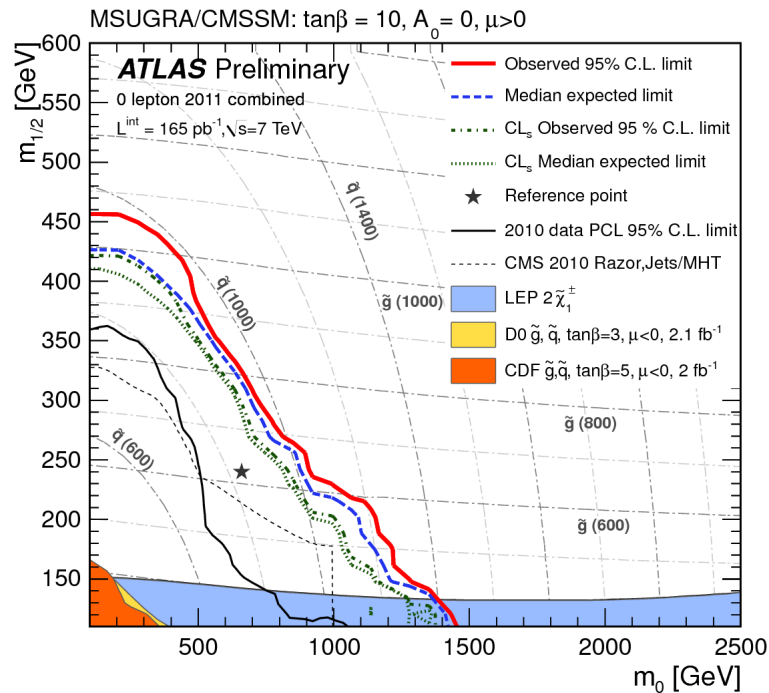


Figure 2.6: A plot of the excluded region in the mSUGRA/CMSSM breaking scenario at the LHC [44] .

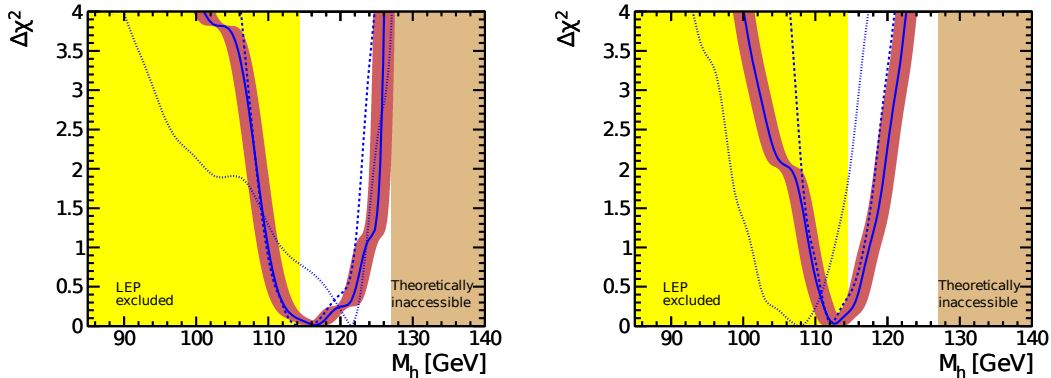


Figure 2.7: The χ^2 plots for m_h in two SUSY breaking scenarios [46]. On the left hand side we have the CMSSM breaking scenario and on the right the NUHM1 model. The dotted lines have not included any LHC data, the dashed lines include CMS data and the solid lines include ATLAS data.

2.3.5.2 Indirect Searches

As we discussed earlier, new physics can have an effect on electroweak observables through new particles entering internal loops. Therefore, one can look at the effect that SUSY can have on our Higgs mass plot Figure 2.3. The direct search limit for a Standard Model Higgs at LEP, 114.4 GeV, and the mass preferred by the electroweak observables is 92 GeV. We show how this plot changes for two specific SUSY breaking scenarios (these plots are presented in [46]) in Figure 2.7. The scenarios we consider are firstly the CMSSM, where the soft-SUSY breaking parameters are assumed to be universal at the GUT scale. This has four input parameters: the universal soft-SUSY breaking parameter m_0 and $m_{1/2}$, a universal trilinear soft-SUSY breaking parameter A_0 , $\tan\beta$ and the sign of μ . We also consider the NUMH1 parameter set where we have one additional parameter which is the soft-SUSY breaking contribution to the masses of the Higgs doublets. The results show that, for the NUMH1 parameter set, the electroweak observable preferred value is actually increased above the direct search limit (for these parameters the LEP direct search limit is modified slightly because the hZZ coupling can be reduced). However, for the CMSSM this direct search limit at LEP is the same as the Standard Model limit and we see that the preferred value is pushed up from the Standard Model case. The tension between the LEP bound and the preferred mass of the Higgs is alleviated, in the SUSY models considered.

Chapter 3

Details of Next to Leading Order Calculations

Over the past few years there has been great progress in the calculation of Next to Leading Order (NLO) corrections to many physical processes for the LHC and also in the development of tools required for their calculation. A recent review of the state of the art is given in [47]. In this chapter we describe the key ingredients of a NLO calculation then go on to describe the technical details involved in our calculation.

3.1 Set up of Calculation

Leading order results suffer from strong dependence on the scales that enter due to the truncation of the perturbative series. Typically, a leading order result will point to the order of magnitude of a cross section and to make a more predictive statement one needs to calculate higher order corrections. We concentrate on the next order in perturbation theory. This includes corrections where a particle is emitted and re-absorbed (virtual) and ones where the particle is not re-absorbed (real). A sample diagram for the process $e^-e^+ \rightarrow 2$ jets at NLO (is shown in Figure 3.1. The results for each component of a generic process can be divergent individually.

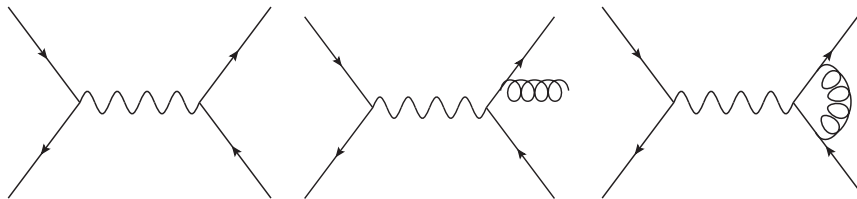


Figure 3.1: From left to right: the born, real correction and virtual correction to the process $e^-e^+ \rightarrow 2$ jets at NLO.

Specifically, one divergence is of ultraviolet nature in the virtual part from the loop integral.

One needs to specify a renormalization procedure in order to obtain a finite (in the ultraviolet region) result.

Once renormalization has been performed other divergences remain. One has infrared divergences coming from the virtual loop integral (present in the renormalised virtual matrix element) and infrared divergences coming from the integral over the soft and collinear region in the phase space of the real emission contribution. These two divergences are expected to cancel between the real and virtual part of the calculation [48, 49, 50] for an inclusive enough observable.

There is a problem in performing a numerical evaluation of the cross section due to the mismatch in the number of particles in the phase space. The crucial point is that the infrared divergences in the renormalized virtual matrix element are explicit in the matrix element and are thus *global* with respect to the phase space; the divergences of the real emission graphs are *local* as they are implicit in the phase space integral. A naïve numerical setup will not incorporate this cancellation.

We follow the strategy of [51] where a *local* counterterm is subtracted from the real emission part before the phase space integral is performed. This same counterterm is then added back after the extra one body phase space integral is performed (in order to match the phase space between the virtual part and the counterterm). Schematically, this looks like

$$d\sigma_{\text{NLO}} = \int_{n+1} [(d\sigma^R)_{\epsilon=0} - (d\sigma^A)_{\epsilon=0}] + \int_n \left[d\sigma^V + \int_1 d\sigma^A \right]_{\epsilon=0}. \quad (3.1)$$

where R stands for the real emission piece, V for the virtual part and A for the local counterterm. Based on the observation that the matrix element factorizes in the soft-collinear region one is able to write down a process independent algorithm for calculating the counter term and the integral of the counter term. This is known as “dipole subtraction” [51]. We adopt this strategy for the real radiation terms in our calculation.

3.2 Hadronic Observables and Scale Dependence at Next to Leading Order

The matrix element for a given process is a function of the relevant initial state and final state configuration: in color, momenta, helicity and polarisations. Once the matrix element squared has been calculated at a given order one needs to integrate over all the possible final states and normalise by the initial state. This means we average (sum) over the initial (final) state discrete variables (polarisations/color/helicities) and for the momenta we divide by the incoming “flux” factor and integrate over the final-state phase space. Thus we arrive at the partonic cross section for 2 pointlike incoming particles for a $2 \rightarrow n$ process:

$$\hat{\sigma}_{ab}(p_a, p_b) = \frac{1}{2\hat{s}_{ab}} \int d\Phi_n |\overline{\mathcal{M}}_{ab}|^2 \quad (3.2)$$

where $\hat{s}_{ab} = (p_a + p_b)^2$ is the partonic centre of mass energy, $d\Phi_n$ is the n-body phase space and \mathcal{M}_{ab} is the matrix element for the partonic process.

We are interested in the hadronic equivalent for LHC processes. We must convolve this partonic cross section with two parton distribution functions (pdfs) and for a given hadronic process sum over all possible initial partonic states present in the pdf. The hadronic cross section is therefore [18]:

$$\sigma = \sum_{a,b} \int dx_a dx_b f_{a/A}(x_a, \mu_F^2) f_{b/B}(x_b, \mu_F^2) \hat{\sigma}_{ab}(x_a P_A, x_b P_B, \mu_F^2, \alpha_s(\mu_R^2)). \quad (3.3)$$

where each parton takes a fraction of the incoming hadronic momenta $p_a = x_a P_a$. We must pick a scale (the factorisation scale μ_F) that splits the process in two: the high energy hard scattering event and the low energy non-perturbative physics that we include in the pdf. If we were to include all orders in perturbation theory the dependence on this scale would vanish from our cross section. However, we calculate at NLO therefore we expect to see some residual scale dependence in our result; by truncating our series we lose predictive power.

We expect scale dependence from another source: the running of α_s . Asymptotic freedom ensures that the expansion of the hard subprocess as a perturbation series in α_s is a good approximation at high energies because our expansion parameter is small. If we truncate this series we also expect a dependence on the renormalization scale to be present in our result.

3.3 Color

When calculating a QCD amplitude the color algebra can be factorised from the rest of the structure. In this section we outline how we treat this and give a couple of examples of how it is used.

The strong force is described by QCD, a gauge theory of $SU(3)$, where the force carrier (the gluon) lies in the adjoint representation and the matter particles (quarks) lie in the fundamental representation. For this section we generalise to $SU(N_c)$ where N_c is the number of colors. The Lie algebra of $SU(N_c)$ is written as

$$[T^A, T^B] = if^{ABC} T^C. \quad (3.4)$$

We let T^A stand for the generators in the fundamental representation and the generators in the adjoint representation are written in terms of the structure constants f^{ABC} . Firstly we normalise our generators:

$$\text{tr}\{T^A T^B\} = T_R \delta^{AB} \quad (3.5)$$

where we make the choice of convention $T_R = 1/2$. We label the two representations with the Casimirs C_A and C_F such that:

$$T_{ik}^A T_{kj}^A = C_F \delta_{ij} \quad (3.6)$$

$$f^{XYA} f^{XYB} = C_A \delta^{AB} \quad (3.7)$$

where $C_A = N_c$ and $C_F = (N_c^2 - 1)/2N_c$ and the summation convention is applied. For $SU(3)$ these values are

$$C_F = \frac{4}{3} \quad C_A = N_c = 3. \quad (3.8)$$

In order to calculate color-factors of diagrams in QCD one can use diagrammatic methods as outlined in [52]. We outline the ‘‘Feynman rules’’ for constructing the color factors in Figure 3.2.

3.3.1 Color Basis

A QCD amplitude will have a colour structure that we wish to strip off so we can write them as

$$\mathcal{M} = \sum_i A_i |c_i\rangle. \quad (3.9)$$

The vectors $|c_i\rangle$ make up our *color basis* and the coefficients of this decomposition, A_i , are known as *partial amplitudes*, which are smaller gauge invariant pieces of our amplitude. There are several ways of completing this decomposition and some are more suited to certain processes [53]. We choose to decompose our amplitudes by using the generators of $SU(N_c)$ as fundamental objects. Therefore our basis will be written in terms of the objects $\{T^A, \delta^{ij}\}$.

The color basis is, in general, not orthogonal therefore we need to calculate the *color-correlation* matrices. This is straightforward; only a certain number of rules are required to calculate this. Arriving at our color factor is a two step process:

1. All structure constants (f^{ABC}) are converted to fundamental generators of $SU(N_c)$ (T^A).
2. Fundamental generators (T^A) can be written in terms of the Kronecker deltas (δ_{ij}).

We now outline the two steps.

3.3.1.1 Step 1

This step can be achieved by inverting the commutation relations. We have the following formulae: the first for when we have a contraction with one generator, the second for when we have no contractions:

$$f^{ABC} T_{ij}^C = -i (T_{ik}^A T_{kj}^B - T_{ik}^B T_{kj}^A) \quad (3.10)$$

$$f^{ABC} = -\frac{i}{T_R} (T_{ij}^A T_{jk}^B T_{ki}^C - T_{ij}^C T_{jk}^B T_{ki}^A). \quad (3.11)$$

We draw the graphical representation of these relations in Figure 3.3 and Figure 3.4.

3.3.1.2 Step 2

All contractions of the generators can be simplified by either using the Fierz-identity:

$$T_{ij}^A T_{kl}^A = T_R \left(\delta_{il} \delta_{kj} - \frac{1}{N_c} \delta_{ij} \delta_{kl} \right). \quad (3.12)$$

or the traceless condition on the generator:

$$\text{tr}\{T^A\} = 0. \quad (3.13)$$

The Fierz identity is drawn in Figure 3.5.

Certain combinations of coefficients can be eliminated by constructing new rules from the above ones. These optional identities are:

$$f^{AXY} f^{BYX} = -2N_c \text{tr}\{T^A T^B\} \quad (3.14)$$

$$f^{AXY} f^{BYZ} f^{CZX} = f^{ABC} T_R N_c \quad (3.15)$$

$$T_{ij}^A T_{jk}^B f^{ABC} = iT_R N_c T_{ik}^C \quad (3.16)$$

$$T_{ij}^A T_{jk}^B T_{kl}^A = -\frac{T_R}{N_c} T_{il}^B. \quad (3.17)$$

The identity (3.14) is simply a rewriting of the usual sum over structure constants (3.7). The second identity here (3.15) can be shown by first eliminating f by applying (3.11) and repeatedly applying (3.12) and (3.13) to arrive at our result. The cyclic property of the trace must also be used. Identity (3.16) can be shown by rewriting the two T generators in terms of symmetric and anti-symmetric tensors and using the relation $f^{AXY} f^{BXY} = N_c \delta^{AB}$. The identity (3.17) can be shown by applying (3.12) and (3.13). We write down the graphical representation of (3.15) in Figure 3.7 and (3.16) in Figure 3.8.

3.3.2 Color Insertion Operators

We define the following notation of color insertion operators:

$$\langle c' | \mathbf{T}_\alpha | c \rangle \quad (3.18)$$

where α stands for the parton in the color basis. If the parton is a quark then \mathbf{T} is a fundamental generator T^A , if the parton is an anti-quark then it is $-T^A$. If the parton is a gluon then \mathbf{T} is f^{ABC} . We now show explicit examples for this.

3.3.3 Example: Neutralino Pair Production

For the process $q\bar{q} \rightarrow \chi^0 \chi^0$ the color structure is simple due to the final state (the Neutralinos) being colorless. Therefore it is sufficient to define only one color vector. We choose the following

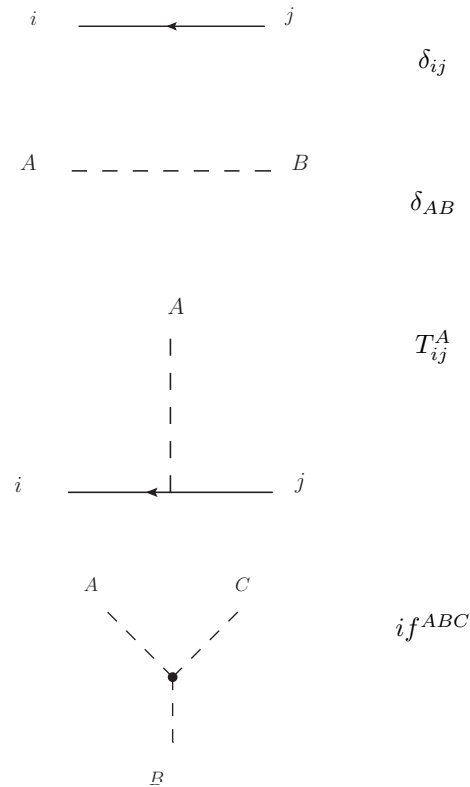


Figure 3.2: Feynman rules for the computation of color factors in the gauge group $SU(N_c)$. The dashed line is the adjoint representation, the arrowed line is the fundamental representation. All tensors are denoted as vertices: the generators in the adjoint representation (the structure constants of the Lie Algebra) are orientated such that the indices are read in counter clockwise fashion. If two legs are swapped one obtains a minus sign.

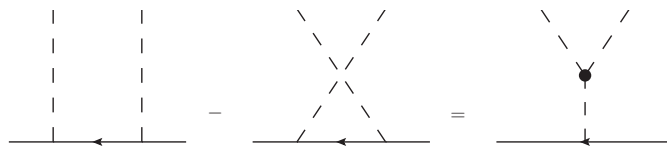


Figure 3.3: Diagrammatic representation of the inversion of the Lie algebra (3.10).

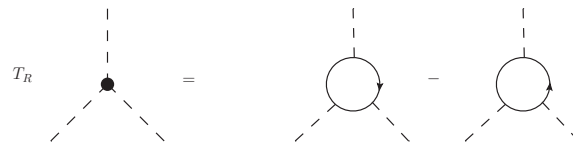


Figure 3.4: Diagrammatic representation of identity of the Lie algebra (3.11).

$$\text{Diagram} = T_R \left(\text{Diagram}_1 - \frac{1}{N_c} \text{Diagram}_2 \right)$$

Figure 3.5: Diagrammatic representation of the Fierz identity (3.12).

$$\begin{aligned} \text{Dashed line} \text{---} \text{Solid Circle} \text{---} \text{Dashed line} &= T_R \text{---} \text{Dashed line} \\ \text{Solid line} \text{---} \text{Dashed Semi-circle} \text{---} \text{Solid line} &= C_F \text{---} \text{Solid line} \\ \text{Dashed line} \text{---} \text{Dashed Circle} \text{---} \text{Dashed line} &= C_A \text{---} \text{Dashed line} \end{aligned}$$

Figure 3.6: The Casimirs written in diagrammatic form.

$$\text{Diagram}_1 = T_R N_c \text{Diagram}_2$$

Figure 3.7: Diagrammatic representation of identity (3.15).

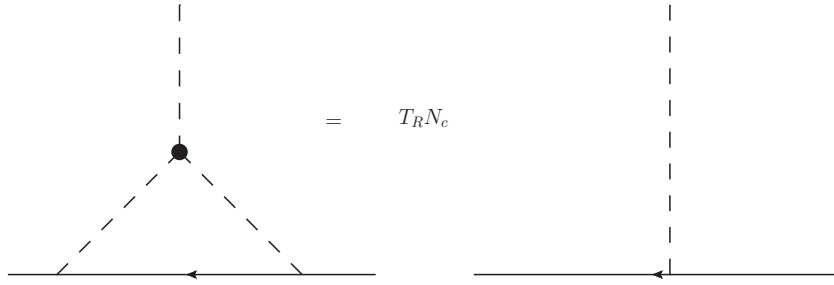


Figure 3.8: Diagrammatic representation of identity (3.16).

color basis:

$$|1\rangle = \delta_{j_2}^{i_1}. \quad (3.19)$$

We label the incoming quark with i_1 and the outgoing anti-quark as j_2 . The heights of the indices denote the “color flow” and the labelling of the color operators follows the numbering of these indices. We can insert a gluon on either the quark or anti-quark. We can use gauge-invariance to write

$$(\mathbf{T}_1 + \mathbf{T}_2)|1\rangle = 0. \quad (3.20)$$

Therefore we can write all the color structures in terms of the Casimirs C_F :

$$\mathbf{T}_1 \cdot \mathbf{T}_2|1\rangle = -\mathbf{T}_1^2|1\rangle = -C_F|1\rangle \quad (3.21)$$

$$\mathbf{T}_1^2|1\rangle = C_F|1\rangle \quad (3.22)$$

$$\mathbf{T}_2^2|1\rangle = C_F|1\rangle. \quad (3.23)$$

Our color correlation “matrix” is simply

$$\langle 1|1\rangle = N_c. \quad (3.24)$$

3.3.4 Example: Neutralino Pair Production plus One Jet

For the process $q\bar{q} \rightarrow g\chi\chi$ the color structure is less trivial than the previous case due to the gluon in the final state. However, as we have only three partons, we can actually write the color algebra in terms of the Casimir operators.

We choose the color “basis” as

$$|1\rangle = T^{A_3}_{j_2}{}^{i_1}. \quad (3.25)$$

Color conservation gives us the following results:

$$\mathbf{T}_2 \cdot \mathbf{T}_3 |1\rangle = \frac{1}{2} [\mathbf{T}_1^2 - \mathbf{T}_2^2 - \mathbf{T}_3^2] |1\rangle \quad (3.26)$$

$$\mathbf{T}_1 \cdot \mathbf{T}_3 |1\rangle = \frac{1}{2} [\mathbf{T}_2^2 - \mathbf{T}_1^2 - \mathbf{T}_3^2] |1\rangle \quad (3.27)$$

$$\mathbf{T}_1 \cdot \mathbf{T}_2 |1\rangle = \frac{1}{2} [\mathbf{T}_3^2 - \mathbf{T}_1^2 - \mathbf{T}_2^2] |1\rangle \quad (3.28)$$

where

$$\mathbf{T}_1^2 |1\rangle = \mathbf{T}_2^2 |1\rangle = C_F |1\rangle \quad (3.29)$$

$$\mathbf{T}_3^2 |1\rangle = C_A |1\rangle = N_c |1\rangle. \quad (3.30)$$

Our color-correlation operators give:

$$\mathbf{T}_1 \cdot \mathbf{T}_3 |1\rangle = \mathbf{T}_2 \cdot \mathbf{T}_3 |1\rangle = -\frac{C_A}{2} |1\rangle \quad (3.31)$$

$$\mathbf{T}_1 \cdot \mathbf{T}_2 |1\rangle = \frac{1}{2N_c} |1\rangle, \quad (3.32)$$

and also

$$\langle 1|1\rangle = C_F N_c. \quad (3.33)$$

3.4 Spinor Helicity Formalism

3.4.1 Definitions

The spinor helicity method was introduced in [54] for massless particles in cross-section calculations. The method is based on two principles: firstly, that one can decompose amplitudes into smaller gauge-invariant pieces and secondly, that these pieces can be written as functions of more fundamental “spinor products” as opposed to Lorentz scalar products of momentum. The final results one arrives at for the amplitudes tend to be more compact and can therefore lead to fast and numerically stable code.

We consider the spinors $u(p)$ and $v(p)$ the solutions to the Dirac equation

$$(\not{p} - m)u(p) = 0 \quad (3.34)$$

$$(\not{p} + m)v(p) = 0. \quad (3.35)$$

We define the usual chirality projection operators $\Pi_- = \frac{1}{2}(\mathbb{I} - \gamma_5)$ and $\Pi_+ = \frac{1}{2}(\mathbb{I} + \gamma_5)$ where \mathbb{I} is the identity matrix in spinor space. In the massless limit the positive and negative energy solutions of the massless four dimensional Dirac equation are identical up to normalisation conventions. We can choose them to be equal to one another. The helicity eigenstates of massless spinors are denoted by

$$\Pi_+ u(k_i) = \Pi_+ v(k_i) = |i\rangle \quad (3.36)$$

$$\Pi_- u(k_i) = \Pi_- v(k_i) = |i] \quad (3.37)$$

$$\bar{u}(k_i)\Pi_- = \bar{v}(k_i)\Pi_- = [i| \quad (3.38)$$

$$\bar{u}(k_i)\Pi_+ = \bar{v}(k_i)\Pi_+ = \langle i| \quad (3.39)$$

where for negative energy solutions, the helicity is the negative of the chirality (or γ_5) eigenvalue i.e.

$$v_{\mp}(p) = \frac{1}{2}(1 \pm \gamma_5)v(p) \quad (3.40)$$

$$u_{\pm}(p) = \frac{1}{2}(1 \pm \gamma_5)u(p). \quad (3.41)$$

Physically, helicity is the dot product of the spin vector and the momentum. This is a well defined quantity for massless particles as one cannot Lorentz boost to a frame that overtakes the particle. Therefore to all observers the particle has the same helicity. Chirality, is the mathematical abstraction of this idea for massive particles. Helicity is no longer constant for massive particles but the chirality is a well defined concept. Because we can no longer use helicity as a quantum number we seem to lose the ability to use the above compact notation. We can work round this by choosing a specific frame in which to define the helicity and then use a *light cone decomposition* of our massive momentum. In this frame we now have a well defined helicity state. Explicitly, for a given lightlike vector q , our massive vector p_I can be written as a sum of two lightlike vectors

$$p_I^\mu = k_i^\mu + \frac{p_I^2}{2p_I \cdot q} q^\mu = k_i^\mu + \frac{m_I^2}{2k_i \cdot q} q^\mu \quad (3.42)$$

$$k_i^2 = q^2 = 0$$

which defines the lightlike vector k_i . The vector q is arbitrary. Using this decomposition we can write the solutions of the massive Dirac equation in terms of massless spinors. These solutions are

$$(\not{p}_I \mp m_I)|I^\pm\rangle = 0 \quad (3.43)$$

$$(\not{p}_I \mp m_I)|I^\pm] = 0 \quad (3.44)$$

and are expressed as

$$|I^\pm\rangle = |i\rangle \pm \frac{m_I}{[iq]}|q\rangle \quad (3.45)$$

$$|I^\pm] = |i] \pm \frac{m_I}{\langle iq\rangle}|q\rangle \quad (3.46)$$

$$\langle I^\pm| = \langle i| \pm \frac{m_I}{[qi]}|q| \quad (3.47)$$

$$[I^\pm| = [i| \pm \frac{m_I}{\langle qi\rangle}\langle q|. \quad (3.48)$$

That these satisfy the Dirac equation can be shown using the completeness property

$$|i\rangle[i| + |i]\langle i| = \not{k}_i. \quad (3.49)$$

We can now write the spinor products for massive particles in terms of massless ones:

$$\langle IJ\rangle = \langle ij\rangle \quad (3.50)$$

$$[IJ] = [ij] \quad (3.51)$$

(due to anti-symmetry conditions) and, despite the similarity of appearance, the mixed angled spinor products are non-zero for massive spinors

$$[IJ] = \left(\frac{m_I}{s_{iq}} + \frac{m_J}{s_{jq}} \right) [i|q|j\rangle \quad (3.52)$$

$$\langle IJ\rangle = \left(\frac{m_I}{s_{iq}} + \frac{m_J}{s_{jq}} \right) \langle i|q|j] \quad (3.53)$$

$$(3.54)$$

where s_{iq} is the Mandelstam variable $(p_i + q)^2 = 2p_i \cdot q$.

3.4.1.1 Numerical Implementation

To evaluate these spinor products numerically we need to choose an explicit representation of the Dirac matrices. At high energy it is convenient to use the Weyl basis

$$\gamma^0 = \begin{pmatrix} \mathbf{0} & \mathbf{1} \\ \mathbf{1} & \mathbf{0} \end{pmatrix}, \gamma^i = \begin{pmatrix} \mathbf{0} & \sigma^i \\ -\sigma^i & \mathbf{0} \end{pmatrix}, \gamma^5 = \begin{pmatrix} \mathbf{1} & \mathbf{0} \\ \mathbf{0} & -\mathbf{1} \end{pmatrix} \quad (3.55)$$

so that the explicit form of the Chiral projection operators is

$$\Pi_+ = \begin{pmatrix} \mathbf{1} & \mathbf{0} \\ \mathbf{0} & \mathbf{0} \end{pmatrix}, \Pi_- = \begin{pmatrix} \mathbf{0} & \mathbf{0} \\ \mathbf{0} & \mathbf{1} \end{pmatrix}. \quad (3.56)$$

where σ^i are the usual Pauli matrices. To gain an explicit representation for the solutions of the massless Dirac equation it is useful to write down the representation of \not{p} in the Weyl basis.

We have

$$\not{p} = \begin{pmatrix} 0 & 0 & p^+ & p^1 - ip^2 \\ 0 & 0 & p^1 + ip^2 & p^- \\ p^- & -p^1 + ip^2 & 0 & 0 \\ -p^1 + ip^2 & p^+ & 0 & 0 \end{pmatrix} \quad (3.57)$$

where $p^\pm = p^0 \pm p^3$. We can choose the massless spinors as follows:

$$u_+(p) = \begin{pmatrix} \sqrt{p^+} \\ \sqrt{p^-} e^{i\phi_p} \\ 0 \\ 0 \end{pmatrix}, u_-(p) = \begin{pmatrix} 0 \\ 0 \\ \sqrt{p^-} e^{-i\phi_p} \\ -\sqrt{p^+} \end{pmatrix} \quad (3.58)$$

where the phase is labelled by the momentum it refers to:

$$e^{\pm i\phi_p} = \frac{p^1 \pm ip^2}{\sqrt{(p^1)^2 + (p^2)^2}} = \frac{p^1 \pm ip^2}{\sqrt{p^+ p^-}}. \quad (3.59)$$

We can write down an explicit expression for our spinor products, in the case where both the energies are positive, $k_i^0 > 0$, $k_j^0 > 0$.

$$\begin{aligned} \langle ij \rangle &= \sqrt{k_i^- k_j^+} e^{i\phi_{k_i}} - \sqrt{k_i^+ k_j^-} e^{i\phi_{k_j}} = \sqrt{|s_{ij}|} e^{i\phi_{ij}} \\ [ij] &= \sqrt{k_i^+ k_j^-} e^{-i\phi_{k_j}} - \sqrt{k_i^- k_j^+} e^{-i\phi_{k_i}} = -\sqrt{|s_{ij}|} e^{-i\phi_{ij}}. \end{aligned} \quad (3.60)$$

where $s_{ij} = 2k_i \cdot k_j$ and

$$\cos \phi_{ij} = \frac{k_i^1 k_j^+ - k_j^1 k_i^+}{\sqrt{|s_{ij}| k_i^+ k_j^+}} \quad (3.61)$$

$$\sin \phi_{ij} = \frac{k_i^2 k_j^+ - k_j^2 k_i^+}{\sqrt{|s_{ij}| k_i^+ k_j^+}}. \quad (3.62)$$

This completes our numerical implementation when both the energies are positive. To define the negative energy case we use the same formula (3.60) for $\langle ij \rangle$ but with $k_i \rightarrow -k_i$ if $k_i^0 < 0$ and with an extra factor of i for each negative energy particle. We then define $[ij]$ using the following identity [55]:

$$\langle ij \rangle [ji] = \bar{u}(k_i) \Pi_+ u(k_j) \bar{u}(k_j) \Pi_- u(k_i) = \text{tr}\{\Pi_- \not{k}_i \not{k}_j\} \quad (3.63)$$

$$= \frac{1}{2} k_i \cdot k_j = s_{ij}. \quad (3.64)$$

3.4.1.2 Collection of useful Identities

We can use the following useful identities in algebraic manipulation:

- Projection operators:

$$|i\rangle[i] = \Pi_+ \not{k}_i \quad (3.65)$$

$$|i]\langle i| = \Pi_- \not{k}_i \quad (3.66)$$

$$|i\rangle[i] + |i]\langle i| = \not{k}_i \quad (3.67)$$

- Gordon identity:

$$\langle i|\gamma^\mu|i] = [i]\gamma^\mu|i\rangle = 2k_i^\mu \quad (3.68)$$

- Anti-symmetry:

$$\langle ij\rangle = -\langle ji\rangle, \quad [ij] = -[ji], \quad \langle ii\rangle = 0 \quad (3.69)$$

- Schouten identities:

$$\langle ij\rangle\langle kl\rangle = \langle ik\rangle\langle jl\rangle + \langle il\rangle\langle kj\rangle \quad (3.70)$$

$$[ij][kl] = [ik][jl] + [il][kj]. \quad (3.71)$$

(this follows from explicitly showing that $|i\rangle\langle j| - |j\rangle\langle i| = \langle ji\rangle\Pi_+$.)

- Complex conjugation:

$$\langle ij\rangle^* = \text{sign}(k_i \cdot k_j)[j\bar{i}] \quad (3.72)$$

- Reversing Spinor Line:

– Even case:

$$\langle i|\gamma^{\mu_1} \dots \gamma^{\mu_{2n}}|j\rangle = -\langle j|\gamma^{\mu_{2n}} \dots \gamma^{\mu_1}|i\rangle \quad (3.73)$$

$$[i]\gamma^{\mu_1} \dots \gamma^{\mu_{2n}}|j] = -[j]\gamma^{\mu_{2n}} \dots \gamma^{\mu_1}|i] \quad (3.74)$$

– Odd case:

$$\langle i|\gamma^{\mu_1} \dots \gamma^{\mu_{2n+1}}|j\rangle = \langle j|\gamma^{\mu_{2n+1}} \dots \gamma^{\mu_1}|i\rangle \quad (3.75)$$

$$[i]\gamma^{\mu_1} \dots \gamma^{\mu_{2n+1}}|j] = [j]\gamma^{\mu_{2n+1}} \dots \gamma^{\mu_1}|i] \quad (3.76)$$

3.4.1.3 Massless Gauge Bosons

We can also cast massless gauge boson polarization vectors in terms of massless helicity spinors as in reference [54]. Again, one needs to define a reference momentum q . The definition is

$$\varepsilon_{\mu}^{\pm} = \pm \frac{\langle q^{\mp} | \gamma_{\mu} | k^{\mp} \rangle}{\sqrt{2} \langle q^{\mp} | k^{\pm} \rangle} \quad (3.77)$$

which gives

$$\varepsilon_{\mu}^{+}(k, q) = \frac{\langle q | \gamma_{\mu} | k \rangle}{\sqrt{2} \langle q k \rangle} \quad (3.78)$$

$$\varepsilon_{\mu}^{-}(k, q) = \frac{[q | \gamma_{\mu} | k \rangle}{\sqrt{2} [k q]} \quad (3.79)$$

and the complex conjugation (for outgoing particles) gives

$$(\varepsilon_{\mu}^{+}(k, q))^* = \frac{[q | \gamma_{\mu} | k \rangle}{\sqrt{2} [k q]} \quad (3.80)$$

$$(\varepsilon_{\mu}^{-}(k, q))^* = \frac{\langle q | \gamma_{\mu} | k \rangle}{\sqrt{2} \langle q k \rangle} \quad (3.81)$$

i.e. complex conjugation reverses the helicity. Since $\not{k} | k^{\pm} \rangle = 0$ the polarisation vector is transverse to our momentum vector, independent of our choice of reference vector q :

$$\varepsilon^{\pm}(k, q) \cdot k = 0. \quad (3.82)$$

The polarisation vectors are also orthonormal: $|\varepsilon|^2 = \varepsilon^{+} \cdot (\varepsilon^{+})^* = -1$ and $\varepsilon^{+} \cdot (\varepsilon^{-})^* = 0$ (by charge conjugation and Fierz rearrangement). Finally, the completeness relation for the polarisation vectors gives:

$$\sum_{\lambda=\pm 1} \varepsilon_{\mu}^{\lambda}(k, q) (\varepsilon_{\nu}^{\lambda}(k, q))^* = -g_{\mu\nu} + \frac{q_{\mu} k_{\nu} + q_{\nu} k_{\mu}}{k \cdot q}. \quad (3.83)$$

which is the same as that for a light-like gauge. There are only two physical polarisations and the polarisation sum is gauge dependent. We have chosen the gauge here $q_{\mu} \varepsilon^{\mu}(k) = 0$ where q_{μ} is a light-like four vector. In the case of the massive spinors the reference vector had the physical significance of defining a frame to allow a definition of helicity; the polarisation vector is constructed such that a shift in the reference vector q is equivalent to a gauge transformation. We can see this by considering the difference between two polarisation vectors at two different

reference vectors q and q' ,

$$\begin{aligned}\Delta\epsilon_\mu^+ &= \epsilon_\mu^+(k, q') - \epsilon_\mu^+(k, q) = \frac{\langle q' | \gamma_\mu | k \rangle}{\sqrt{2}\langle q' k \rangle} - \frac{\langle q | \gamma_\mu | k \rangle}{\sqrt{2}\langle q k \rangle} \\ &= - \left(\frac{\langle q' | \gamma_\mu | k \rangle \langle k q \rangle + \langle q | \gamma_\mu | k \rangle \langle k q' \rangle}{\sqrt{2}\langle q' k \rangle \langle q k \rangle} \right) = - \frac{\sqrt{2}\langle q' q \rangle}{\langle q' k \rangle \langle q k \rangle} k^\mu,\end{aligned}\quad (3.84)$$

and noting that the shift in reference momentum induces a shift in polarisation vector proportional to k^μ .

3.4.1.4 Massive Gauge bosons

We can extend our formalism to include massive gauge bosons also, where $k^2 = m^2$. The three conditions we need to satisfy in the massive case are as follows [56]:

- transversality

$$k^\mu \epsilon_\mu^\pm(k) = 0 \quad (3.85)$$

- orthonormality

$$\epsilon^{\lambda_1}(k) \cdot (\epsilon^{\lambda_2}(k))^* = -\delta_{\lambda_1 \lambda_2} \quad (3.86)$$

- completeness

$$\sum_{\lambda=-1,0,+1} \epsilon_\mu^\lambda(k) (\epsilon_\nu^\lambda(k))^* = -g_{\mu\nu} + \frac{k_\mu k_\nu}{m^2}. \quad (3.87)$$

Again we can use the light cone splitting, where we define a new massless vector k' in terms of our massive vector k and a lightlike reference vector q :

$$\begin{aligned}k^\mu &= k'^\mu + \frac{m_I^2}{2k' \cdot q} q^\mu \\ k'^2 &= q^2 = 0.\end{aligned}\quad (3.88)$$

We can choose two of the polarisation vectors to be the same as the massless case

$$\epsilon_\mu^+(k, q, k') = \frac{\langle q | \gamma_\mu | k' \rangle}{\sqrt{2}\langle q k' \rangle} \quad (3.89)$$

$$\epsilon_\mu^-(k, q, k') = \frac{[q | \gamma_\mu | k' \rangle}{\sqrt{2}[k' q]}. \quad (3.90)$$

and then the third polarisation vector is

$$\begin{aligned}
 \varepsilon_\mu^0(k, q, k') &= \frac{1}{m} \left(k'_\mu - \frac{m^2}{2k' \cdot q} q_\mu \right) \\
 &= \frac{1}{m} (2k'_\mu - k_\mu) \\
 &= \frac{1}{m} \left(k'_\mu - \frac{m^2}{[qk'] \langle k'q \rangle} q_\mu \right).
 \end{aligned} \tag{3.91}$$

3.4.2 Chisholm Identities

In the previous section we have constructed a formalism in which massive fermions and boson can be written in terms of massless helicity spinors. In the following section we described how any amplitude can be reduced to products of spinors $\langle ij \rangle$ and $[ij]$ to be evaluated numerically.

After we rewrite the massive spinors and vector boson polarisation vectors in terms of massless helicity spinors as explained above our expression consists of Dirac matrices sandwiched between two spinor lines. These Dirac matrices can be contracted with a vector (e.g. \not{p}) or with another Dirac matrix either in the same spinor chain or in another. Whilst, in principle, this could be completed numerically, it is much more efficient to algebraically reduce these expressions. To this end we can repeatedly apply the *Chisholm identities* [1]. In what follows we let Γ stand for a string of Dirac matrices with an odd number of elements and therefore $\Gamma\gamma^\rho$ is an even string. We have the following two contraction identities

$$\begin{aligned}
 \gamma^\mu \Gamma \gamma_\mu &= -2\overleftarrow{\Gamma} \\
 \gamma^\mu \Gamma \gamma^\rho \gamma_\mu &= 2(\gamma^\rho \Gamma + \overleftarrow{\Gamma} \gamma^\rho)
 \end{aligned} \tag{3.92}$$

with $\overleftarrow{\Gamma}$ labels the reverse sequence of Dirac matrices in Γ . We can convert any spinor line into a trace using the following procedure:

$$\begin{aligned}
 \langle i | \cdots | j \rangle &= \langle i | \cdots | j \rangle \frac{[jp] \langle pq \rangle [qi]}{[jp] \langle pq \rangle [qi]} \\
 &= \frac{\text{tr} \{ \Pi_- \not{k}_i \cdots \not{k}_j \not{p} \not{q} \}}{[j] \not{p} \not{q} | i].}
 \end{aligned} \tag{3.93a}$$

Likewise we derive

$$[i] \cdots [j] = \frac{\text{tr} \{ \Pi_+ \not{k}_i \cdots \not{k}_j \not{p} \not{q} \}}{\langle j | \not{p} \not{q} | i \rangle} \tag{3.93b}$$

$$\langle i | \cdots | j \rangle = \frac{\text{tr} \{ \Pi_- \not{k}_i \cdots \not{k}_j \not{p} \}}{\langle j | \not{p} | i \rangle} \tag{3.93c}$$

$$[i] \cdots | j \rangle = \frac{\text{tr} \{ \Pi_+ \not{k}_i \cdots \not{k}_j \not{p} \}}{[j] \not{p} | i \rangle}. \tag{3.93d}$$

The Chisholm identity is

$$\text{tr}\{\gamma^{\mu_1} \dots \gamma^{2m+1} \gamma^\rho\} \gamma_\rho = 2(\gamma^{\mu_1} \dots \gamma^{2m+1} + \gamma^{2m+1} \dots \gamma^{\mu_1}). \quad (3.94)$$

The application of these identities to spinor chains yields:

$$\langle i|\Gamma\gamma^\mu\Gamma'|j\rangle\gamma_\mu = 2\Gamma'|j\rangle\langle i|\Gamma - 2\overleftarrow{\Gamma}|i\rangle\langle j|\overleftarrow{\Gamma}' \quad (3.95a)$$

$$[i|\Gamma\gamma^\mu\Gamma'|j\rangle\gamma_\mu = 2\Gamma'|j][i|\Gamma - 2\overleftarrow{\Gamma}|i][j|\overleftarrow{\Gamma}' \quad (3.95b)$$

$$\langle i|\Gamma\gamma^\mu\Gamma'|j\rangle\gamma_\mu = 2\Gamma'|j][i|\Gamma + 2\overleftarrow{\Gamma}|i][j|\overleftarrow{\Gamma}' \quad (3.95c)$$

$$[i|\Gamma\gamma^\mu\Gamma'|j\rangle\gamma_\mu = 2\Gamma'|j][i|\Gamma - 2\overleftarrow{\Gamma}|i][j|\overleftarrow{\Gamma}'. \quad (3.95d)$$

where Γ and Γ' represent a string of either an odd or an even number of Dirac matrices. These are simply derived using (3.93a). These identities are only valid when the left hand side is non-zero (for example in (3.95a) if $\Gamma'\gamma^\mu\Gamma'$ is an odd number then this is zero). So in implementing these identities one must count the number of Dirac matrices lying between the spinors.

Repeated application of (3.95) and (3.92) ensures that any amplitude (with no free Lorentz indices) can be reduced to spinor products which is ideal for a numerical implementation.

3.5 Majorana Fermions

Majorana fermions arise in supersymmetric extensions to the Standard Model. For example, the supersymmetric partner of the gluon is the gluino and has the kinetic term (we drop color indices)

$$\mathcal{L}_{\text{gluino}} \supset \frac{1}{2} \bar{g} i \gamma_\mu \partial^\mu g. \quad (3.96)$$

In supersymmetric theories, SUSY treats left and right handed particles separately. For example, a quark has two superpartners: the left and right handed squarks. On the contrary if one tries to write down a supersymmetric partner for the gluon (the gluino) one arrives at a Weyl fermion. It for this reason that the ‘‘natural’’ representation for supersymmetric fermions is Weyl fermions. To write the gluino as a Dirac fermion one is forced to write it as a Majorana fermion. The same can be said when we write down the supersymmetric partners of any of the bosons in our theory: the supersymmetric partners of the Z, A and Higgs bosons that combine to form the Neutralinos.

A Majorana fermion is its own anti-particle i.e. it is invariant under charge conjugation:

$$\tilde{\psi}_M = C \bar{\psi}_M^T = \psi_M. \quad (3.97)$$

The charge-conjugation matrix has the properties:

$$C^\dagger = C^{-1}, \quad C^T = -C, \quad C\Gamma_i^T C^{-1} = \eta_i \Gamma_i \quad (3.98)$$

with

$$\eta_i = \begin{cases} +1 & \text{for } \Gamma_i = 1, \gamma_5, \gamma_\mu \gamma_5 \\ -1 & \text{for } \Gamma_i = \gamma_\mu. \end{cases} \quad (3.99)$$

Because the Majorana fermion is its own anti-particle then it follows that any vertex involving them must violate fermion number flow; the fermion flow in the Feynman diagram is ill-defined. A consistent way of dealing with this was proposed in [57]. There are two drawbacks with this approach; charge conjugation matrices are explicitly introduced into the Feynman rules and the relative sign of the Feynman graphs needs to be determined from the original Wick contractions i.e. one has to take a step back from the Feynman rules.

We follow the approach in [58] which has been implemented in [59]. Dirac fermions have an arrow denoting the fermion number flow, and Majorana fermions do not have an arrow. The idea is that we place all fermions (Majorana or not) on an equal footing by realizing that each vertex can be written in one of two equivalent ways: one in which the fermion flow follows the fermion number flow, and the other “flipped” vertex, where the fermion flows in the opposite direction. In our implementation we impose a fermion flow on the vertex and “flip” the vertices and spinors where necessary; we follow the imposed fermion flow and when the “flipped” version of the vertex is encountered we simply apply the flipping rules. For our purposes, the number of flipping rules required is quite small. Explicitly they are

$$\begin{aligned} (\gamma^\mu)' &= -\gamma^\mu \\ (\Pi_\pm)' &= \Pi_\pm \end{aligned} \quad (3.100)$$

and for the spinors

$$\begin{aligned} |p\rangle' &= \langle p| \\ |p\rangle' &= [p]. \end{aligned} \quad (3.101)$$

This leads to the following rule for the fermionic propagator:

$$S'(p) = \frac{1}{-\not{p} - m} = S(-p). \quad (3.102)$$

Another appealing feature of this method is that the relative sign between graphs can be determined directly from our Feynman graphs without reverting back to the original Wick contractions. To compute a consistent relative sign of Feynman graphs each graph must be multiplied by $(-1)^{P+L}$ where

- P : the parity of the permutation of external spinors with respect to some reference order,
- L : the number of closed fermion loops.

This sign is determined after the flipping rules are applied.

3.5.1 Working with Majorana Spinors

We provide some examples to illustrate the points above [1].

3.5.1.1 Charge Conjugation of a Vector Current

We illustrate our approach through the following simple example. The vector current, $\langle p^+ | \gamma^\mu | q^+ \rangle$, satisfies the charge conjugation relation

$$\langle p^+ | \gamma^\mu | q^+ \rangle = \langle q^- | \gamma^\mu | p^- \rangle, \quad (3.103)$$

which we can show explicitly using charge conjugation relations. This charge conjugation operation is equivalent to us reversing the fermion flow arrow. Therefore we can use Equations (3.100) to show this equivalence holds:

$$\langle p^+ | \gamma^\mu | q^+ \rangle = [p | \mu | q] \rightarrow (-1)^P \langle q | \gamma^{\mu'} | p \rangle = (-1)^P (-1) \langle q | \gamma^\mu | p \rangle \quad (3.104)$$

$$= \langle q | \gamma^\mu | p \rangle = \langle q^- | \gamma^\mu | p^- \rangle \quad (3.105)$$

where we have used (3.99) and (3.101) and we have defined our reference order as (p, q) giving $(-1)^P = -1$. This result is true for both Dirac and Majorana fermions.

3.5.1.2 Majorana Exchange

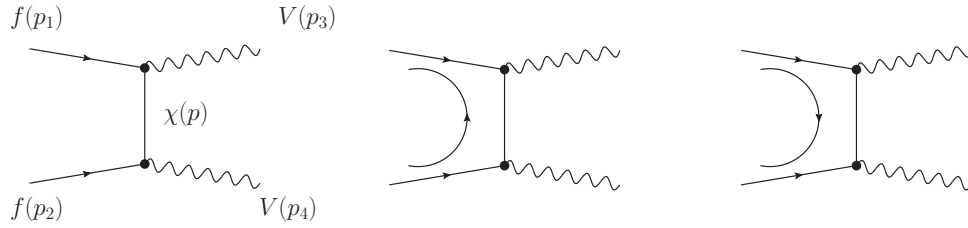


Figure 3.9: The process $(ff \rightarrow VV)$ mediated by the exchange of a Majorana fermion (χ) as discussed in the example. The left hand figure shows the original diagram; the middle figure shows the first choice of fermion orientation; and the figure on the right shows the second choice of orientation.

We now consider two Dirac fermions scattering to two vector bosons via a t-channel Majorana fermion exchange. There are two equivalent orientations to choose from as shown in Figure 3.9. We write our amplitude as

$$\mathcal{A} = \mathcal{A}^{\mu\nu} \epsilon_\mu^*(p_3) \epsilon_\nu^*(p_4). \quad (3.106)$$

Our first choice of orientation gives

$$\mathcal{A}_1^{\mu\nu} = \langle p_1 | (\gamma^\mu)' S(p) \gamma^\nu | p_2 \rangle \quad (3.107)$$

and the second orientation gives

$$\mathcal{A}_2^{\mu\nu} = (-1) \langle p_2 | (\gamma^\nu)' S(-p) \gamma^\mu | p_1 \rangle \quad (3.108)$$

where we have chosen the reference order (p_1, p_2) . Applying our flipping rules to Equation (3.107) gives the result:

$$\mathcal{A}_1^{\mu\nu'} = (-1)^P \langle p_2 | (\gamma^\nu)' S(-p) \gamma^\mu | p_1 \rangle = \mathcal{A}_2^{\mu\nu}. \quad (3.109)$$

Therefore the amplitude is independent of the original choice of fermion orientation.

3.6 Tests of Implementation

As a test of our implementation of the spinor helicity formalism and of the treatment of Majorana fermions we checked against the software program MadGraph [3] at tree level for a variety of processes. We performed a sweep in the phase space of the outgoing particles. We found agreement in every test within machine precision. We plot two of our results in Figure 3.10 for $2 \rightarrow 3$ processes where we can see the variation of the tree level matrix element squared against the polar angle of the first outgoing particle. The first result for $gg \rightarrow \tilde{u}_L \tilde{u}_L^\dagger Z$ shows that the relative sign has been handled correctly and also our implementation for the massive gauge boson Z is correctly handled. For the process $u\bar{u} \rightarrow \chi_1^0 \chi_1^0 g$ we see that our *massive* Majorana fermions χ_1 have been treated correctly and also the relative sign between graphs has been computed correctly.

3.7 Regularisation Scheme

We are interested in the virtual contribution in a NLO calculation. These contributions involve an integral over the unresolved loop momenta that can be divergent in both the infrared and the ultraviolet. One must regulate this divergence to obtain a useful result by choosing a *regularisation scheme* [11]. *Dimensional regularisation* is the regularisation of loop integrals by continuing the loop momenta into $n = 4 - 2\epsilon$ dimensions. Once we have dealt with this loop integral we are left with a certain amount of freedom in how we treat the other objects (gamma matrices, momentum, polarisation vectors) and this freedom has been explored extensively in the literature. We summarize the main choices here: they are *conventional dimensional regularisation* (**CDR**), the *'t Hooft-Veltman* convention (**HV**) and *dimensional reduction* (**DRED**). We outline the choices we can make below.

- Dirac Algebra:

We can choose to extend this to n dimensions or to leave it in 4-dimensions.

- Momenta:

The internal momenta must be n dimensional. However, we can choose to retain the external momenta in the physical 4 dimensional space or extend it also to the n dimensional space. Extending it to n dimensions occurs in the (**CDR**) scheme and is generally out of favour as keeping it in 4 dimensions can simplify final expressions.

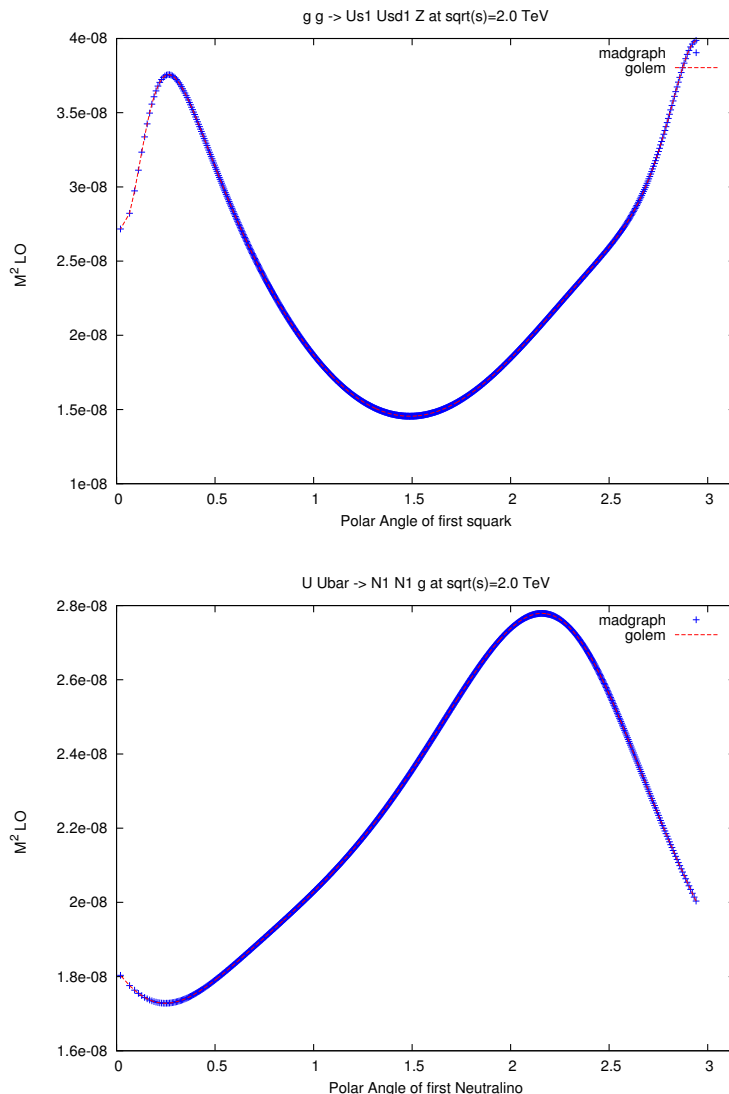


Figure 3.10: Comparison of our implementation of flipping rules in our MSSM model file with the implementation in MadGraph [3] for the processes $gg \rightarrow \tilde{u}_L \tilde{u}_L^\dagger Z$ and $u\bar{u} \rightarrow \chi_1^0 \chi_1^0 g$. We see that we have agreement throughout phase-space.

- Vector Boson polarisations:

Corresponding to our choice of dimension of external momenta the number of external gluon polarisations is either 2 or $n-2 = 2-2\epsilon$. The number of internal gluon polarisations is chosen to be either $n-2$ or kept fixed as 2.

- Quark Helicities:

We choose the number of massless quark helicities as 2.

We summarize the choice of the three different schemes in the table 3.1.

Scheme	CDR	HV	DRED
Dirac algebra	$\gamma^\mu = \hat{\gamma}^\mu + \bar{\gamma}^\mu$	$\gamma^\mu = \hat{\gamma}^\mu + \bar{\gamma}^\mu$	$\gamma^\mu = \hat{\gamma}^\mu$
γ_5	(3.119)	(3.120)	(3.119)
internal momenta	n ($k = \hat{k} + \bar{k}$)	n ($k = \hat{k} + \bar{k}$)	n ($k = \hat{k} + \bar{k}$)
external momenta	n ($p = \hat{p} + \bar{p}$)	4 ($p = \hat{p}$)	4 ($p = \hat{p}$)
Number of internal gluons	$n - 2$	$n - 2$	2
Number of external gluons	$n - 2$	2	2
Number of internal quarks	2	2	2
Number of external quarks	2	2	2

Table 3.1: Summary of the different choices of dimensions for objects in different dimensional regularisation schemes. We note that the common feature is the regulation of the loop integral by extending the dimension to $n = 4 - 2\epsilon$.

3.7.1 The 't Hooft Veltman Scheme

In our calculation we use the 't Hooft Veltman scheme (**HV**) [11]. In this scheme the Dirac algebra is extended to n dimensions. In this section we describe how we handle the extra dimensional pieces in the numerator algebra and how we extend γ_5 to n dimensions. It has been shown that, using this scheme, one can derive the axial anomaly in an unambiguous manner at the two loop level [60].

3.7.1.1 Dimension splitting

We split our n dimensional metric tensor g into two non-overlapping parts

$$g^{\mu\nu} = \hat{g}^{\mu\nu} + \bar{g}^{\mu\nu}. \quad (3.110)$$

with the 4 dimensional metric \hat{g} and the $n - 4$ dimensional metric \bar{g} . Our spinor helicity results in Section 3.4 now hold for the metric \hat{g} . We have the following rules:

$$\hat{g}_\mu^\mu \equiv \hat{g}^{\mu\nu} g_{\nu\mu} = 4 \quad (3.111)$$

$$\bar{g}_\mu^\mu \equiv \bar{g}^{\mu\nu} g_{\nu\mu} = n - 4 \quad (3.112)$$

$$\bar{g}^{\mu\nu} \hat{g}_{\nu\rho} = 0. \quad (3.113)$$

One can visualise the splitting easily if one thinks of the metric as a matrix in block diagonal form. We have

$$g^{\mu\nu} \rightarrow \left(\begin{array}{c|c} \hat{g}^{\mu\nu} & 0 \\ \hline 0 & \bar{g}^{\mu\nu} \end{array} \right). \quad (3.114)$$

A typical expression in **HV** contains a combination of two metrics we need a method to disentangle the two parts. We start from the identity

$$\text{tr}\{\mathbb{I}\} \text{tr}\{\hat{\gamma}^{\alpha_1} \dots \hat{\gamma}^{\alpha_p} \bar{\gamma}^{\beta_1} \dots \bar{\gamma}_{\beta_q}\} = \text{tr}\{\hat{\gamma}^{\alpha_1} \dots \hat{\gamma}^{\alpha_p}\} \text{tr}\{\bar{\gamma}^{\beta_1} \dots \bar{\gamma}_{\beta_q}\} \quad (3.115)$$

a proof of which is given in [61]. We split all γ matrices in our expression and commute them to opposite ends of the spinor chain using the following rule:

$$\{\hat{\gamma}^\mu, \bar{\gamma}^\nu\} = 0 \quad (3.116)$$

i.e.

$$\{\hat{\gamma}^\mu, \bar{\gamma}^\nu\} = \hat{g}^{\mu\alpha} \bar{g}^{\nu\beta} \{\gamma_\alpha, \gamma_\beta\} = \hat{g}^{\mu\alpha} \bar{g}^{\nu\beta} 2g_{\alpha\beta} = \hat{g}_\alpha^\mu \bar{g}^{\alpha\nu} = 0. \quad (3.117)$$

We have already described how to deal with the 4 dimensional pieces; for the $n - 4$ part we can use the following reduction formula [1]:

$$\text{tr}\{\bar{\gamma}^{\beta_1} \dots \bar{\gamma}^{\beta_n}\} = \sum_{i=2}^n (-1)^i \bar{g}^{\beta_1 \beta_i} \text{tr}\{\bar{\gamma}^{\beta_2} \dots \bar{\gamma}^{\beta_{i-1}} \bar{\gamma}^{\beta_{i+1}} \dots \bar{\gamma}^{\beta_n}\}. \quad (3.118)$$

3.7.1.2 Dealing with γ_5

In chiral theories, one also needs to extend our definition of, what is essentially a four dimensional object, γ_5 to n dimensions. The naïve way of doing this

$$\{\gamma^\mu, \gamma_5\} = 0 \quad \forall \mu \quad (3.119)$$

leads to ambiguities beyond tree level [11]. If, however, we adopt the following prescription for γ_5 :

$$\begin{aligned} \{\gamma^\mu, \gamma_5\} &= 0 \quad \mu \in \{0, 1, 2, 3\} \\ [\gamma^\mu, \gamma_5] &= 0 \quad \text{otherwise} \end{aligned} \quad (3.120)$$

where the γ_5 is essentially living in a 4 dimensional subspace we can avoid these ambiguities. In our dimensional splitting notation the above condition reads

$$[\gamma_5, \bar{\gamma}^\mu] = 0 \quad (3.121)$$

i.e. γ_5 is kept in 4 dimensions allowing us to write down an explicit expression for γ_5 in terms of our four dimensional Dirac matrices:

$$\gamma_5 = \frac{i}{4!} \epsilon_{\mu\nu\gamma\delta} \hat{\gamma}^\mu \hat{\gamma}^\nu \hat{\gamma}^\gamma \hat{\gamma}^\delta. \quad (3.122)$$

Therefore, when γ_5 is present in an expression it is shuffled to the four dimensional trace part of (3.115) using the relations (3.120).

3.7.2 Regularisation scheme dependence

The regularisation scheme we choose can respect or break the symmetry of the Lagrangian and it is highly desirable to retain the symmetries of a Lagrangian at the one-loop level. For

example regularisation using a cut-off regulator breaks the gauge invariance of the photon as the one-loop correction introduces a “mass” for the photon and dimensional regularisation is preferred as it respects gauge invariance. In supersymmetric theories dimensional regularisation does not respect the supersymmetric transformations. We can see this as follows: the simplest supersymmetric Lagrangian is given by

$$\mathcal{L} = -\frac{1}{4}G^{\mu\nu}G_{\mu\nu} + \frac{i}{2}\bar{\lambda}\gamma^\mu\partial_\mu\lambda + \frac{1}{2}D^2. \quad (3.123)$$

A necessary condition for supersymmetry is the equality of bosonic and fermionic degrees of freedom. In dimensional regularisation we have that the gauge field has $(n - 2)$ degrees of freedom, whereas the fermion (here λ is a Majorana fermion) has 2 degrees of freedom. Therefore we expect supersymmetric relations not to hold away from $n = 4$. We explicitly show that the SUSY Yang-Mills Lagrangian is invariant in 4-dimensions in Appendix B and this is broken when we move to generic n dimensions by the *Siegel ambiguity* [62]. Dimensional reduction does respect supersymmetry as the gauge fields have 2 degrees of freedom.

There can be finite differences between the two schemes in one-loop calculations resulting from the treatment of the metric tensor associated with the gauge field [63]. In dimensional regularisation these are extended to $n = 4 - 2\epsilon$ dimensions which can result in ϵ in the numerator. These ϵ terms can hit a ϵ pole when multiplied by a divergent loop integral. In dimensional reduction these terms are not present therefore we have a finite difference between the two schemes. We can restore supersymmetry at the one-loop level by including these finite differences in the dimensional regularisation result.

3.7.3 Examples

We give a couple of examples of the differences between results from the **HV** and **DRED** regularisation schemes.

3.7.4 Boson quark quark vertex

The tree level coupling for this vertex is $ie\gamma^\mu$. We consider the correction with one virtual gluon. For the massless quark case we get the result

$$\bar{u}(p_3)\Gamma^\mu u(p_2) = f_1(s)\bar{u}(p_3)(ie\gamma^\mu)u(p_2) \quad (3.124)$$

where r_Γ is defined in Section D.1.6. Our result is

$$f_1(s) = r_\Gamma \frac{C_F\alpha_s}{4\pi} \left(\frac{4\pi\mu^2}{s}\right)^\epsilon \left(-\frac{2}{\epsilon^2} - \frac{3}{\epsilon} + \pi^2 - 8\right). \quad (3.125)$$

The dimensional reduction result is

$$f_1(s) = r_\Gamma \frac{C_F\alpha_s}{4\pi} \left(\frac{4\pi\mu^2}{s}\right)^\epsilon \left(-\frac{2}{\epsilon^2} - \frac{3}{\epsilon} + \pi^2 - 8 + 1\right). \quad (3.126)$$

3.7.5 Chiral Coupling

If we have a chiral coupling the situation is a little different. If our tree level coupling is parameterized as

$$i\gamma^\mu (g_L \Pi_- + g_R \Pi_+) \quad (3.127)$$

then our vertex correction can be written as

$$\bar{u}(p_3)\Gamma^\mu u(p_1) = \bar{u}(p_3)i\gamma^\mu (f_1(s)\Pi_- + f_2(s)\Pi_+) u(p_1) \quad (3.128)$$

which gives (upon expansion)

$$f_1(s) = r_\Gamma \frac{C_F \alpha_s}{4\pi} \left(\frac{4\pi\mu^2}{s} \right)^\epsilon \left[g_L \left(-\frac{2}{\epsilon^2} - \frac{3}{\epsilon} + \pi^2 - 6 \right) - 2g_R \right] \quad (3.129)$$

$$f_2(s) = r_\Gamma \frac{C_F \alpha_s}{4\pi} \left(\frac{4\pi\mu^2}{s} \right)^\epsilon \left[g_R \left(-\frac{2}{\epsilon^2} - \frac{3}{\epsilon} + \pi^2 - 6 \right) - 2g_L \right]. \quad (3.130)$$

The dimensional reduction results are similar but we now have

$$f_1(s) = r_\Gamma \frac{C_F \alpha_s}{4\pi} \left(\frac{4\pi\mu^2}{s} \right)^\epsilon \left[g_L \left(-\frac{2}{\epsilon^2} - \frac{3}{\epsilon} + \pi^2 - 6 \right) - 2g_R + g_R \right] \quad (3.131)$$

$$f_2(s) = r_\Gamma \frac{C_F \alpha_s}{4\pi} \left(\frac{4\pi\mu^2}{s} \right)^\epsilon \left[g_R \left(-\frac{2}{\epsilon^2} - \frac{3}{\epsilon} + \pi^2 - 6 \right) - 2g_L + g_L \right]. \quad (3.132)$$

Chapter 4

Loop Integrals

4.1 Reduction Scheme

The virtual part of a NLO calculation will contain an integral over the unresolved loop momenta. As we explained in the previous chapter these integrals can lead to divergences either in the infrared or collinear region (IR) or in the ultraviolet region (UV). These divergences mean that a purely numerical evaluation of the integral is not possible. We regularise our divergent integrals by letting $n = 4 - 2\epsilon$ and our final results appear as a Laurent series in ϵ . Schematically we have

$$\mathcal{A}_V = \frac{A}{\epsilon^2} + \frac{B}{\epsilon} + C + D\epsilon + \mathcal{O}(\epsilon^2) \quad (4.1)$$

where the first term is present only when we have a infrared and collinear singularity and the second term can be of IR or UV origin. In general the coefficients of the series will depend on the kinematic variables present in the process.

Loop integrals can have a non-trivial numerator structure and their calculation can be lengthy. In this section we outline a reduction scheme for loop integrals that can be implemented in an automated way.

4.1.1 Overview

We consider one-loop N -point diagrams. They are expressed as integrals in momentum space either with powers of the loop momentum in the numerator (*tensor integral*) or without (*scalar integral*). Our strategy is to reduce any integral appearing to a basis set of master integrals that can be computed once and for all. In our case (at one-loop) the number of such integrals is manageable. Other techniques such as the method of *integration by parts* [64] can also be used.

The traditional method of tensor reduction was introduced in [65] where all tensor integrals are reduced to scalar integrals (we call this basis **SI**). This method leads to numerical instabilities due to the appearance of Gram determinants in the denominator of intermediate expressions

that can become small in certain kinematic regions. This is an artificial reduction scheme dependent issue. One could avoid this by cancelling the Gram determinants between certain classes of diagrams (an approach followed in [66]). However, we aim for a completely automated approach that avoids intermediate steps such as these.

The final integral basis is not unique. We therefore choose a different basis that avoids these inverse Gram determinants. There exists a trade-off in any reduction scheme between the simplicity of the objects at the end of the reduction and the number of terms introduced in order to arrive at these objects. In our calculation we follow the reduction scheme laid out in [67] and implemented in the program [68, 2]. Our choice of the end point of our reduction is listed in Table 4.1 and we call it the Golem Basis (**GB**). The integrals in **GB** can have Feynman parameters in the numerator and we label the N -point, n dimensional integral as I_N^n . We can write any N -point amplitude as a linear combination of the integrals in **GB** without encountering any inverse Gram determinants.

Basis Integral	UV divergent	IR divergent
I_4^{n+2}	no	no
I_4^{n+4}	yes	no
I_3^n	no	yes
I_3^{n+2}	yes	no
I_2^n	yes	no

Table 4.1: Basis integrals of our reduction scheme. All integrals here can have Feynman parameters in the numerator. An N -point integral in n dimensions is written as I_N^n .

We can further reduce this basis to **SI** (with no Feynman parameters in the numerator). It is at this step that one cannot avoid introducing inverse Gram determinants. A reduction to the purely scalar integrals would be desirable as their computation would be the quickest but we arrive at the same numerical problem as mentioned above. Therefore our approach reduces **GB** to **SI** *only if* the Gram determinant is not dangerous. If this is not the case then a direct numerical evaluation of **GB** is completed.

4.1.2 Form Factor Representation

The general one-loop N -point tensor integral of rank r in n dimensions can be written as

$$I_N^{n,\mu_1,\dots,\mu_r}(a_1, a_2, \dots, a_r) = \int \frac{d^n k}{i\pi^{\frac{n}{2}}} \frac{q_{a_1}^{\mu_1} \dots q_{a_r}^{\mu_r}}{(q_1^2 - m_1^2 + i\delta) \dots (q_N^2 - m_N^2 + i\delta)}. \quad (4.2)$$

where N labels the number of propagators. The propagators have the momenta $q_i = k + r_i$ where r_i is a combination of external momenta. r_i is defined such that $p_i = r_i - r_{i-1}$ and $r_0 = r_N$. Momentum conservation leads to the constraint

$$\sum_{i=1}^N p_i = 0 \quad (4.3)$$

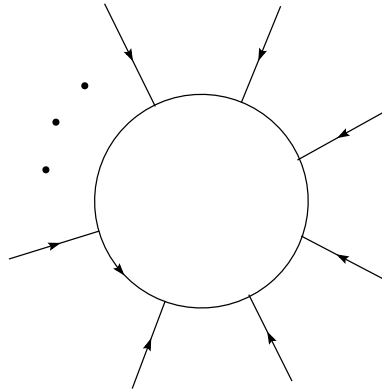


Figure 4.1: Generic N -point loop graph. The momentum in the loop is defined as q_i where i labels the propagator and $q_i = k + r_i$ where k is the loop momentum and r_i is a combination of the incoming, external momenta.

(all the external momenta are defined as incoming) giving $q_i = p_i + q_{i-1}$ ($q_0 = q_N$). Therefore we choose one of the vectors r_i to be zero. Common choices are $r_N = 0$ or $r_1 = 0$.

Our choice in (4.2) in terms of combination of momentum vectors $q_i = k + r_i$ can be contrasted to the conventional expression for a tensor integral written as

$$I_N^{n,\mu_1,\dots,\mu_r}(N,\dots,N) = \int \frac{d^n k}{i\pi^{\frac{n}{2}}} \frac{k^{\mu_1} \dots k^{\mu_r}}{(q_1^2 - m_1^2 + i\delta) \dots (q_N^2 - m_N^2 + i\delta)}. \quad (4.4)$$

The conventional representation is simply a special case of our general representation (4.2) where we set $r_N = 0$ and the momenta in the numerator are all set to $q_N = k$. If one carries out a reduction procedure starting from this form one obtains integrals that are not of a standard type, so a shift operation $k \rightarrow k + r_j$ is necessary to remap to the standard form. For a rank r integral the shift operation gives rise to 2^r terms. Our representation (4.2) is manifestly translation invariant thus avoiding such a proliferation of terms. We wish to also define a translation invariant form factor representation for (4.2). To this end we define the shift invariant vector Δ_{ij} where

$$\Delta_{ij}^\mu = r_i^\mu - r_j^\mu = q_i^\mu - q_j^\mu. \quad (4.5)$$

We express tensor integrals in terms of these Lorentz tensors and the set of form factors: $A_{l_1,\dots,l_r}^{N,r}, B_{l_1,\dots,l_r}^{N,r}, C_{l_1,\dots,l_r}^{N,r}$.

Our tensor definition is as follows, where S stands for the kinematic configuration of the

integral:

$$\begin{aligned}
 I_N^{n, \mu_1 \dots \mu_r}(a_1, \dots, a_r; S) = & \\
 & \sum_{j_1 \dots j_r \in S} [\Delta_{j_1} \dots \Delta_{j_r}]_{\{a_1 \dots a_r\}}^{\{\mu_1 \dots \mu_r\}} A_{j_1 \dots j_r}^{N, r}(S) \\
 & + \sum_{j_1 \dots j_{r-2} \in S} [g \Delta_{j_1} \dots \Delta_{j_{r-2}}]_{\{a_1 \dots a_r\}}^{\{\mu_1 \dots \mu_r\}} B_{j_1 \dots j_{r-2}}^{N, r}(S) \\
 & + \sum_{j_1 \dots j_{r-4} \in S} [g \Delta_{j_1} \dots \Delta_{j_{r-4}}]_{\{a_1 \dots a_r\}}^{\{\mu_1 \dots \mu_r\}} C_{j_1 \dots j_{r-4}}^{N, r}(S). \tag{4.6}
 \end{aligned}$$

The distribution of the r Lorentz indices μ_i and the momentum labels a_i is best demonstrated through examples:

$$I_N^n(S) = A^{N, 0}(S) \tag{4.7}$$

$$I_N^{n, \mu_1}(a_1; S) = \sum_{l \in S} \Delta_{l a_1}^{\mu_1} A_l^{N, 1}(S) \tag{4.8}$$

$$I_N^{n, \mu_1 \mu_2}(a_1, a_2; S) = \sum_{l_1, l_2 \in S} \Delta_{l_1 a_1}^{\mu_1} \Delta_{l_2 a_2}^{\mu_2} A_{l_1 l_2}^{N, 2}(S) + g^{\mu_1 \mu_2} B^{N, 2}(S) \tag{4.9}$$

$$\begin{aligned}
 I_N^{n, \mu_1 \mu_2 \mu_3}(a_1, a_2, a_3; S) = & \sum_{l_1, l_2, l_3 \in S} \Delta_{l_1 a_1}^{\mu_1} \Delta_{l_2 a_2}^{\mu_2} \Delta_{l_3 a_3}^{\mu_3} A_{l_1 l_2 l_3}^{N, 3}(S) \\
 & + \sum_{l \in S} (g^{\mu_1 \mu_2} \Delta_{l a_3}^{\mu_3} + g^{\mu_1 \mu_3} \Delta_{l a_2}^{\mu_2} + g^{\mu_2 \mu_3} \Delta_{l a_1}^{\mu_1}) B_l^{N, 3}(S) \tag{4.10}
 \end{aligned}$$

$$\begin{aligned}
 I_N^{n, \mu_1 \mu_2 \mu_3 \mu_4}(a_1, a_2, a_3, a_4; S) = & \sum_{l_1 \dots l_4 \in S} \Delta_{l_1 a_1}^{\mu_1} \Delta_{l_2 a_2}^{\mu_2} \Delta_{l_3 a_3}^{\mu_3} \Delta_{l_4 a_4}^{\mu_4} A_{l_1 l_2 l_3 l_4}^{N, 4}(S) \\
 & + \sum_{l_1, l_2 \in S} (g^{\mu_1 \mu_2} \Delta_{l_1 a_3}^{\mu_3} \Delta_{l_2 a_4}^{\mu_4} + g^{\mu_1 \mu_3} \Delta_{l_1 a_2}^{\mu_2} \Delta_{l_2 a_4}^{\mu_4} + g^{\mu_1 \mu_4} \Delta_{l_1 a_2}^{\mu_2} \Delta_{l_2 a_3}^{\mu_3} \\
 & + g^{\mu_2 \mu_3} \Delta_{l_1 a_1}^{\mu_1} \Delta_{l_2 a_4}^{\mu_4} + g^{\mu_2 \mu_4} \Delta_{l_1 a_1}^{\mu_1} \Delta_{l_2 a_3}^{\mu_3} + g^{\mu_3 \mu_4} \Delta_{l_1 a_1}^{\mu_1} \Delta_{l_2 a_2}^{\mu_2}) B_{l_1 l_2}^{N, 4}(S) \\
 & + (g^{\mu_1 \mu_2} g^{\mu_3 \mu_4} + g^{\mu_1 \mu_3} g^{\mu_2 \mu_4} + g^{\mu_2 \mu_3} g^{\mu_1 \mu_4}) C^{N, 4}(S). \tag{4.11}
 \end{aligned}$$

We can see that these form factors are shift-invariant by setting all the $a_j = N$ and $r_N = 0$ to obtain the conventional representation. The set of form factors can be written in terms of **GB** as we shall explain shortly. If the phase space point is not dangerous we can iteratively reduce **GB** to **SI**; we can express the form factors in terms of **SI** but at the expense of introducing inverse Gram determinants.

4.1.3 Tensor Reduction

In this section we derive a result that shows us that we can express a tensor integral in terms of higher order scalar integrals. This is a crucial result for us as it relates tensor integrals with the **GB** integrals. Therefore it holds the key to writing down our set of form factors in terms of **GB**. After completing the square in the denominator of our integral as demonstrated in Appendix C.1 any odd power of loop momenta in the numerator causes the integral to vanish after integration. Therefore we can express the numerator as follows:

$$l^{\mu_1} \dots l^{\mu_{2m}} = A [g^{\dots} \dots g^{\dots}]^{\mu_1 \dots \mu_{2m}} (l^2)^m. \quad (4.12)$$

where $[g^{\dots} \dots g^{\dots}]^{\mu_1 \dots \mu_{2m}}$ is the sum of all distinct distributions of indices over the metric tensors. There are m metric tensors in each product in the sum. And there are $(2m - 1)!!$ products in each sum. That is, the number of distinct ways of grouping $2m$ objects into pairs is $(2m - 1) \times (2m - 3) \times \dots \times 1$. Due to symmetry each product has the same coefficient A .

A is the number of ways of contracting the indices for each product of metrics where $g_{\mu}^{\mu} = n$. There are m metrics, therefore the first line can either close a metric or join to one of the $2(m - 1)$ metrics. Likewise, the second metric can close a metric or join to one of the $2(m - 2)$ metrics left. This continues until there is no other metrics to join and the only possibility is to join it to itself (for the m^{th} iteration). So we get

$$A = \frac{1}{\prod_{k=1}^m (n + 2(k - 1))}. \quad (4.13)$$

A simple example of this would be when we have two metrics, and the result is

$$k^{\mu} k^{\nu} k^{\rho} k^{\sigma} = \frac{k^4}{n(n + 2)} (g^{\mu\nu} g^{\rho\sigma} + g^{\mu\rho} g^{\nu\sigma} + g^{\mu\sigma} g^{\nu\rho}) \quad (4.14)$$

which we can verify by contracting with $g^{\mu\nu} g^{\rho\sigma}$. We rewrite

$$\prod_{k=1}^m (n + 2(k - 1)) = \frac{2^m \Gamma(m + \frac{n}{2})}{\Gamma(\frac{n}{2})} \quad (4.15)$$

which is easily proven by induction. Therefore our final result is

$$k^{\mu_1} \dots k^{\mu_{2m}} = \frac{\Gamma(\frac{n}{2})}{2^m \Gamma(m + \frac{n}{2})} [g^{\dots} \dots g^{\dots}]^{\mu_1 \dots \mu_{2m}} (k^2)^m. \quad (4.16)$$

We can therefore strip away the Lorentz indices according to the following formula:

$$\int \frac{d^n k}{i\pi^{\frac{n}{2}}} \frac{k^{\mu_1} \dots k^{\mu_{2m}}}{(k^2 - R^2)^N} = (-1)^N [g^{\dots} \dots g^{\dots}]^{\mu_1 \dots \mu_{2m}} \left(-\frac{1}{2}\right)^m \frac{\Gamma(N - (n + 2m)/2)}{\Gamma(N)} (R^2)^{-N + (n + 2m)/2}. \quad (4.17)$$

We can see that the inclusion of powers of k on the numerator allow us to rewrite our tensor

integral in terms of scalar integrals of shifted dimension i.e. if we have $2m$ powers of the loop momentum in the numerator the corresponding scalar integral (once we have stripped away the Lorentz indices) can be recast as a $n + 2m$ dimensional integral. We can derive a similar result for our general tensor integral (4.2) except the difference lies in the treatment of the numerator. Firstly, we parameterize the integral in the same way. We obtain a symmetric denominator using the steps as before. To this end, we recall that we needed to shift the loop momentum a finite amount $k = l - Q$. This has an effect on the numerator giving:

$$I_N^{\mu_1 \cdots \mu_r} = \Gamma(N) \int_0^\infty \prod_{i=1}^N dz_i \delta(1 - \sum_{i=1}^N z_i) \times \\ \times \int \frac{d^n l}{i\pi^{\frac{n}{2}}} [l^2 - R^2 + i\delta]^{-N} (l - Q)^{\mu_1} (l - Q)^{\mu_2} \cdots (l - Q)^{\mu_r}. \quad (4.18)$$

Again, we must see how the tensor structure can be written. We have

$$\mathcal{N}^{\mu_1 \cdots \mu_r} = (l - Q)^{\mu_1} (l - Q)^{\mu_2} \cdots (l - Q)^{\mu_r} \\ = \sum_{k=0}^r \underbrace{[l \cdots l]_k}_{k} \underbrace{[Q \cdots Q]_{r-k}}_{r-k}^{\mu_1 \cdots \mu_r}. \quad (4.19)$$

There are $\binom{r}{k}$ ways of distributing the indices for each term in the sum. All these distributions are included and represented by the dots in the expression. If k is odd then the integral above vanishes so we rewrite $k = 2m$. Therefore, as before, there are $(2m - 1)!!$ ways of writing the l tensor in terms of metric tensors. The Q vector is simply the sum $Q^\mu = z_i r_i^\mu$ so

$$\mathcal{N}^{\mu_1 \cdots \mu_r} = \sum_{m=0}^{\lfloor r/2 \rfloor} \underbrace{[l \cdots l]_{2m}}_{2m} \underbrace{[Q \cdots Q]_{r-2m}}_{r-2m}^{\mu_1 \cdots \mu_r} \quad (4.20) \\ = \sum_{m=0}^{\lfloor r/2 \rfloor} (l^2)^m \frac{\Gamma(\frac{n}{2})}{2^m \Gamma(m + \frac{n}{2})} \sum_{j_1, \dots, j_{r-2m}=1}^N [z_{j_1} \cdots, z_{j_{r-2m}}] \left[\underbrace{g \cdots g}_m r_{j_1} \cdots r_{j_{r-2m}} \right]^{\mu_1 \cdots \mu_r}$$

and $\lfloor r/2 \rfloor$ is the nearest integer less or equal to $r/2$.

Using (4.17) we can rewrite this in terms of fundamental scalar integrals with Feynman parameters in the numerator:

$$I_N^{\mu_1 \cdots \mu_r} = \sum_{m=0}^{\lfloor r/2 \rfloor} \left(-\frac{1}{2}\right)^m \sum_{j_1, \dots, j_{r-2m}=1}^{N-1} [g \cdots g r_{j_1} \cdots r_{j_{r-2m}}]^{\mu_1 \cdots \mu_r} I_N^{n+2m}(j_1, \dots, j_{r-2m}). \quad (4.21)$$

where

$$I_N^n(j_1, \dots, j_p) = (-1)^N \Gamma(N - \frac{n}{2}) \int \prod_{i=1}^N dz_i \delta(1 - \sum_{l=1}^N z_l) z_{j_1} \cdots z_{j_p} (R^2)^{n/2-N}. \quad (4.22)$$

This is a key result. We are now able to write down our form factors in terms of **GB** e.g. for the 3-point case we have:

$$\begin{aligned}
 A^{3,0}(S) &= I_3^n(S) \\
 A_l^{3,1}(S) &= -I_3^n(l; S) \\
 B^{3,2}(S) &= -\frac{1}{2}I_3^{n+2}(S) \\
 A_{l_1, l_2}^{3,2}(S) &= I_3^n(l_1, l_2; S) \\
 B_l^{3,3} &= \frac{1}{2}I_3^{n+2}(l; S) \\
 A_{l_1, l_2, l_3}^{3,3}(S) &= -I_3^n(l_1, l_2, l_3, S).
 \end{aligned} \tag{4.23}$$

In Section 4.1.4 we outline how one can further reduce these expression i.e. express our **GB** in terms of **SI**.

4.1.4 Subtraction for Scalar Integrals

We shall show here that we can rewrite our previous integrals in terms of integrals with $N \leq 4$. The idea is that we can split the integral into an infrared finite part, I_{fin} , and a possibly infrared divergent part, I_{red} . We introduce a linear combination of propagators into the numerator with coefficients b_l and look to cancel them:

$$I_N^n = I_{\text{red}} + I_{\text{fin}} = \int \frac{d^n k}{i\pi^{\frac{n}{2}}} \frac{\sum_{l=1}^N b_l (q_l^2 - m_l^2)}{\prod_{l=1}^N (q_l^2 - m_l^2 + i\delta)} + \int \frac{d^n k}{i\pi^{\frac{n}{2}}} \frac{[1 - \sum_{l=1}^N b_l (q_l^2 - m_l^2)]}{\prod_{l=1}^N (q_l^2 - m_l^2 + i\delta)}. \tag{4.24}$$

We carry out the usual Feynman parameterization and momentum shift to give

$$I_{\text{fin}} = \Gamma(N) \int_0^\infty \prod_{i=1}^N dz_i \delta(1 - \sum_{i=1}^N z_i) \int \frac{d^n l}{i\pi^{\frac{n}{2}}} \frac{[1 - \sum_{l=1}^N b_l (\tilde{q}_l^2 - m_l^2)]}{[l^2 - R^2]^N} \tag{4.25}$$

where we have shifted the loop momenta appearing in the q vector:

$$\tilde{q}_l = r_l + l - \sum_{k=1}^N r_k z_k = l + \sum_{k=1}^N (\delta_{lk} - z_k) r_k. \tag{4.26}$$

We use the result for the shifted momenta:

$$\begin{aligned}
 \tilde{q}_j^2 &= l^2 + \left(\sum_{i=1}^N z_i (r_j - r_i) \right)^2 + 2l \cdot \left(\sum_{i=1}^N z_i (r_j - r_i) \right) \\
 &= l^2 + \sum_{i=1}^N z_i S_{ij} + m_j^2 + R^2 + 2l \cdot \left(\sum_{i=1}^N z_i (r_j - r_i) \right)
 \end{aligned} \tag{4.27}$$

where we have used the useful identity

$$\left(\sum_{i=1}^N z_i (r_j - r_i) \right)^2 = \sum_{i=1}^N z_i S_{ij} + m_j^2 + R^2. \quad (4.28)$$

Now we can rewrite the square bracket as

$$-(l^2 + R^2) \sum_{j=1}^N b_j + \sum_{j=1}^N z_j (1 - (\mathcal{S} \cdot b)_j) + \text{odd in } l. \quad (4.29)$$

So if we can solve, for b ,

$$(\mathcal{S} \cdot b)_j = 1, j = 1, \dots, N \quad (4.30)$$

then our equation simplifies to give

$$I_{\text{fin}} = -\Gamma(N) \left(\sum_{l=1}^N b_l \right) \int_0^\infty \prod_{j=1}^N dz_j \delta(1 - \sum_{j=1}^N z_j) \int \frac{d^n l}{i\pi^{\frac{n}{2}}} \frac{l^2 + R^2}{(l^2 - R^2)^N}. \quad (4.31)$$

Using (C.39) we obtain the following result

$$I_{\text{fin}} = - \left(\sum_{l=1}^N b_l \right) (N - n - 1) I_N^{n+2}. \quad (4.32)$$

Therefore if $\det \mathcal{S} \neq 0$ then we can decompose any N -point scalar integral as

$$I_N^n = \sum_{j=1}^N b_j I_{N-1}^D(S \setminus \{j\}) - (N - n - 1) B I_N^{n+2} \quad (4.33)$$

$$b_j = \sum_{i=1}^N \mathcal{S}_{ij}^{-1}, B = \sum_{j=1}^N b_j. \quad (4.34)$$

where $S \setminus \{j\}$ represents a diagram with the j propagator pinched.

4.1.4.1 The Gram matrix

We have the relation

$$\sum_{j=1}^N b_j \det \mathcal{S} = (-1)^{N+1} \det \mathcal{G} \quad (4.35)$$

where $\det \mathcal{G}$ is the Gram matrix $G_{ij} = 2r_i \cdot r_j$. We can construct the matrices \mathcal{S} and \mathcal{G} from 4-dimensional external momenta and they have the following properties:

$$\det \mathcal{G} = 0 \text{ for } N \geq 6 \tag{4.36}$$

$$\det \mathcal{S} = 0 \text{ for } N \geq 7. \tag{4.37}$$

The first relation, (4.36), is an important result and implies that the coefficient $\sum_{j=1}^N b_j = 0$ for all integrals with $N \geq 6$. This implies that the second integral in (4.33) vanishes and we can always write these integrals as combinations of lower point integrals. So the N -point integral can be written as a sum of the $N - 1$ -point integrals and this can be continued recursively until $N = 5$. Then the procedure above is followed. But for $N = 5$ our I_{fin} coefficient $N - n - 1$ is of order ϵ which multiplies the convergent integral I_N^{n+2} . For our applications (and all one-loop calculations) this term can be dropped and we can write a scalar pentagon in terms of the sum of the five boxes that result from pinching the five different propagators.

So to summarize, using the procedure above any arbitrary scalar N -point function can be algebraically reduced to 3-point functions and $(n + 2)$ dimensional 4-point functions. The infrared poles lie in the 3-point functions and are naturally separated from the rest of the functions.

4.1.4.2 The case $\det \mathcal{S} = 0$

If $\det \mathcal{S} = 0$ then (4.30) cannot be solved and a different procedure based on the pseudo-inverse must be pursued. The details are in [67]. The conclusion is that one can find the solution b for arbitrary N . However, numerical instabilities may still occur in special momentum configurations. Unlike, traditional methods where the instabilities are an artifact of the tensor reduction scheme (vanishing Gram determinants in the reduction of tensor integrals) these singularities are due to physical singularities including soft/collinear or threshold singularities.

4.1.5 Subtraction for Tensor integrals

We now carry out the same argument as before but for the class of tensor integrals. Again, we look to split an arbitrary N -point, rank r , tensor integral into two pieces: an infrared finite and an infrared divergent part. The infrared divergent part will be an $N - 1$ -point integral, like in the previous case and will also be of rank $r - 1$. We begin with our definition of a tensor

integral from (4.4)

$$\begin{aligned}
 I_N^{n,\mu_1,\dots,\mu_r} &= \int \frac{d^n k}{i\pi^{\frac{n}{2}}} \frac{k^{\mu_1} \dots k^{\mu_r}}{(q_1^2 - m_1^2 + i\delta) \dots (q_N^2 - m_N^2 + i\delta)} \\
 &= I_{\text{fin}}^{\mu_1,\dots,\mu_r} + I_{\text{red}}^{\mu_1,\dots,\mu_r} \\
 &= \int \frac{d^n k}{i\pi^{\frac{n}{2}}} \frac{\left[k^{\mu_1} + \sum_{j=1}^N C_j^\mu (q_j^2 - m_j^2) \right] k^{\mu_2} \dots k^{\mu_r}}{(q_1^2 - m_1^2 + i\delta) \dots (q_N^2 - m_N^2 + i\delta)} \\
 &\quad - \int \frac{d^n k}{i\pi^{\frac{n}{2}}} \frac{\sum_{j=1}^N C_j^\mu (q_j^2 - m_j^2) k^{\mu_2} \dots k^{\mu_r}}{(q_1^2 - m_1^2 + i\delta) \dots (q_N^2 - m_N^2 + i\delta)}.
 \end{aligned} \tag{4.38}$$

We follow the usual procedure of shifting k in order to symmetrize the denominator. This shifts the numerator also and, using (4.27), we can write the term in square brackets as:

$$\begin{aligned}
 A^\mu &= k^{\mu_1} + \sum_{j=1}^N C_j^\mu (q_j^2 - m_j^2) = l^\mu - \sum_{i=1}^N z_i r_i^\mu + \sum_{j=1}^N C_j^\mu (q_j^2 - m_j^2) \\
 &= l^\mu + (l^2 + R^2) \sum_{j=1}^N C_j^\mu + \sum_{i=1}^N z_i \left\{ \sum_{j=1}^N C_j^\mu [\mathcal{S}_{ij} + 2l \cdot (r_j - r_i)] - r_i^\mu \right\}.
 \end{aligned} \tag{4.39}$$

In analogy to the scalar condition, (4.30), if we can solve for C_μ

$$\sum_{j=1}^N \mathcal{S}_{ij} C_j^\mu = r_i^\mu \tag{4.40}$$

then the terms in A^μ are either proportional to l or R^2 . If (4.40) is satisfied then we can write A^μ as

$$A^\mu = l_\nu \left[g^{\mu\nu} + 2 \sum_{j=1}^N C_j^\mu (r_j - r_a)^\nu + 2 \sum_{i=1}^N z_i \sum_{j=1}^N C_j^\mu (r_a - r_i)^\nu \right] + (l^2 + R^2) \sum_{j=1}^N C_j^\mu. \tag{4.41}$$

In the previous step we have introduced an arbitrary vector r_a in order to split the sum over the Feynman parameters. Plugging this into our expression we get two integrals that can be related to higher dimensional scalar integrals using (4.21). In fact, to get the explicit form, one needs to slightly modify the derivation as we shift only $r-1$ k vectors in the numerator in the same way. The resultant integral I_{fin} is infrared finite and therefore we separated our rank r , N -point tensor integral into an infrared finite part and a rank $r-1$, $N-1$ -point tensor integral.

Like the scalar case, if $\det \mathcal{S} = 0$, one can still find solutions based on the pseudo-inverse approach. In fact one can make a stronger statement, and say that for $N \geq 6$ all integrals can be reduced iteratively to 5-point integrals.

4.1.6 Landau conditions

The conditions for an integral to contain an infrared singularity were first written down by Landau [69]. The Landau equations take the form [70] in the representation (C.2):

$$\begin{aligned} \sum_{i=1}^N q_i z_i &= 0 \text{ for all } i \text{ or} \\ z_i(q_i^2 - m_i^2) &= 0 \text{ for all } i. \end{aligned} \tag{4.42}$$

The first condition corresponds to the sum of all the momentum as we traverse around the loop; if this vanishes we can visualise the loop vanishing to a point. The second condition corresponds to (if all the Feynman parameters are non-zero) all the internal propagators being on-shell simultaneously. This is known as a *leading* singularity and corresponds to a kinematic point which is either a physical threshold or an anomalous threshold. If the conditions are satisfied by one of the Feynman parameters being zero we have a *lower-order* singularity, so called because one would obtain the same singularity if the corresponding internal propagator was contracted to a point; the vanishing of its corresponding z effectively removes the propagator from the graph.

We can also consider the Landau singularities after the integration of the loop momenta has been carried out. Because the k integral has been carried out the condition is now:

$$\mathcal{F} = 0. \tag{4.43}$$

where as before $\mathcal{F} = z_i S_{ij} z_j$. This leads to the Landau conditions

$$\begin{aligned} z_i &= 0 \text{ or} \\ \frac{\partial \mathcal{F}}{\partial z_i} &= 0 \text{ for all } i. \end{aligned} \tag{4.44}$$

Since \mathcal{F} is a homogeneous function of z_i we have (due to Euler's theorem)

$$\sum_i z_i \frac{\partial \mathcal{F}}{\partial z_i} \propto \mathcal{F} \tag{4.45}$$

hence (4.43) is satisfied when the other two conditions are. The first condition $\frac{\partial \mathcal{F}}{\partial z_i} = 0$ corresponds to the leading singularities above. For NLO calculations we are interested in soft and collinear singularities when external virtualities and internal masses have fixed values. We start from these conditions when looking at the infrared divergent triangle integrals.

4.2 Evaluation of 3-point functions

If $\det \mathcal{S}$ is zero we saw that we run into problems in our reduction reduction to **GB**. All the infrared divergences are isolated to the triangle functions in **GB** with or without Feynman parameters in the numerator. In this section we evaluate the necessary infrared divergent scalar

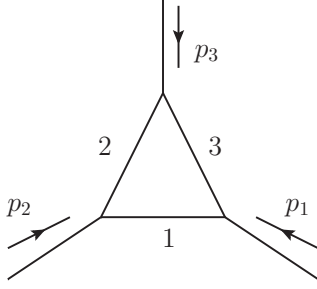


Figure 4.2: The kinematic setup for our triangle integrals.

triangle integrals in n dimensions. We define the scalar N -point integral to be

$$I_N^n = \int \frac{d^n k}{i\pi^{n/2}} \frac{1}{\prod_{i=1}^N (q_i^2 - m_i^2 + i\delta)} \quad (4.46)$$

in n dimensions. Graphically, the kinematics are set up as in Figure 4.2. with propagator momenta

$$\begin{aligned} q_1 &= k - p_1 \\ q_2 &= k - p_1 - p_2 \\ q_3 &= k \end{aligned}$$

and the propagator masses are labelled as m_1^2 , m_2^2 and m_3^2 as shown in the diagram. We use the following Mandelstam variables:

$$s_i = p_i \cdot p_i.$$

Here we are interested in 3-point integrals. The n dimensional integral is written as

$$\begin{aligned} I_3^n(s_1, s_2, s_3, m_1^2, m_2^2, m_3^2) = & \quad (4.47) \\ & -\Gamma(3 - n/2) \int dx_1 dx_2 dx_3 \delta(1 - x_1 - x_2 - x_3) \mathcal{F}^{-3+n/2} \\ & \mathcal{F} = (-s_1)x_3x_1 + (-s_2)x_1x_2 + (-s_3)x_2x_3 + \sum_{j=1}^3 m_j^2 x_j - i\delta \end{aligned}$$

The definition above relates to the Veltman-Passarino convention as follows [65] :

$$I_3^n = (s_1, s_2, s_3, m_1^2, m_2^2, m_3^2) = C_0(s_1, s_2, s_3, m_3^2, m_1^2, m_2^2) \quad (4.48)$$

We will present results for the following integrals sorted with respect to the number of internal masses present (as seen in Figure 4.3):

- Triangles with no internal mass
 - 4.2.1.1 $I_3^n(s_1, 0, 0, 0, 0, 0)$
 - 4.2.1.2 $I_3^n(s_1, s_2, 0, 0, 0, 0)$
 - 4.2.1.3 $I_3^n(s_1, s_1, 0, 0, 0, 0)$
- Triangles with one internal mass
 - 4.2.2.1 $I_3^n(s_1, s_2, 0, m_1^2, 0, 0)$
 - 4.2.2.2 $I_3^n(m_1^2, s_2, 0, m_1^2, 0, 0)$
 - 4.2.2.3 $I_3^n(s_1, s_1, 0, m_1^2, 0, 0)$
 - 4.2.2.4 $I_3^n(m_1^2, m_1^2, 0, m_1^2, 0, 0)$
- Triangles with two internal masses
 - 4.2.3.1 $I_3^n(m_1^2, s_2, m_2^2, m_1^2, m_2^2, 0)$
 - 4.2.3.2 $I_3^n(m_1^2, s_2, m_1^2, m_1^2, m_1^2, 0)$

These results were checked against the program [71].

4.2.1 Triangles with no internal mass

4.2.1.1 The integral $I_3^n(s_1, 0, 0, 0, 0, 0)$

Kinematics are setup as in Figure 4.3(a):

$$s_1 \neq 0, \quad s_2 = s_3 = m_j^2 = 0$$

$$\begin{aligned}
 I_3^n(s_1, 0, 0, 0, 0, 0) &= \mu^{-2\epsilon} \mu^{2\epsilon} \frac{\Gamma(1+\epsilon)\Gamma(1-\epsilon)^2}{\Gamma(1-2\epsilon)} \frac{1}{\epsilon^2} \frac{(-s_1 - i\delta)^{-\epsilon}}{s_1} \\
 &= \mu^{-2\epsilon} \frac{\Gamma(1+\epsilon)\Gamma(1-\epsilon)^2}{\Gamma(1-2\epsilon)} \frac{1}{s_1} \left(\frac{1}{\epsilon^2} - \frac{1}{\epsilon} \log \left(\frac{-s_1 - i\delta}{\mu^2} \right) \right. \\
 &\quad \left. + \frac{1}{2} \log^2 \left(\frac{-s_1 - i\delta}{\mu^2} \right) \right) + \mathcal{O}(\epsilon).
 \end{aligned} \tag{4.49}$$

4.2.1.2 The integral $I_3^n(s_1, s_2, 0, 0, 0, 0)$

Kinematics are setup as in Figure 4.3(b):

$$s_1 \neq 0, \quad s_2 \neq 0, \quad s_3 = m_j^2 = 0.$$

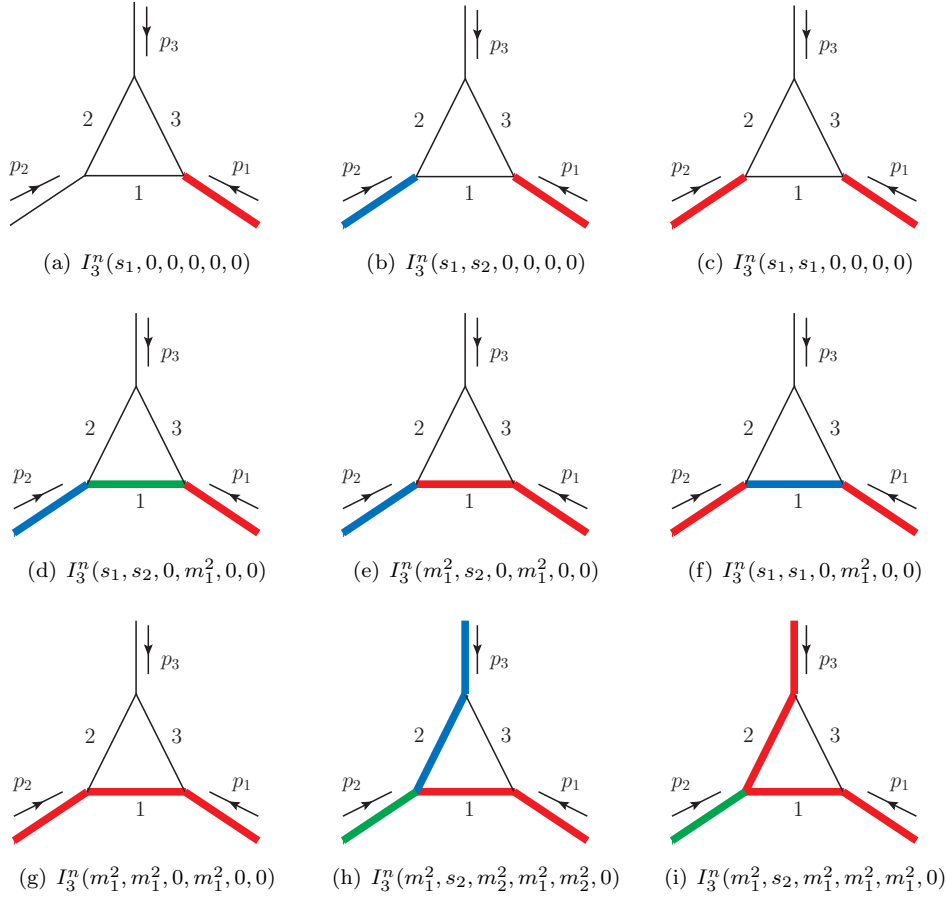


Figure 4.3: The set of infrared divergent integrals.

$$\begin{aligned}
 I_3^n(s_1, s_2, 0, 0, 0, 0) &= \mu^{-2\epsilon} \mu^{2\epsilon} \frac{\Gamma(1+\epsilon)}{\epsilon^2} \frac{\Gamma(1-\epsilon)^2}{\Gamma(1-2\epsilon)} \frac{1}{s_1 - s_2} [(-s_1 - i\delta)^{-\epsilon} - (-s_2 - i\delta)^{-\epsilon}] \quad (4.50) \\
 &= \mu^{-2\epsilon} \frac{\Gamma(1+\epsilon)}{\epsilon^2} \frac{\Gamma(1-\epsilon)^2}{\Gamma(1-2\epsilon)} \frac{1}{s_1 - s_2} \left[\left(\frac{-s_1 - i\delta}{\mu^2} \right)^{-\epsilon} - \left(\frac{-s_2 - i\delta}{\mu^2} \right)^{-\epsilon} \right]
 \end{aligned}$$

4.2.1.3 The integral $I_3^n(s_1, s_1, 0, 0, 0, 0)$

Kinematics are setup as in Figure 4.3(c):

$$s_1 = s_2 \neq 0, \quad s_3 = m_j^2 = 0.$$

$$\begin{aligned}
I_3^n(s_1, s_1, 0, 0, 0, 0) &= \mu^{-2\epsilon} \mu^{2\epsilon} \frac{\Gamma(1+\epsilon) \Gamma(1-\epsilon)^2}{\epsilon \Gamma(1-2\epsilon)} (-s_1 - i\delta)^{-1-\epsilon} \\
&= \mu^{-2\epsilon} \frac{\Gamma(1+\epsilon) \Gamma(1-\epsilon)^2}{\Gamma(1-2\epsilon)} \frac{1}{s_1} \left(-\frac{1}{\epsilon} + \log \left(\frac{-s_1 - i\delta}{\mu^2} \right) \right) + \mathcal{O}(\epsilon).
\end{aligned} \tag{4.51}$$

We see that the ϵ pole structure of $I_3^n(s_1, s_2, 0, 0, 0, 0)$ changes in the limit $s_2 \rightarrow s_1$. This limit does not commute with the ϵ expansion.

4.2.2 Triangles with one internal mass

4.2.2.1 The integral $I_3^n(s_1, s_2, 0, m_1^2, 0, 0)$

Kinematics are setup as in Figure 4.3(d):

$$s_1 \neq 0, s_2 \neq 0, m_1^2 \neq 0, s_3 = m_2^2 = m_3^2 = 0.$$

$$\begin{aligned} I_3^n(s_1, s_2, 0, m_1^2, 0, 0) = & \mu^{-2\epsilon} \frac{\Gamma(1+\epsilon)}{s_1 - s_2} \left[\left(\frac{1}{\epsilon} - \log \left(\frac{m_1^2 - i\delta}{\mu^2} \right) \right) \log \left(\frac{-s_2 + m_1^2 - i\delta}{-s_1 + m_1^2 - i\delta} \right) \right. \\ & - \log^2 \left(\frac{-s_2 + m_1^2 - i\delta}{m_1^2} \right) + \log^2 \left(\frac{-s_1 + m_1^2 - i\delta}{m_1^2} \right) \\ & \left. + \text{Li}_2 \left(\frac{s_1 + i\delta}{m_1^2} \right) - \text{Li}_2 \left(\frac{s_2 + i\delta}{m_1^2} \right) \right] + \mathcal{O}(\epsilon). \end{aligned} \quad (4.52)$$

In this formula, a complex mass with negative imaginary part may be used. In the limit $m_1^2 \rightarrow 0$ we find the result of $I_3^n(s_1, s_2, 0, 0, 0, 0)$ given above. The results for the real and imaginary parts are plotted in Figure 4.4.

			ϵ^{-2}		ϵ^{-1}		ϵ^0	
s_1	s_2	m_1^2	Re	Im	Re	Im	Re	Im
11.0	7.0	5.0	0.00000000	0.00000000	-0.27465307	0.00000000	0.27532857	-1.37070786
7.0	3.0	5.0	0.00000000	0.00000000	0.00000000	0.78539816	-2.06952942	0.43952121
7.0	-3.0	5.0	0.00000000	0.00000000	0.13862944	0.31415927	-0.86348936	0.17580848
3.0	-3.0	5.0	0.00000000	0.00000000	0.23104906	0.00000000	-0.05946265	0.00000000
-3.0	-5.0	5.0	0.00000000	0.00000000	0.11157178	0.00000000	-0.16216272	0.00000000

Table 4.2: Kinematic points for $I_3^n(s_1, s_2, 0, m_1^2, 0, 0)$.

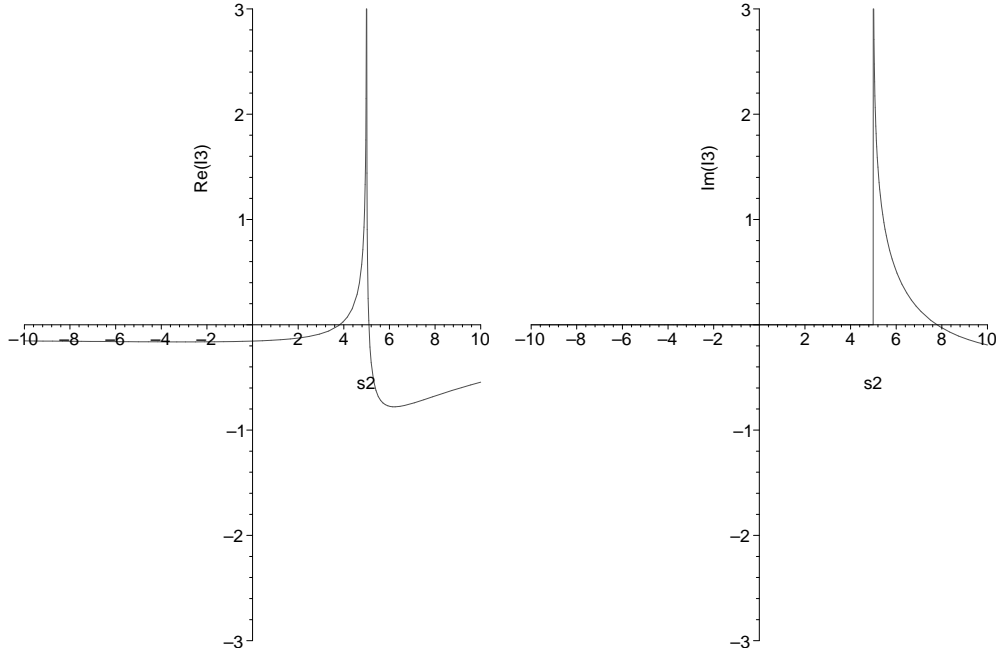


Figure 4.4: Graphs of the real part (left) and imaginary part (right) of the ϵ^0 term of $I_3^n(s_1, s_2, 0, m_1^2, 0, 0)$ against s_2 with fixed $m_1^2 = 5.0$ and $s_1 = -5.0$.

4.2.2.2 The integral $I_3^n(m_1^2, s_2, 0, m_1^2, 0, 0)$

Kinematics are setup as in Figure 4.3(e):

$$s_1 = m_1^2 \neq 0, \quad s_2 \neq 0, \quad s_3 = m_2^2 = m_3^2 = 0$$

$$\begin{aligned} & I_3^n(m_1^2, s_2, 0, m_1^2, 0, 0) \\ &= \mu^{-2\epsilon} \frac{\Gamma(1+\epsilon)}{(-s_2 + m_1^2)} \left[-\frac{1}{2\epsilon^2} + \frac{1}{\epsilon} \left\{ \log\left(\frac{-s_2 + m_1^2 - i\delta}{\mu^2}\right) - \frac{1}{2} \log\left(\frac{m_1^2 - i\delta}{\mu^2}\right) \right\} \right. \\ &+ \frac{1}{2} \left\{ 2 \log\left(\frac{-s_2 - i\delta}{-s_2 + m_1^2 - i\delta}\right) \log\left(\frac{-s_2 + m_1^2 - i\delta}{m_1^2 - i\delta}\right) + \frac{\pi^2}{3} \right. \\ &\left. \left. - 2\text{Li}_2\left(\frac{m_1^2 - i\delta}{-s_2 + m_1^2 - i\delta}\right) - \log^2\left(\frac{-s_2 + m_1^2 - i\delta}{\mu^2}\right) + \frac{1}{2} \log^2\left(\frac{m_1^2 - i\delta}{\mu^2}\right) \right\} \right] + \mathcal{O}(\epsilon). \end{aligned} \quad (4.53)$$

We see that the ϵ pole structure of $I_3^n(s_1, s_2, 0, m_1^2, 0, 0)$ changes in the limit $s_1 \rightarrow m_1^2$. This limit does not commute with the ϵ expansion. In this formula, a complex mass with negative imaginary part may be used. To compare to [71] we must consider the factor

$$\frac{\Gamma(1-\epsilon)^2}{\Gamma(1-2\epsilon)} = 1 - \frac{\pi^2}{6}\epsilon^2 + \mathcal{O}(\epsilon^3) \quad (4.54)$$

that does not appear in our definition of our integral. This factor combines with the double pole in ϵ to give an extra finite contribution to the result. This factor is not added to the results below. The results for the real and imaginary parts are plotted in Figure 4.5.

		ϵ^{-2}		ϵ^{-1}		ϵ^0	
s_2	m_1^2	Re	Im	Re	Im	Re	Im
7.0	5.0	0.25000000	0.00000000	0.05578589	1.57079633	-3.76904155	0.87904242
3.0	5.0	-0.25000000	0.00000000	-0.05578589	-0.00000000	-0.37001728	-0.00000000
-3.0	5.0	-0.06250000	0.00000000	0.15934032	-0.00000000	-0.13710131	0.00000000

Table 4.3: Kinematic points for $I_3^n(m_1^2, s_2, 0, m_1^2, 0, 0)$

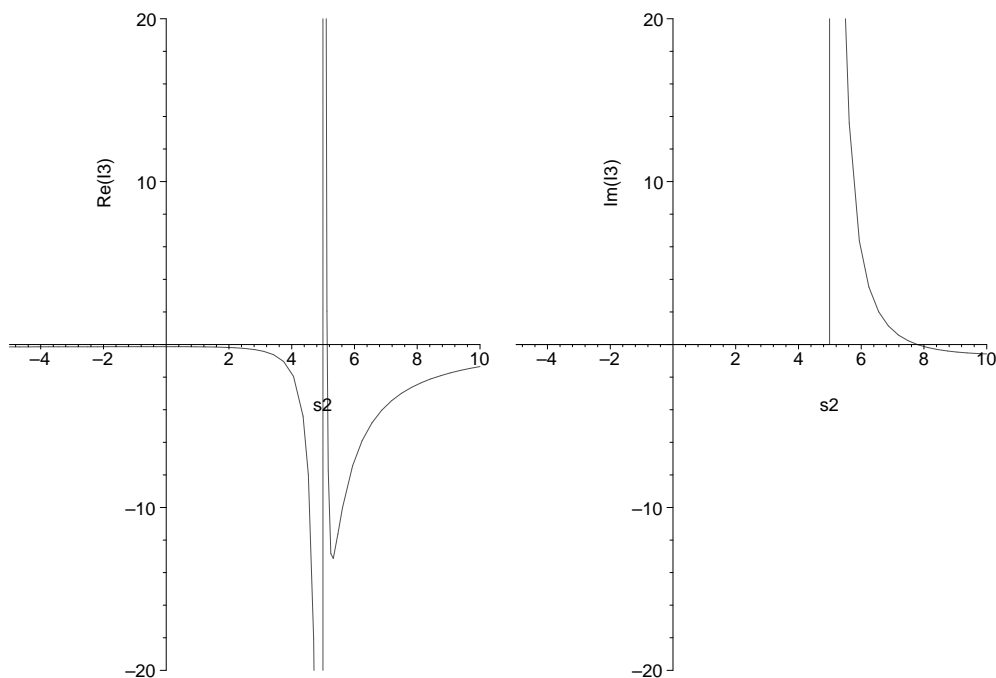


Figure 4.5: Graphs of the real part (left) and imaginary part (right) of the ϵ^0 term of $I_3^n(m_1^2, s_2, 0, m_1^2, 0, 0)$ against s_2 with fixed $m_1^2 = 5.0$ and $s_1 = -5.0$.

4.2.2.3 The integral $I_3^n(s_1, s_1, 0, m_1^2, 0, 0)$

Kinematics are setup as in Figure 4.3(f):

$$s_1 = s_2 \neq 0, \quad s_3 = m_2^2 = m_3^2 = 0.$$

$$\begin{aligned} I_3^n(s_1, s_1, 0, m_1^2, 0, 0) & \quad (4.55) \\ &= \mu^{-2\epsilon} \mu^{2\epsilon} \frac{\Gamma(1+\epsilon)}{(-s_1 + m_1^2)} \left[\frac{1}{\epsilon} (-s_1 + m_1^2 - i\delta)^{-\epsilon} - \frac{m_1^2}{s_1} \log \left(\frac{-s_1 + m_1^2 - i\delta}{m_1^2 - i\delta} \right) \right] \\ &= \mu^{-2\epsilon} \frac{\Gamma(1+\epsilon)}{(-s_1 + m_1^2)} \left[\frac{1}{\epsilon} - \log \left(\frac{-s_1 + m_1^2 - i\delta}{\mu^2} \right) - \frac{m_1^2}{s_1} \log \left(\frac{-s_1 + m_1^2 - i\delta}{m_1^2 - i\delta} \right) \right] + \mathcal{O}(\epsilon). \end{aligned}$$

We see that the ϵ pole structure of $I_3^n(s_1, s_2, 0, m_1^2, 0, 0)$ changes in the limit $s_2 \rightarrow s_1$. In this formula, a complex mass with negative imaginary part may be used. The results for the real and imaginary parts are plotted in Figure 4.6.

		ϵ^{-2}		ϵ^{-1}		ϵ^0	
s_1	m_1^2	Re	Im	Re	Im	Re	Im
7.0	5.0	0.00000000	0.00000000	-0.50000000	0.00000000	0.01932690	-2.69279370
3.0	5.0	0.00000000	0.00000000	0.50000000	0.00000000	0.41700202	0.00000000
-3.0	5.0	0.00000000	0.00000000	0.12500000	0.00000000	-0.16201277	0.00000000

Table 4.4: Kinematic points for $I_3^n(s_1, s_1, 0, m_1^2, 0, 0)$.

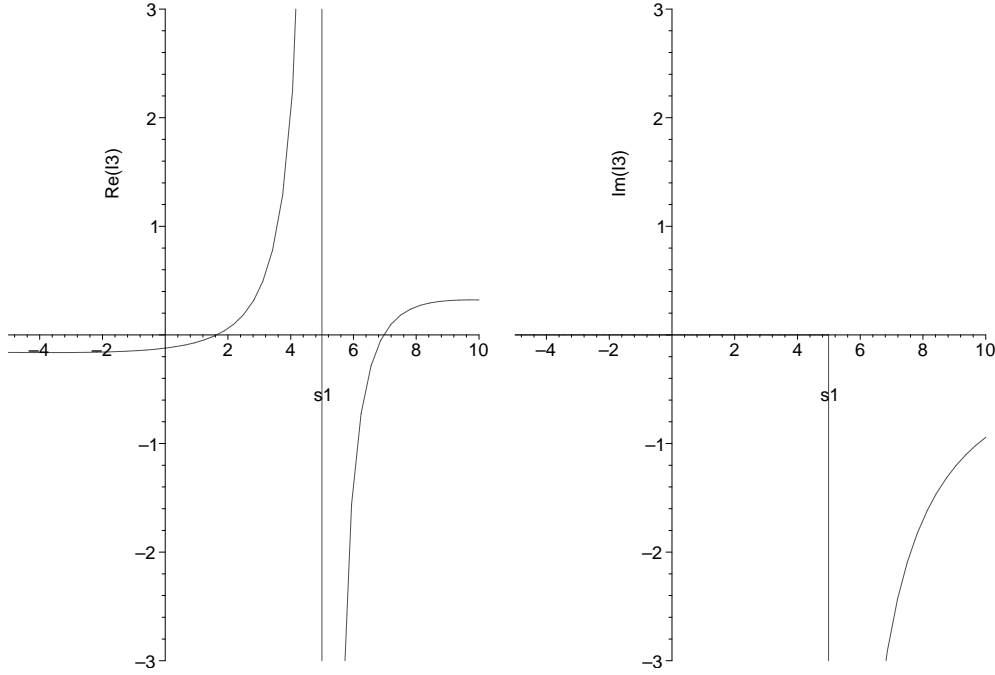


Figure 4.6: Graphs of the real part (left) and imaginary part (right) of the ϵ^0 term of $I_3^n(s_1, s_1, 0, m_1^2, 0, 0)$ against s_1 with fixed $m_1^2 = 5.0$.

4.2.2.4 The integral $I_3^n(m_1^2, m_1^2, 0, m_1^2, 0, 0)$

Kinematics are setup as in Figure 4.3(g):

$$s_1 = s_2 = m_1^2 \neq 0, \quad s_3 = m_2^2 = m_3^2 = 0$$

$$\begin{aligned} I_3^n(m_1^2, m_1^2, 0, m_1^2, 0, 0) &= \mu^{-2\epsilon} \mu^{2\epsilon} \frac{\Gamma(1+\epsilon)}{2\epsilon} \frac{1}{(m_1^2)^{1+\epsilon}} \left(\frac{1}{-1-2\epsilon} \right) \\ &= \mu^{-2\epsilon} \Gamma(1+\epsilon) \left(\frac{\mu^2}{m_1^2} \right)^\epsilon \frac{1}{m_1^2} \left(-\frac{1}{2\epsilon} + 1 + \mathcal{O}(\epsilon) \right) \\ &= \mu^{-2\epsilon} \frac{\Gamma(1+\epsilon)}{m_1^2} \left(-\frac{1}{2\epsilon} - \frac{1}{2} \log \left(\frac{\mu^2}{m_1^2} \right) + 1 \right) + \mathcal{O}(\epsilon). \end{aligned} \quad (4.56)$$

We evaluate for one positive $m_1^2 = 5.0$ and obtain the result $-0.10000000 \frac{1}{\epsilon} + 0.36094380$.

4.2.3 Triangles with two internal masses

4.2.3.1 The integral $I_3^n(m_1^2, s_2, m_2^2, m_1^2, m_2^2, 0)$

Kinematics are setup as in Figure 4.3(h):

$$s_2 \neq 0, s_1 = m_1^2 \neq 0, s_3 = m_2^2 \neq 0, m_3^2 = 0.$$

$$\begin{aligned}
 I_3^n(m_1^2, s_2, m_2^2, m_1^2, m_2^2, 0) = & \quad (4.57) \\
 & \mu^{-2\epsilon} \frac{\Gamma(1+\epsilon)}{2(-s_2)(u_+ - u_-)} \left[\frac{1}{\epsilon} \left[\log\left(\frac{u_+}{-u_-}\right) - \log\left(\frac{u_+ - 1}{1 - u_-}\right) \right] \right. \\
 & - \log\left(\frac{1 - u_-}{u_+ - 1}\right) \log\left(\frac{m_1^2 - i\delta}{\mu^2}\right) \\
 & - \log\left(\frac{u_+}{-u_-}\right) \log\left(\frac{m_2^2 - i\delta}{\mu^2}\right) \\
 & + 2 \log(u_+ - u_-) [\log(u_+ - 1) - \log(u_+)] \\
 & - \frac{1}{2} \log^2(-u_-) + \frac{1}{2} \log^2(u_+) + \frac{1}{2} \log^2(1 - u_-) - \frac{1}{2} \log^2(u_+ - 1) \\
 & + \log(u_+) \log(-u_-) - \log(u_+ - 1) \log(1 - u_-) \\
 & \left. - 2\text{Li}_2\left(\frac{u_+ - 1}{u_+ - u_-}\right) + 2\text{Li}_2\left(\frac{u_+}{u_+ - u_-}\right) \right] + \mathcal{O}(\epsilon)
 \end{aligned}$$

where the following quantities are defined

$$\begin{aligned}
 u_{\pm} &= \frac{1}{-2s_2} (-s_2 + m_2^2 - m_1^2 \pm \beta) \\
 \beta &= \sqrt{\lambda(s_2, m_1^2, m_2^2) + i\delta \text{sgn}(s_2)}
 \end{aligned}$$

and also in this case the relations $s_2 u_+ u_- = m_2^2 - i\delta$ and $s_2(u_+ - 1)(u_- - 1) = m_1^2 - i\delta$ have been used. Note that in the Euclidean region $s_2 < 0$ we have $u_+ > 1$ and $u_- < 0$ and the $i\delta$ can be omitted. The results for this graph are plotted in Figure 4.7. The representation found here is more compact than the one found in [71] (there are only two dilogarithms) and is valid for arbitrary values of s_2 .

			ϵ^{-2}		ϵ^{-1}		ϵ^0	
s_2	m_1^2	m_2^2	Re	Im	Re	Im	Re	Im
25.0	9.0	3.0	0.00000000	0.00000000	-0.08890625	0.40223972	-0.94912920	-0.35879704
10.0	9.0	3.0	0.00000000	0.00000000	0.13503949	0.00000000	-0.16794830	-0.00000000
1.0	9.0	3.0	0.00000000	0.00000000	0.09439224	0.00000000	-0.15265716	-0.00000000
-5.0	9.0	3.0	0.00000000	0.00000000	0.07991448	0.00000000	-0.14241331	-0.00000000

Table 4.5: Kinematic points for $I_3^n(m_1^2, s_2, m_2^2, m_1^2, m_2^2, 0)$.

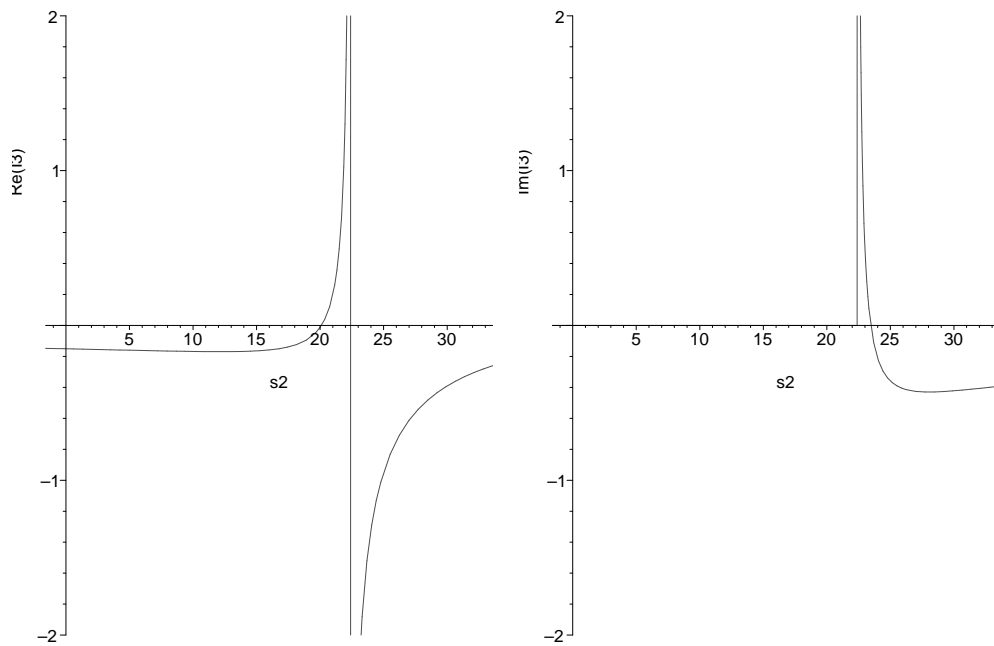


Figure 4.7: Graphs of the real part (left) and imaginary part (right) of the ϵ^0 term of $I_3^n(m_1^2, s_2, m_2^2, m_1^2, m_2^2, 0)$ against s_2 with fixed $m_1^2 = 9.0$ and $m_2^2 = 3.0$.

4.2.3.2 The integral $I_3^n(m_1^2, s_2, m_1^2, m_1^2, m_1^2, 0)$

Kinematics are setup as in Figure 4.3(i):

$$s_2 \neq 0, s_1 = s_3 = m_1^2 = m_2^2 \neq 0, m_3^2 = 0.$$

We can safely take the limit of the above result $m_2^2 \rightarrow m_1^2$ without changing the pole structure. No new singularities arise. In this limit our variables relate to each other as follows

$$\begin{aligned} 1 - u_- &= u_+ \\ u_+ - 1 &= -u_- \end{aligned}$$

Now

$$u_{\pm} = \frac{1}{2} \left(1 \pm \sqrt{1 - \frac{4(m_1^2 - i\delta)}{s_1}} \right)$$

$$\begin{aligned} I_3^n(m_1^2, s_2, m_1^2, m_1^2, m_1^2, 0) &= \tag{4.58} \\ \mu^{-2\epsilon} \frac{\Gamma(1 + \epsilon)}{2(-s_2)(u_+ - u_-)} &\left[\frac{2}{\epsilon} \log\left(\frac{u_+}{-u_-}\right) \right. \\ -2 \log\left(\frac{u_+}{-u_-}\right) &\left(\log\left(\frac{m_1^2 - i\delta}{\mu^2}\right) + \log(u_+ - u_-) \right) \\ -\log^2(-u_-) + \log^2(u_+) &- 2\text{Li}_2\left(\frac{-u_-}{u_+ - u_-}\right) + 2\text{Li}_2\left(\frac{u_+}{u_+ - u_-}\right) \left. \right] + \mathcal{O}(\epsilon) \end{aligned}$$

The results for this graph are plotted in Figure 4.8

		ϵ^{-2}		ϵ^{-1}		ϵ^0	
s_2	m_1^2	Re	Im	Re	Im	Re	Im
25.0	5.0	0.00000000	0.00000000	-0.08608179	0.28099259	-0.56766811	-0.45224013
13.0	5.0	0.00000000	0.00000000	0.19660467	0.00000000	-0.17380014	0.00000000
-5.0	5.0	0.00000000	0.00000000	0.08608179	0.00000000	-0.15125481	-0.00000000

Table 4.6: Kinematic points for $I_3^n(m_1^2, s_2, m_1^2, m_1^2, m_1^2, 0)$.

4.3 Evaluation of 2-point functions

We consider the analytic calculation of bubble integrals. Graphically, the kinematics are set up

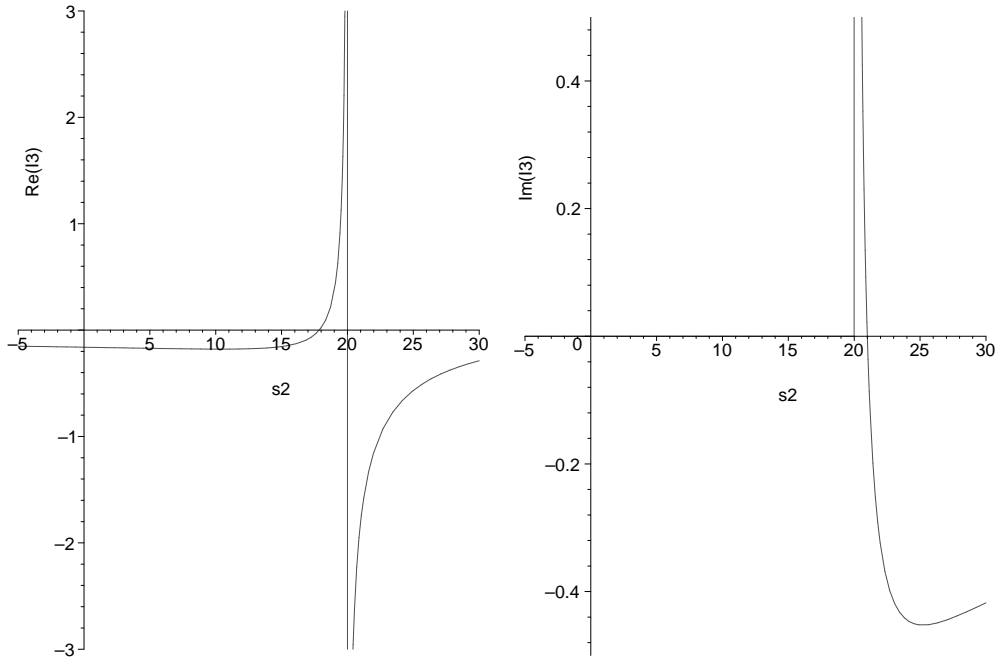


Figure 4.8: Graphs of the real part (left) and imaginary part (right) of the ϵ^0 term of $I_3^n(m_1^2, s_2, m_1^2, m_1^2, m_1^2, 0)$ against s_2 with fixed $m_1^2 = 5.0$.

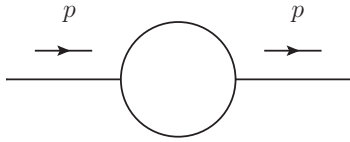


Figure 4.9: Kinematics for bubble integrals.

as in Figure 4.9. Propagator momenta are defined as:

$$q_1 = k - p \quad (4.59)$$

$$q_2 = k \quad (4.60)$$

and we have one Mandelstam variable:

$$s = p \cdot p. \quad (4.61)$$

The n -dimensional 2-point integral is written as:

$$I_2^n(s; m_1^2, m_2^2) = \Gamma\left(2 - \frac{n}{2}\right) \int_0^1 dx [\mathcal{F}]^{-2 + \frac{n}{2}} \quad (4.62)$$

where

$$\mathcal{F} = (-s)x\bar{x} + xm_1^2 + \bar{x}m_2^2 - i\delta \quad (4.63)$$

The definition above relates to the Veltman-Passarino convention as follows:

$$I_3^n = (s_1, m_1^2, m_2^2) = B_0(s_1, m_2^2, m_1^2) \quad (4.64)$$

Of course the scalar integral is symmetric in the two masses.

We will present results for the following integrals sorted with respect to the number of internal masses present:

- Bubbles with no internal mass
 - 4.3.1.1 $I_2^n(s; 0, 0)$
- Bubbles with one internal mass
 - 4.3.2.1 $I_2^n(s; m^2, 0)$
 - 4.3.2.2 $I_2^n(m^2; m^2, 0)$
- Bubbles with two internal masses
 - 4.3.3.1 $I_2^n(s; m_1^2, m_2^2)$
 - 4.3.3.3 $I_2^n(s; m^2, m^2)$
- Tadpole Integral
 - 4.5.0.8 $I_1^n(m^2)$

These results were checked against the program QCDloop [71] and we have plotted the results here.

4.3.1 Bubbles with no internal mass

4.3.1.1 The integral $I_2^n(s; 0, 0)$

The kinematics are defined as follows:

$$s_1 \neq 0, m_j^2 = 0.$$

$$\begin{aligned} I_2^n(s; 0, 0) &= \mu^{-2\epsilon} \mu^{2\epsilon} \frac{r_\Gamma}{(-s)^\epsilon} \frac{1}{\epsilon} \frac{1}{1-2\epsilon} \\ &= \mu^{-2\epsilon} r_\Gamma \left(\frac{\mu^2}{-s-i\delta} \right)^\epsilon \left[\frac{1}{\epsilon} + 2 \right] + \mathcal{O}(\epsilon) \\ &= \mu^{-2\epsilon} r_\Gamma \left(\frac{1}{\epsilon} + 2 - \log \left(\frac{-s-i\delta}{\mu^2} \right) \right) + \mathcal{O}(\epsilon). \end{aligned} \quad (4.65)$$

			ϵ^{-1}		ϵ^0	
s	m_1^2	m_2^2	Re	Im	Re	Im
5.0	0.0	0.0	1.00000000	0.00000000	0.39056209	3.14159265

 Table 4.7: Kinematic points for $I_2^n(s; 0, 0)$.

The limit $s \rightarrow 0$ does not commute with the expansion in ϵ . By definition $I_2^n(0; 0, 0) = 0$ because we have cancelling behaviour from the UV and IR poles. If we do distinguish between the two different poles our result is

$$I_2^n(0; 0, 0) \propto \frac{1}{\epsilon_{\text{UV}}} - \frac{1}{\epsilon_{\text{IR}}}. \quad (4.66)$$

4.3.2 Bubbles with one internal mass

4.3.2.1 The integral $I_2^n(s; m^2, 0)$

The kinematics are defined as:

$$s \neq 0, \quad m^2 \neq 0.$$

$$\begin{aligned} I_2^n(s; m^2, 0) &= \mu^{-2\epsilon} \mu^{2\epsilon} \Gamma(1 + \epsilon) (m^2)^{-\epsilon} \left[\frac{1}{\epsilon} + 2 + \frac{m^2 - s}{s} \log \left(\frac{-s + m^2 - i\delta}{m^2 - i\delta} \right) \right] + \mathcal{O}(\epsilon) \quad (4.67) \\ &= \mu^{-2\epsilon} \Gamma(1 + \epsilon) \left[\frac{1}{\epsilon} + 2 + \frac{m^2 - s}{s} \log \left(\frac{-s + m^2 - i\delta}{m^2 - i\delta} \right) - \log \left(\frac{m^2 - i\delta}{\mu^2} \right) \right] + \mathcal{O}(\epsilon) \end{aligned}$$

We plot the results in Figure 4.10.

			ϵ^{-1}		ϵ^0	
s	m_1^2	m_2^2	Re	Im	Re	Im
7.0	5.0	0.0	1.00000000	0.00000000	0.65235944	0.89759790
3.0	5.0	0.0	1.00000000	0.00000000	-0.22029840	-0.00000000
-3.0	5.0	0.0	1.00000000	0.00000000	-0.86278092	0.00000000

 Table 4.8: Kinematic points for $I_2^n(s; m^2, 0)$.

4.3.2.2 The integral $I_2^n(m^2; m^2, 0)$

$$\begin{aligned} I_2^n(m^2; 0, m^2) &= \mu^{-2\epsilon} \mu^{2\epsilon} \Gamma(1 + \epsilon) (m^2)^{-\epsilon} \left[\frac{1}{\epsilon} + 2 \right] + \mathcal{O}(\epsilon) \\ &= \mu^{-2\epsilon} \Gamma(1 + \epsilon) \left[\frac{1}{\epsilon} + 2 - \log \left(\frac{m^2 - i\delta}{\mu^2} \right) \right] + \mathcal{O}(\epsilon) \quad (4.68) \end{aligned}$$

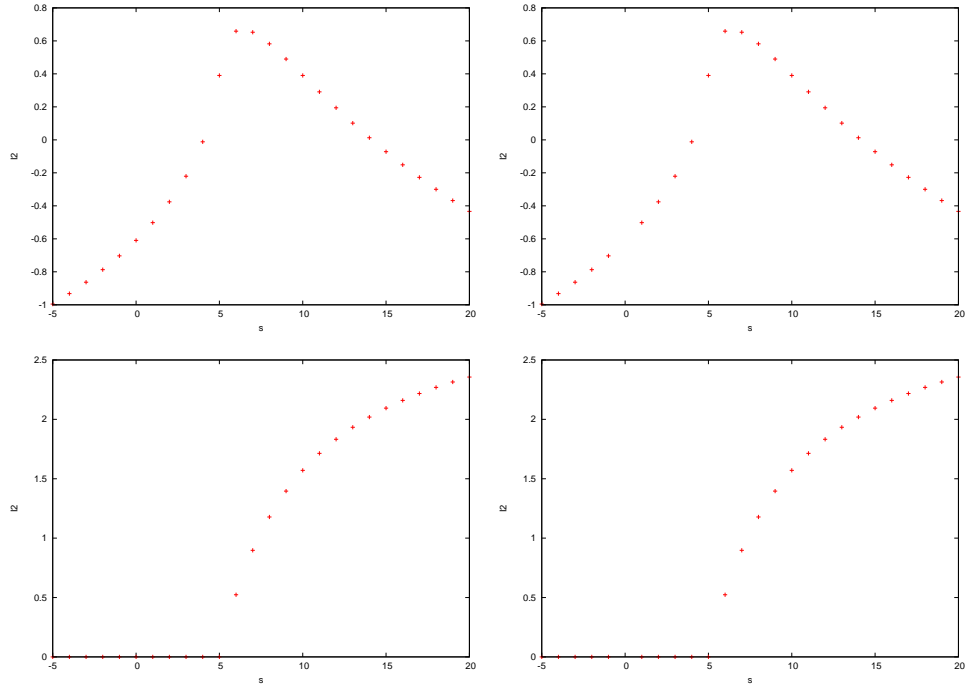


Figure 4.10: Graphs of the real part (upper) and imaginary part (lower) of the ϵ^0 term of $I_2^n(s; m^2, 0)$ for my implementation (right) against [71] (left).

We can take the limit $s \rightarrow m^2$ of $I_2^n(s; m^2, 0)$. The log term in the square brackets of equation (4.67) is zero:

$$\begin{aligned} \lim_{s \rightarrow m^2} I_2^n(s; m^2, 0) &= \mu^{-2\epsilon} \mu^{2\epsilon} \Gamma(1 + \epsilon) (m^2)^{-\epsilon} \left[\frac{1}{\epsilon} + 2 \right] + \mathcal{O}(\epsilon) \\ &= \mu^{-2\epsilon} \Gamma(1 + \epsilon) \left[\frac{1}{\epsilon} + 2 - \log \left(\frac{m^2 - i\delta}{\mu^2} \right) \right] + \mathcal{O}(\epsilon). \end{aligned} \quad (4.69)$$

We plot the result in Figure 4.11.

			ϵ^{-1}		ϵ^0	
s	m_1^2	m_2^2	Re	Im	Re	Im
5.0	5.0	0.0	1.00000000	0.00000000	0.39056209	0.00000000

Table 4.9: Kinematic points for $I_2^n(m^2; m^2, 0)$.

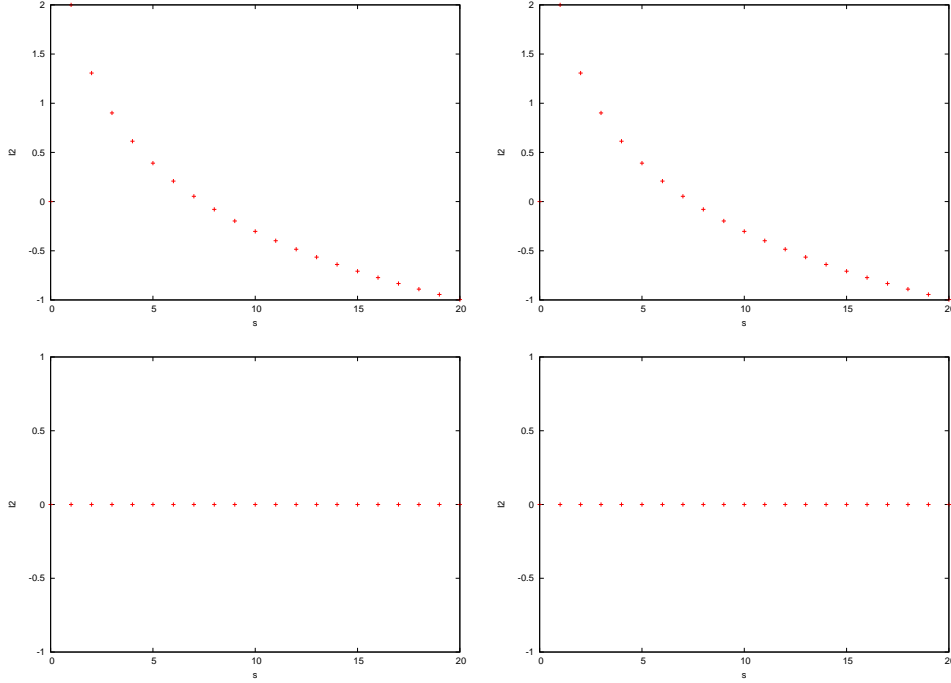


Figure 4.11: Graphs of the real part (upper) and imaginary part (lower) of the ϵ^0 term of $I_2^n(m^2; m^2, 0)$ for my implementation (right) against [71] (left) where we vary $s = m^2$.

4.3.2.3 The integral $I_2^n(0; m^2, 0)$

The limit $s \rightarrow 0$ of the integral $I_2^n(s; m^2, 0)$ commutes with the ϵ expansion. So we can take the limit of the above integral or calculate it independently to obtain:

$$\begin{aligned} I_2^n(0; 0, m^2) &= \mu^{-2\epsilon} \mu^{2\epsilon} \Gamma(1 + \epsilon) (m^2)^{-\epsilon} \left[\frac{1}{\epsilon} + 1 \right] + \mathcal{O}(\epsilon) \\ &= \mu^{-2\epsilon} \Gamma(1 + \epsilon) \left[\frac{1}{\epsilon} + 1 - \log \left(\frac{m^2 - i\delta}{\mu^2} \right) \right] + \mathcal{O}(\epsilon). \end{aligned} \quad (4.70)$$

In taking the limit of $I_2^n(s; m^2, 0)$ we use

$$\lim_{s \rightarrow 0} \left[\frac{m^2 - s}{s} \log \left(\frac{-s + m^2}{m^2} \right) \right] = -1. \quad (4.71)$$

We can also easily verify the relation:

$$I_1^n(m^2) = m^2 I_2^n(0; 0, m^2). \quad (4.72)$$

4.3.3 Bubbles with two internal masses

4.3.3.1 The integral $I_2^n(s, m_1^2, m_2^2)$

$$\begin{aligned}
 I_2^n(s; m_1^2, m_2^2) &= \mu^{-2\epsilon} \mu^{2\epsilon} \Gamma(1 + \epsilon) \left\{ \frac{1}{\epsilon} - \log[-(s - i\delta)(x_+ - 1)(1 - x_-)] - 2 \right. \\
 &\quad \left. - \left[x_+ \log\left(\frac{x_+ - 1}{x_+}\right) + x_- \log\left(\frac{x_- - 1}{x_-}\right) \right] \right\} + \mathcal{O}(\epsilon) \\
 &= \mu^{-2\epsilon} \Gamma(1 + \epsilon) \left\{ \frac{1}{\epsilon} - \log\left[\frac{-(s - i\delta)(x_+ - 1)(1 - x_-)}{\mu^2}\right] - 2 \right. \\
 &\quad \left. - \left[x_+ \log\left(\frac{x_+ - 1}{x_+}\right) + x_- \log\left(\frac{x_- - 1}{x_-}\right) \right] \right\} + \mathcal{O}(\epsilon)
 \end{aligned} \tag{4.73}$$

where we define

$$x_{\pm} = \frac{(s - m_1^2 + m_2^2) \pm \sqrt{\lambda(s, m_1^2, m_2^2) + i\delta \operatorname{sgn}(s)}}{2s}. \tag{4.74}$$

We plot our results in Figure 4.12.

			ϵ^{-1}		ϵ^0	
s	m_1^2	m_2^2	Re	Im	Re	Im
25.0	9.0	3.0	1.00000000	0.00000000	0.00331684	0.98146492
10.0	9.0	3.0	1.00000000	0.00000000	-1.38191285	0.00000000
1.0	9.0	3.0	1.00000000	0.00000000	-1.71665616	0.00000000
-5.0	9.0	3.0	1.00000000	0.00000000	-1.88165529	-0.00000000

Table 4.10: Kinematic points for $I_2^n(0; m^2, 0)$.

4.3.3.2 The limit $s \rightarrow 0$

We have the result

$$\begin{aligned}
 \lim_{s \rightarrow 0} I_2^n(s; m_1^2, m_2^2) &= \mu^{-2\epsilon} \mu^{2\epsilon} \Gamma(1 + \epsilon) \left[\frac{1}{\epsilon} + 1 - \frac{1}{m_1^2 - m_2^2} (m_1^2 \log(m_1^2 - i\delta) - m_2^2 \log(m_2^2 - i\delta)) \right] \\
 &= \mu^{-2\epsilon} \Gamma(1 + \epsilon) \left[\frac{1}{\epsilon} + 1 \right. \\
 &\quad \left. - \frac{1}{m_1^2 - m_2^2} \left(m_1^2 \log \frac{(m_1^2 - i\delta)}{\mu^2} - m_2^2 \log \frac{(m_2^2 - i\delta)}{\mu^2} \right) \right] + \mathcal{O}(\epsilon).
 \end{aligned} \tag{4.75}$$

4.3.3.3 The integral $I_2^n(s, m^2, m^2)$

$$\begin{aligned}
 I_2^n(s; m^2, m^2) &= \mu^{-2\epsilon} \mu^{2\epsilon} \Gamma(1 + \epsilon) (m^2)^{-\epsilon} \left[\frac{1}{\epsilon} + 2 + \beta \log\left(\frac{-x_-}{x_+}\right) \right] + \mathcal{O}(\epsilon) \\
 &= \mu^{-2\epsilon} \Gamma(1 + \epsilon) \left[\frac{1}{\epsilon} + 2 + \beta \log\left(\frac{-x_-}{x_+}\right) - \log\left(\frac{m^2 - i\delta}{\mu^2}\right) \right] + \mathcal{O}(\epsilon)
 \end{aligned} \tag{4.76}$$

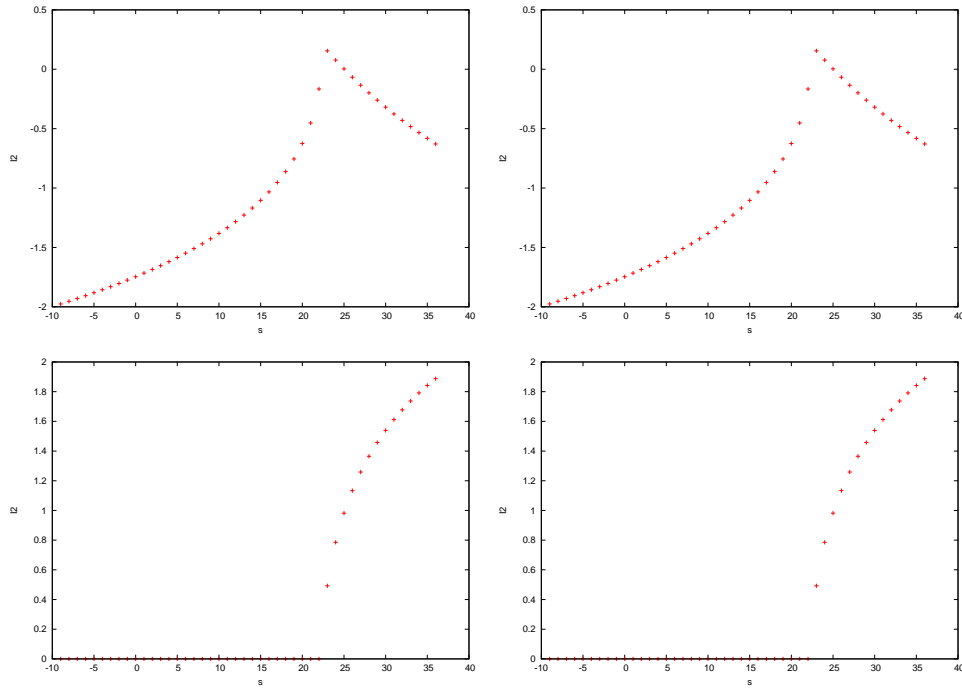


Figure 4.12: Graphs of the real part (upper) and imaginary part (lower) of the ϵ^0 term of $I_2^n(s, m_1^2, m_2^2)$ for my implementation (right) against [71] (left).

where

$$x_{\pm} = \frac{1}{2}(1 + \beta) \quad (4.77)$$

and

$$\beta = \sqrt{1 - \frac{4m^2}{s}}. \quad (4.78)$$

The above result can be derived in the limit $m_1^2 \rightarrow m_2^2$ of $I_2^n(s; m_1^2, m_2^2)$. Again, we have the same problem in the limit $s \rightarrow 0$. The result in this limit is simply:

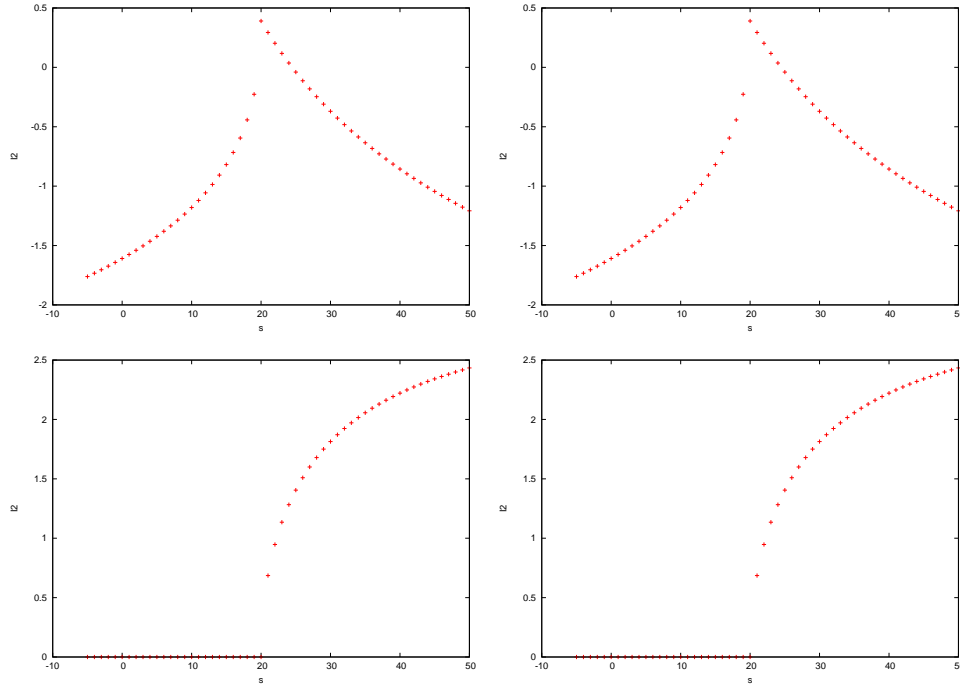
$$\lim_{s \rightarrow 0} I_2^n(s; m^2, m^2) = \mu^{-2\epsilon} \Gamma(1 + \epsilon) \left[\frac{1}{\epsilon} - \log \left(\frac{m^2 - i\delta}{\mu^2} \right) \right] + \mathcal{O}(\epsilon). \quad (4.79)$$

We include this behaviour in our plot Figure 4.13.

4.4 Derivatives of Bubbles

For our renormalization condition we need to know the derivatives of some of the bubble integrals. We need the following:

			ϵ^{-1}		ϵ^0	
s	m_1^2	m_2^2	Re	Im	Re	Im
25.0	5.0	5.0	1.00000000	0.00000000	-0.03984685	1.40496295
13.0	5.0	5.0	1.00000000	0.00000000	-0.98567057	0.00000000
-5.0	5.0	5.0	1.00000000	0.00000000	-1.76148262	-0.00000000

Table 4.11: Kinematic points for $I_2^n(s, m^2, m^2)$.Figure 4.13: Graphs of the real part (upper) and imaginary part (lower) of the ϵ^0 term of $I_2^n(s, m^2, m^2)$ for my implementation (right) against [71] (left).

- Derivatives of Bubbles

- 4.4.0.4 $I_2^{n'}(m^2; 0, m^2)$

- 4.4.0.5 $I_2^{n'}(0; m^2, m^2)$

- 4.4.0.6 $I_2^{n'}(0; m^2, 0)$

- 4.4.0.7 $I_2^{n'}(0; m_1^2, m_2^2)$

where

$$I_2^{n'}(s; m_1^2, m_2^2) = \frac{\partial I_2^n(s; 0, m^2)}{\partial s}. \quad (4.80)$$

4.4.0.4 The integral $I_2^{n'}(m^2; 0, m^2)$

$$I_2^{n'}(m^2; 0, m^2) = \left. \frac{\partial I_2^n(s; 0, m^2)}{\partial s} \right|_{s=m^2}. \quad (4.81)$$

We use an important property of Feynman integrals that we can interchange the integral and derivative give:

$$\begin{aligned} I_2^{n'}(m^2; 0, m^2) &= \Gamma(\epsilon) \int dx \left(\frac{\partial}{\partial s} (-sx\bar{x} + m^2\bar{x} - i\delta)^{-\epsilon} \right)_{s=m^2} \\ &= (-1)^2 \epsilon \Gamma(\epsilon) \int dx (m^2)^{-1-\epsilon} x\bar{x}^{-2\epsilon-1}. \end{aligned} \quad (4.82)$$

Our final result is

$$\begin{aligned} I_2^{n'}(m^2; 0, m^2) &= \Gamma(1+\epsilon)(m^2)^{-1-\epsilon} B(2, -2\epsilon) \\ &= -\mu^{-2\epsilon} \mu^{2\epsilon} \Gamma(1+\epsilon) \frac{(m^2)^{-\epsilon}}{m^2} \left(\frac{1}{2\epsilon} + 1 \right) + \mathcal{O}(\epsilon) \\ &= -\mu^{-2\epsilon} \Gamma(1+\epsilon) \frac{1}{m^2} \left[\frac{1}{2\epsilon} + 1 - \frac{1}{2} \log \left(\frac{m^2 - i\delta}{\mu^2} \right) \right] + \mathcal{O}(\epsilon) \end{aligned} \quad (4.83)$$

where $B(\alpha, \beta)$ is defined in (D.8).

4.4.0.5 The integral $I_2^{n'}(0; m^2, m^2)$

We need the integral

$$\begin{aligned} I_2^{n'}(0; m^2, m^2) &= \Gamma(\epsilon) \int dx \left(\frac{\partial}{\partial s} (-sx\bar{x} + m^2\bar{x} + m^2x - i\delta)^{-\epsilon} \right)_{s=0} \\ &= (-1)^2 \epsilon \Gamma(\epsilon) \int dx (m^2)^{-1-\epsilon} x\bar{x}. \end{aligned} \quad (4.84)$$

Our final result is therefore:

$$\begin{aligned} I_2^{n'}(0; m^2, m^2) &= \Gamma(1+\epsilon) \frac{(m^2)^{-\epsilon}}{6m^2} \\ &= \mu^{-2\epsilon} \Gamma(1+\epsilon) \frac{1}{6m^2} + \mathcal{O}(\epsilon). \end{aligned} \quad (4.85)$$

4.4.0.6 The integral $I_2^{n'}(0; m^2, 0)$

The integral is

$$\begin{aligned} I_2^{n'}(0; m^2, 0) &= \Gamma(\epsilon) \int dx \left(\frac{\partial}{\partial s} (-sx\bar{x} + m^2x - i\delta)^{-\epsilon} \right)_{s=0} \\ &= (-1)^2 \epsilon \Gamma(\epsilon) \int dx (m^2)^{-1-\epsilon} x^{-\epsilon} \bar{x} \\ &= (-1)^2 \Gamma(1+\epsilon) B(1-\epsilon, 2). \end{aligned} \quad (4.86)$$

Our final result is therefore:

$$\begin{aligned} I_2^{n'}(0; m^2, m^2) &= \Gamma(1 + \epsilon) \frac{(m^2)^{-\epsilon}}{2m^2} + \mathcal{O}(\epsilon) \\ &= \mu^{-2\epsilon} \Gamma(1 + \epsilon) \frac{1}{2m^2} + \mathcal{O}(\epsilon). \end{aligned} \quad (4.87)$$

4.4.0.7 The integral $I_2^{n'}(0; m_1^2, m_2^2)$

$$I_2^{n'}(0; m_1^2, m_2^2) = \mu^{-2\epsilon} \Gamma(1 + \epsilon) \frac{1}{2(m_1^2 - m_2^2)^3} \left(m_1^4 - m_2^4 - 2m_1^2 m_2^2 \log \frac{m_1^2}{m_2^2} \right) + \mathcal{O}(\epsilon). \quad (4.88)$$

4.5 Tadpole Integral

4.5.0.8 The integral $I_1^n(m^2)$

The one-point integral is defined as

$$I_1^n(m^2) = \int \frac{d^n k}{i\pi^{\frac{n}{2}}} \frac{1}{k^2 - m^2 + i\delta} \quad (4.89)$$

with one internal mass. The integral is trivial as we have only one Feynman parameter, x , and a delta function $\delta(1 - x)$.

$$\begin{aligned} I_1^n(m^2) &= \frac{\Gamma(1 + \epsilon)}{\epsilon(1 - \epsilon)} m^2 (m^2)^{-\epsilon} \\ &= \Gamma(1 + \epsilon) m^2 (m^2)^{-\epsilon} \left(\frac{1}{\epsilon} + 1 \right) + \mathcal{O}(\epsilon^2) \\ &= \mu^{-2\epsilon} \Gamma(1 + \epsilon) m^2 \left[\frac{1}{\epsilon} + 1 - \log \left(\frac{m^2 - i\delta}{\mu^2} \right) \right] + \mathcal{O}(\epsilon). \end{aligned} \quad (4.90)$$

4.6 Evaluation of Three Point Tensor Integrals

As part of our analysis we also computed the form factors associated with the 3-point tensor integrals for each kinematic configuration in Section 4.2. We get the following tensor decomposition:

$$I_3^N(S) = \int \frac{d^n k}{i\pi^{\frac{n}{2}}} \frac{1}{[(k + r_1)^2 - m_1^2][(k + r_2)^2 - m_2^2][(k + r_3)^2 - m_3^2]} \quad (4.91)$$

$$I_3^{3,\mu}(S) = \int \frac{d^n k}{i\pi^{\frac{n}{2}}} \frac{k^\mu}{[(k + r_1)^2 - m_1^2][(k + r_2)^2 - m_2^2][(k + r_3)^2 - m_3^2]} \quad (4.92)$$

$$= r_1^\mu A_1^{3,1}(S) + r_2^\mu A_2^{3,1}(S) \quad (4.93)$$

$$I_3^{3,\mu\nu}(S) = \int \frac{d^n k}{i\pi^{\frac{n}{2}}} \frac{k^\mu k^\nu}{[(k + r_1)^2 - m_1^2][(k + r_2)^2 - m_2^2][(k + r_3)^2 - m_3^2]} \quad (4.94)$$

$$= r_1^\mu r_1^\nu A_{1,1}^{3,2}(S) + r_1^\mu r_2^\nu A_{1,2}^{3,2}(S) + r_2^\mu r_1^\nu A_{2,1}^{3,2}(S) + r_2^\mu r_2^\nu A_{2,2}^{3,2}(S) + g^{\mu\nu} B^{3,2}(S) \quad (4.95)$$

and likewise for the rank three tensor.

We compared two implementations of the form factors. The first using the numerical integrals in the **GB** and the second by reducing them further to **SI**. The relationship between the two approaches is given by (4.23). We document one example of the reduction of **GB** to scalar integrals, and give numerical results for the rest. The two results agreed for all points tested. Where a numerical integration was used the agreement was limited by the accuracy specified by the integrator.

4.6.1 Explicit results for $I_3^n(s_1, s_2, 0; m_1^2, 0, 0)$

We present the results for the rank one and two tensor integral with the above kinematics. Using the notation of (4.23), we decompose the integrals as

$$I_3^n(1; S) = \frac{1}{(s_1 - s_2)} [I_2(s_2; m_1^2, 0) - I_2^n(s_1; m_1^2, 0)] \quad (4.96)$$

$$I_3^n(2; S) = \frac{1}{s_1 - s_2} \{ (s_1 - m_1^2) I_3^n(s_1, s_2, 0; m_1^2, 0, 0) + I_2^n(s_2; m_1^2, 0) + I_2^n(s_1; m_1^2, 0) \} \quad (4.97)$$

and for the rank two case:

$$I_3^n(1, 1; S) = \frac{1}{(s_1 - s_2)} \left\{ \left[\frac{m_1^2 - s_1}{2s_1} \right] I_2(s_1; m_1^2, 0) + \left[\frac{s_2 - m_1^2}{2s_2} \right] I_2(s_2; m_1^2, 0) \right\} \quad (4.98)$$

$$I_3^n(1, 2; S) = \frac{1}{(s_1 - s_2)^2} \left\{ \left[\frac{s_1 - m_1^2}{2} + \frac{s_1 - m_1^2}{2} \epsilon \right] I_2(s_1; m_1^2, 0) \right. \\ \left. + \left[\frac{s_1 s_2 - s_2 m_1^2 + s_1 m_1^2}{2s_2} - \frac{m_1^2 - s_2}{2} \epsilon \right] I_2(s_2; m_1^2, 0) \right\} \quad (4.99)$$

$$I_3^n(2, 2; S) = \frac{-1}{(s_1 - s_2)^2} \left\{ \left[\frac{3s_1(s_1 - m_1^2)}{(s_1 - s_2)} + \frac{3s_1(s_1 - m_1^2)}{(s_1 - s_2)} \epsilon \right] I_2(s_1; m_1^2, 0) \right. \\ \left. + \left[\frac{-s_1^2 m_1^2 - 3s_1^2 s_2 + s_2^3 + 4s_1 s_2 m_1^2 - 4s_1 s_2^2 + 3s_2^2 m_1^2}{2(s_1 - s_2)s_2} + \frac{s_1(m_1^2 - s_2)}{s_1 - s_2} \epsilon \right] I_2(s_2; m_1^2, 0) \right. \\ \left. + [(s_1^2 - m_1^2)^2] I_3^n(s_1, s_2, 0; m_1^2, 0, 0) \right\} \quad (4.100)$$

where we have expanded the coefficients in ϵ . This is sufficient for these integrals because the basis integrals are at most divergent to $\sim 1/\epsilon$. However, for other kinematic configurations there may be a double pole so the ϵ^2 terms must be included. The form factors that multiply the metric tensors $B^{3,2}$ can be related to scalar integrals in $n+2$ dimensions and are not calculated here.

4.6.2 Numerical Results

We compute the numerical results for the kinematic regions that were in the previous section. We present the results in Appendix F.

Chapter 5

Neutralino Pair Production at Next to Leading Order

5.1 Outline

As a test of our implementation we calculate the process $pp \rightarrow \chi_1^0 \chi_1^0$ at Next to Leading Order (NLO). This process is of phenomenological interest; in the MSSM, for large regions of parameter space, the neutralino, χ_1^0 , is the lightest supersymmetric particle (LSP). Due to the conservation of R-parity the LSP is the end product of any decay chain of a superpartner. The Neutralino is a weakly interacting massive particle and provides a perfect candidate for cold dark matter.

In this section we outline our renormalization procedure and then we go on to present the details of our calculation.

5.2 Renormalization

To render our virtual matrix element finite in the ultraviolet limit we need to subtract the ultraviolet divergences present in our virtual part of the amplitude. For neutralino pair production we must calculate the quark and squark wavefunction renormalization constants and the mass counterterm for the squark propagator. In this section we outline the results of this renormalization procedure. For brevity we define the prefactor

$$P = \frac{(4\pi)^\epsilon \alpha_s}{4\pi} \tag{5.1}$$

which comes about naturally from our definitions of scalar integrals:

$$g^2 \int \frac{d^n k}{(2\pi)^n} = \int \frac{d^n k}{i\pi^{\frac{n}{2}}} \frac{i\alpha_s (4\pi)^\epsilon}{(4\pi)} \tag{5.2}$$

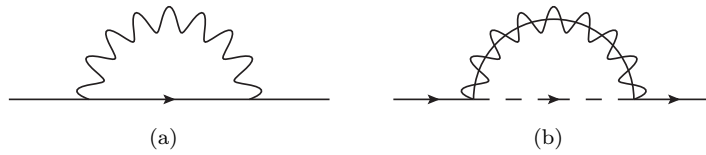


Figure 5.1: Quark self energy contributions.

and $\int \frac{d^n k}{i\pi^{\frac{n}{2}}}$ is the prefactor of the scalar integrals we use. We drop the factor of i from our definition of the self-energies, so that the self energy is real.

5.2.1 Self Energies

5.2.1.1 Quark Propagator

We use a covariant decomposition for the massless quark self energy

$$\Sigma_{q\bar{q}}^{ij}(-p, p) = f(p^2)\not{p}\delta^{ij}. \quad (5.3)$$

which gives

$$f = \frac{\text{tr}(\Sigma_{q\bar{q}}\not{p})}{4p^2}. \quad (5.4)$$

For Figure 5.1(a) we have the result

$$\frac{f_{5.1(a)}(p^2)}{P} = C_F I_2^n(s; 0, 0)(1 - \epsilon) \quad (5.5)$$

where here including the red term gives the dimensional regularisation result (black only is the dimensional reduction result) and for Figure 5.1(b)

$$\frac{f_{5.1(b)}(p^2)}{P} = \sum_{q=q_L, q_R} \frac{C_F}{2} \left\{ I_2^n(s; m_{\bar{q}}^2, m_{\bar{g}}^2) + \frac{m_{\bar{g}}^2 - m_{\bar{q}}^2}{s} [I_2^n(s; m_{\bar{q}}^2, m_{\bar{g}}^2) - I_2^n(0; m_{\bar{q}}^2, m_{\bar{g}}^2)] \right\}. \quad (5.6)$$

where we sum over the two intermediate squark states.

5.2.1.2 Squark Propagator

The decomposition of the squark self energy is simple. We obtain for the left handed squark:

$$\Sigma_\phi = f. \quad (5.7)$$

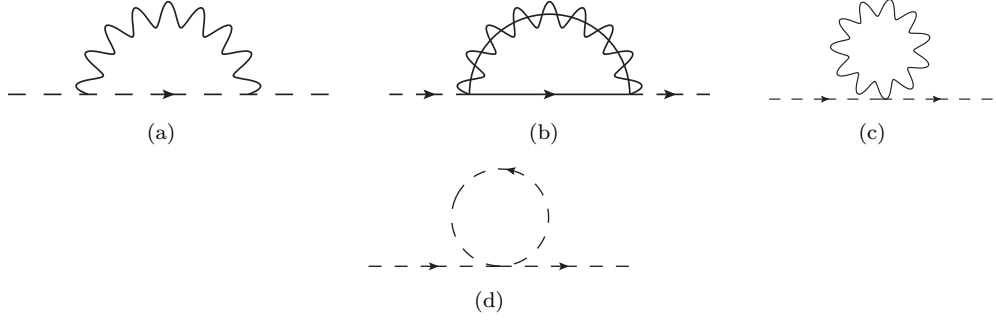


Figure 5.2: Squark self energy contributions. Figure 5.2(c) is zero due to the massless gluon.

The results for diagrams 5.2(a) and 5.2(b) are

$$f_{5.2(a)}/P = C_F \left\{ (-2s - m_q^2) I_2^n(s; 0, m_q^2) - m_q^2 [I_2^n(s; 0, m_q^2) - I_2^n(0; 0, m_q^2)] + \frac{1}{6}s - \frac{1}{2}m_q^2 \right\} \quad (5.8)$$

$$f_{5.2(b)}/P = C_F \left\{ \left[(3 - \epsilon) - \frac{m_g^2}{s}(6 - \epsilon) \right] \frac{2s}{3 - 2\epsilon} I_2^n(s; m_g^2, 0) \right. \\ \left. + \left[(3 - \epsilon) + \epsilon \frac{m_g^2}{s} \right] \frac{2m_g^2}{3 - 2\epsilon} [I_2^n(s; 0, m_g^2) - I_2^n(0; 0, m_g^2)] \right\} \quad (5.9)$$

$$= C_F \left\{ 2s I_2^n(s; m_g^2, 0) - 4m_g^2 I_2^n(s; m_g^2, 0) + 2m_g^2 [I_2^n(s; 0, m_g^2) - I_2^n(0; 0, m_g^2)] \right. \\ \left. - \frac{2}{3}(3m_g^2 - s) \right\} \quad (5.10)$$

where the red text corresponds to the extra terms in the dimensional reduction result (i.e. black text only is the dimensional regularisation result). These arise from terms proportional to ϵ multiplying a divergent integral.

Also we state the result for the second diagram but with an internal massive quark with mass m_q :

$$f_{5.2(a)}'/P = C_F \left\{ \frac{2}{3 - 2\epsilon} [s(3 - \epsilon) - 6m_q^2 + (m_q^2 - m_g^2)\epsilon] [I_2^n(s; m_g^2, m_q^2)] \right. \\ \left. + \frac{2}{3 - 2\epsilon} \left[(3 - \epsilon)(m_q^2 - m_g^2) + \epsilon \frac{(m_q^2 - m_g^2)^2}{s} \right] [I_2^n(s; m_g^2, m_q^2) - I_2^n(0; m_g^2, m_q^2)] \right. \\ \left. + 4m_g^2 \left[\frac{3 - \epsilon}{3 - 2\epsilon} I_2^n(0; m_g^2, 0) \right] \right\}. \quad (5.11)$$

We also get a contribution from the diagram with the 4 squark interaction. The result is

$$f_{5.2(d)}/P = C_F I_2^n(0; 0, m_q^2) m_q^2. \quad (5.12)$$

The color structure means that the diagram with an squark propagator of a different chirality

to the legs is zero.

5.2.1.3 Mixed Squark Propagator

The squark propagator can also mix. This can come about through Figure 5.2(b). The result is

$$f_{5.2(b),ij}/P = C_F \left\{ \frac{2\epsilon(s - 3m_{\tilde{g}}^2)}{3 - 2\epsilon} I_2^n(s; m_{\tilde{g}}^2, 0) + \frac{2m_{\tilde{g}}^2\epsilon}{3 - 2\epsilon} \left(1 + \frac{m_{\tilde{g}}^2}{s} \right) [I_2^n(s; 0, m_{\tilde{g}}^2) - I_2^n(0; 0, m_{\tilde{g}}^2)] \right\} \quad (5.13)$$

or, equivalently,

$$f_{5.2(b),ij}/P = C_F \left\{ \frac{2(s - m_{\tilde{g}}^2)^2\epsilon}{(3 - 2\epsilon)s} I_2^n(s; m_{\tilde{g}}^2, 0) - \frac{2(s + m_{\tilde{g}}^2)m_{\tilde{g}}^2\epsilon}{(3 - 2\epsilon)s} I_2^n(0; 0, m_{\tilde{g}}^2) \right\} \quad (5.14)$$

Comments:

- It is clear from looking at the diagram that the result should be proportional to ϵ as the trace contains a term that looks like $\Pi_+(\not{k} + \not{p})\Pi_+$ which disappears in 4 dimensions. However, in the ϵ dimensions it is non-vanishing. This is in contrast to the same flavour mixing that contains $\Pi_- \not{q} \Pi_-$.
- Evaluated at a squark mass $m_{\tilde{q}}$ we get a simple result because the expression is proportional to ϵ :

$$\Sigma(m_{\tilde{q}}^2) = \frac{2}{3}(m_{\tilde{q}}^2 - 3m_{\tilde{g}}^2). \quad (5.15)$$

5.2.2 Renormalization Conditions

We choose to renormalize in the on-shell scheme.

5.2.2.1 Squark Renormalization

The squark's renormalized self-energy is

$$\Sigma^R(s, m_{\tilde{q}}^2) = (s - m_{\tilde{q}}^2) + A(s, m_{\tilde{q}}^2) + \delta Z_{\tilde{q}}(s - m_{\tilde{q}}^2) - \delta m_{\tilde{q}}^2 \quad (5.16)$$

and the renormalization condition is that the renormalized one-loop self energy is equal to the bare propagator

$$\lim_{s \rightarrow m_{\tilde{q}}^2} \Sigma^R(s, m_{\tilde{q}}^2) = s - m_{\tilde{q}}^2. \quad (5.17)$$

We expand A :

$$f(s, m_{\tilde{q}}^2) = A(m_{\tilde{q}}^2, m_{\tilde{q}}^2) + (s - m_{\tilde{q}}^2)A'(m_{\tilde{q}}^2, m_{\tilde{q}}^2) + \mathcal{O}(s - m_{\tilde{q}}^2)^2 \quad (5.18)$$

and then (5.17) fixes our renormalization constants:

$$\delta Z_{\bar{q}} = -A'(m_{\bar{q}}^2, m_{\bar{q}}^2) \quad (5.19)$$

$$\delta m_{\bar{q}}^2 = A(m_{\bar{q}}^2, m_{\bar{q}}^2). \quad (5.20)$$

The function A is the unrenormalized one-loop self energy and is related to the previous section by

$$A(s, m_{\bar{q}}^2) = Pf(s, m_{\bar{q}}^2). \quad (5.21)$$

5.2.2.2 Explicit Results

5.2.2.3 Squark Mass Counterterm

For clarity the renormalization constants are presented for each diagram individually.

$$\delta m_{\bar{q}}^{2,(5.2(a))} = C_F \left[-4m_{\bar{q}}^2 I_2^n(m_{\bar{q}}^2, 0, m_{\bar{q}}^2) + m_{\bar{q}}^2 I_2^n(0, 0, m_{\bar{q}}^2) - \frac{1}{3} m_{\bar{q}}^2 \right] \quad (5.22)$$

$$\delta m_{\bar{q}}^{2,(5.2(b))} = C_F \left[2(m_{\bar{q}}^2 - m_{\bar{g}}^2) I_2^n(m_{\bar{q}}^2, 0, m_{\bar{g}}^2) - 2m_{\bar{g}}^2 I_2^n(0, 0, m_{\bar{g}}^2) + \left(\frac{2}{3} m_{\bar{q}}^2 - 2m_{\bar{g}}^2 \right) \right] \quad (5.23)$$

$$\delta m_{\bar{q}}^{2,(5.2(d))} = C_F [m_{\bar{q}}^2 I_2^n(0, 0, m_{\bar{q}}^2)] \quad (5.24)$$

$$(5.25)$$

Comments:

- Upon adding all contributions the pole term has a dependence on the gluino mass. The squark mass dependence cancels between Figure 5.2(a) and Figure 5.2(d).
- As expected the extra finite dimensional regularisation terms comes solely from the gluon contribution.

5.2.2.4 Squark Wave Function Renormalisation

$$\delta Z_{\bar{q}}^{(5.2(a))} = 4m_{\bar{q}}^2 I_2^{n'}(m_{\bar{q}}^2, m_{\bar{q}}^2, 0) + 2I_2^n(m_{\bar{q}}^2, m_{\bar{q}}^2, 0) \quad (5.26)$$

$$\delta Z_{\bar{q}}^{(5.2(b))} = 2(m_{\bar{g}}^2 - m_{\bar{q}}^2) I_2^{n'}(m_{\bar{q}}^2, 0, m_{\bar{g}}^2) - 2I_2^n(m_{\bar{q}}^2, 0, m_{\bar{g}}^2) - \frac{2}{3} \quad (5.27)$$

$$\delta Z_{\bar{q}}^{(5.2(d))} = 0 \quad (5.28)$$

Comments:

- There is no UV pole coming from the squark renormalization as we get a cancellation between Figure 5.2(a) and Figure 5.2(b). However, as we use the on-shell scheme there is a finite piece.
- Again, we have a finite, regularisation-dependent piece coming from Figure 5.2(b).

- The first condition gives an infrared divergence in the derivative of the scalar bubble at equal masses. In the paper [72] this exact is avoided by applying the renormalization condition at an arbitrary scale $s = \mu^2$. Therefore we avoid introducing an infrared pole here. We now proceed to outline the results at this new point.

5.2.2.5 μ result

We rewrite the above results at an arbitrary scale, μ :

$$\delta Z_{\tilde{q}} = -\Sigma'_{\tilde{q}}(\mu^2). \quad (5.29)$$

Therefore, our conditions are now:

$$\delta Z_{\tilde{q}}^{(5.2(a))} = 2(\mu^2 + m_{\tilde{q}}^2)I_2^{n'}(\mu^2, m_{\tilde{q}}^2, 0) + 2I_2^n(\mu^2, m_{\tilde{q}}^2, 0) - \frac{1}{6} \quad (5.30)$$

$$\delta Z_{\tilde{q}}^{(5.2(b))} = 2(m_{\tilde{g}}^2 - \mu^2)I_2^{n'}(\mu^2, 0, m_{\tilde{g}}^2) - 2I_2^n(\mu^2, 0, m_{\tilde{g}}^2) - \frac{2}{3} \quad (5.31)$$

$$\delta Z_{\tilde{q}}^{(5.2(d))} = 0 \quad (5.32)$$

and in our calculation we choose μ^2 to be the renormalization scale. We avoid this problem for the quarks, simply because we take the massless quark approximation.

5.2.3 Mixing Squark Renormalization

For the diagrams where the squarks are mixed we have the following renormalised self energy:

$$\Sigma_{ij}^R(s, m_{\tilde{q}}^2) = A_{ij}(s, m_{\tilde{q}}^2) + \frac{1}{2}(\delta Z_{ij}(s) + \delta Z_{ji})s - (\delta m_{\tilde{q}}^2)_{ij}. \quad (5.33)$$

The on-shell condition is therefore

$$\delta Z_{ij} = 2 \frac{\Sigma_{ij}(m_{\tilde{q}_i}^2)}{m_{\tilde{q}_i}^2 - m_{\tilde{q}_j}^2} \quad (5.34)$$

where

$$\Sigma_{12}^{(5.2(b))}(m_{\tilde{q}}^2) = -2m_{\tilde{g}}^2 + \frac{2}{3}m_{\tilde{q}}^2 = \Sigma_{21}. \quad (5.35)$$

5.2.3.1 Quark Renormalization

We write the renormalized quark self energy as (where the quark is massless)

$$\Sigma^R(s) = \not{p} + \not{p}A(s) + \delta Z_q \not{p}. \quad (5.36)$$

The renormalization condition is

$$\lim_{s \rightarrow 0} \Sigma^R(s)u(p) = \not{p}u(p) \quad (5.37)$$

which is satisfied by

$$\delta Z_q = -A(0). \quad (5.38)$$

5.2.3.2 Explicit Results

$$\delta Z^{(5.1(a))} = -C_F I_2^n(0, 0, 0)(1 - \epsilon) \quad (5.39)$$

$$\delta Z^{(5.1(b))} = -\frac{C_F}{2} \sum_{q=q_L, q_R} \left[I_2^n(0, m_q^2, m_g^2) + (m_g^2 - m_q^2) I_2^{n'}(0, m_q^2, m_g^2) \right]. \quad (5.40)$$

5.2.4 Finite Squark Quark Neutralino Coupling

As explained in Section 3.7.2 dimensional regularisation does not respect supersymmetry. We must compensate this scheme dependent breaking of supersymmetry by introducing a finite counterterm for the quark-squark-neutralino coupling [73, 74]. We have the following shift for the quark-squark-neutralino coupling:

$$g \rightarrow g \left(1 - \frac{\alpha_s}{6\pi} \right). \quad (5.41)$$

In our implementation we absorb this finite shift into the counter term for the squark propagator. Each self energy must compensate for the shift in two couplings (one at either end of the propagator) therefore we shift the squark wave function term by the following amount:

$$\delta Z \rightarrow \delta Z - \frac{\alpha_s}{4\pi} \left(\frac{4}{3} \right). \quad (5.42)$$

For the relevant set of diagrams, as given in Figure 5.3, we plot in Figure 5.4 the ratio of the dimensional regularisation result to the dimensional reduction results before and after the finite term is included. We perform a scan over the outgoing polar angle of the first neutralino and the plot is for one helicity configuration. We found the two results to agree after the finite shift i.e. the sum of these diagrams is scheme independent only when the finite shift is included.

5.3 Results for $pp \rightarrow \chi_1^0 \chi_1^0$.

5.3.1 Comparison to the Literature

A calculation of neutralino pair production but with the e^+e^- initial state was presented in [75]. A calculation of neutralino pair production for the LHC was presented in [74]. Their results give the total cross sections for various neutralino pair combinations and the corresponding K-factors (the ratio of the NLO result to the LO result).

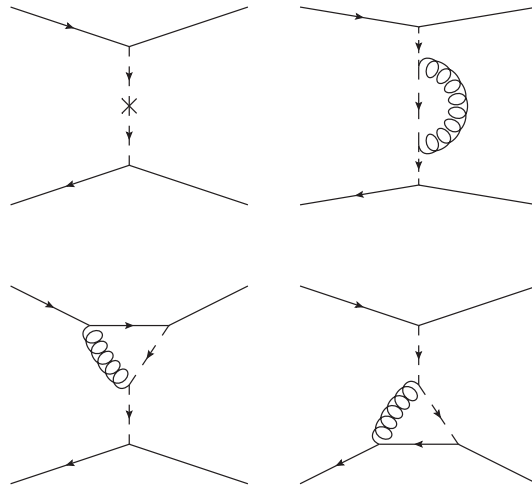


Figure 5.3: The subset of diagrams corresponding to Figure 5.4.

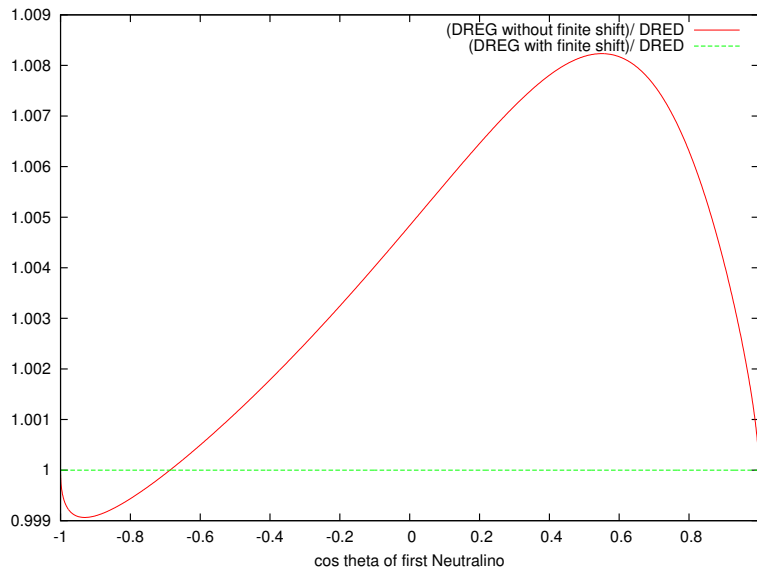
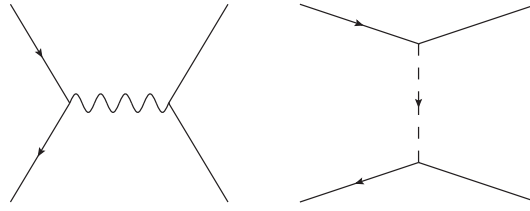
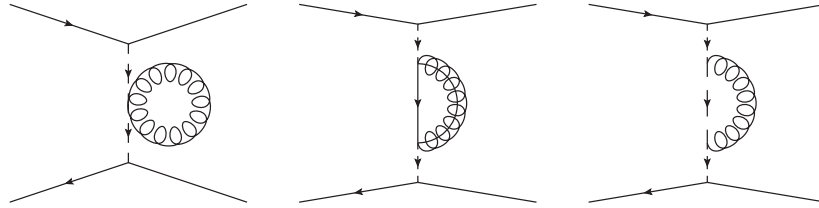
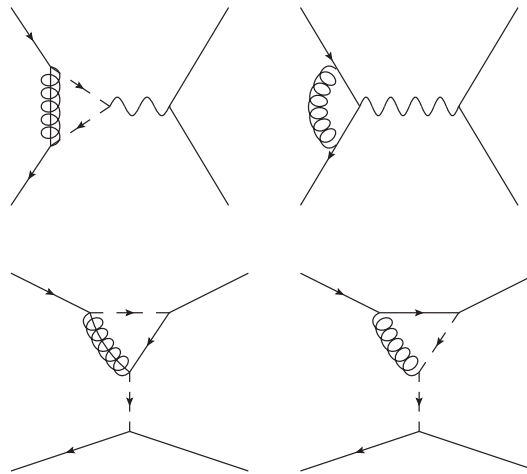
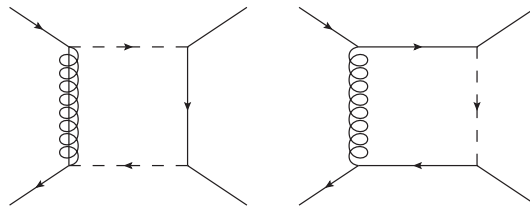
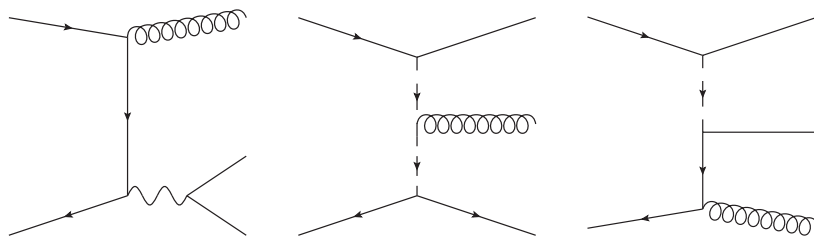


Figure 5.4: The ratio of the dimensional regularised and renormalised virtual matrix elements squared to the corresponding dimensional reduction result is plotted here for the diagrams in Figure 5.3 for one helicity configuration. The red result is before we include the finite counterterm (5.42) and the green result after. We keep the energy and the azimuthal angle constant but vary the polar angle θ of the first outgoing Neutralino. We see that the sum of the diagrams is scheme independent after the inclusion of the finite shift.

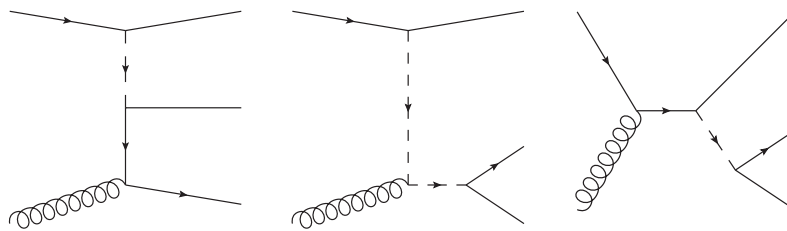
(a) Tree level diagrams for $q\bar{q} \rightarrow \chi_1^0 \chi_1^0$.(b) Bubble diagrams for $q\bar{q} \rightarrow \chi_1^0 \chi_1^0$.(c) Triangle diagrams for $q\bar{q} \rightarrow \chi_1^0 \chi_1^0$.(d) Box diagrams for $q\bar{q} \rightarrow \chi_1^0 \chi_1^0$.

5.3.2 Details of our Calculation

The generic diagrams calculated are presented in Figure 5.5 using the Feynman rules defined in Appendix A. The code used for the virtual part is outlined in Appendix E. For the infrared



(e) Real emission diagrams for the channel $q\bar{q} \rightarrow \chi_1^0 \chi_1^0 g$.



(f) Real emission diagrams for the channel $qg \rightarrow \chi_1^0 \chi_1^0 q$.

Figure 5.5: Diagrams for the process $pp \rightarrow \chi_1^0 \chi_1^0$. They are drawn using the Feynman rules defined in Appendix A.

subtraction terms [76] is used. This is based on the Catani-Seymour dipole subtraction method [51] implemented in the MadGraph/MadEvent setup [3] incorporating the ideas in [77]. For the real emission part MadGraph/MadEvent [3] is used. Our renormalization procedure is outlined in Section 5.2; we use the on-shell scheme.

We work in the 5 flavour massless quark scheme $q \in \{u, d, s, t, b\}$. At the partonic level we see flavour symmetry amongst the set of down type quarks and amongst the set of up type quarks. We use the parton distribution set Martin-Stirling-Thorne-Watt Parton Distribution Functions (MSTW08) [78].

For the SUSY parameters we use the modified benchmarks point SPS1amod suggested in [79]. This is a modification of the benchmark point SPS1a first suggested in [41]. SPS1a has lighter squarks than other benchmark points. The modification is the tuning of the SUSY breaking parameter $A_t \equiv -733$ GeV such that the lightest Higgs boson's mass lies above the LEP exclusion bound at $m_h = 118$ GeV. In this scenario χ_1^0 is the lightest supersymmetric particle. The SPS1amod scenario, due to its low squark masses should give an indication of the upper bound on the result that will decrease with heavier sparticles. We calculate the run at 7 TeV centre of mass scale to correspond to the current running energy of the LHC.

5.4 Details of Checks

The following checks of the calculation were performed. As a preliminary check, the number of diagrams was checked against the program [59]. Our results were checked robustly through two methods. Firstly, our unrenormalized virtual matrix element, using traditional Feynman rule based tensor reduction methods as outlined in this thesis, was compared to the unrenormalized virtual matrix element generated using the unitarity methods outlined in [80, 81]. The diagrams are generated using the same program [82] but with two different model files: one which was made by hand and the other from an interface with [83]. These two results were compared for a single phase space point for individual diagrams at one helicity and then the sum over diagrams and helicities was compared. A second check was performed on the renormalized virtual matrix element. After performing our renormalization procedure we are left with only infrared poles. We checked that the coefficients of the IR poles cancelled with the poles coming from the dipole subtraction terms. We found agreement to 10 decimal places on comparison of phase space points.

5.5 Observables

We plot the $m_{\chi_1^0 \chi_1^0}$ reconstructed mass differential distribution in Figure 5.6 and see that it is not what one would naïvely expect at NLO. The NLO contribution is significantly larger than the LO one and the scale variation is actually increased rather than reduced in moving to NLO. The individual contributions to this graph are shown in Figure 5.7 and the dominant contribution to the NLO cross section is the real emission part. Therefore we can understand our original plot as follows: at NLO a new initial state $qg(\rightarrow \chi_1^0 \chi_1^0 q)$ opens up which is of

leading order type and because of the gluon in the pdf this is dominating the real radiation contribution as can be seen in Figure 5.8. Therefore we see large scale dependence in this result. We also have a contribution from the initial state $\bar{q}g(\rightarrow \chi_1^0\chi_1^0\bar{q})$ but this contribution is not as large (the asymmetry between these two channels is due to the asymmetry of the anti-quark and quark in the parton distribution function). We suppress this contribution by applying a jet veto where we discard all events with $p_T^{jet} > 20$ GeV and $\eta < 4.5$. It is our intention to examine only the radiative corrections to the original process, where the gluons that appear in the real emission part are due to soft and collinear emission. The jet veto suppresses contributions that belong to the distinct process of neutralino pair plus one hard jet at leading order. The effect of the jet veto on the real radiation contributions can be seen in Figure 5.9. This result is plotted in Figure 5.10.

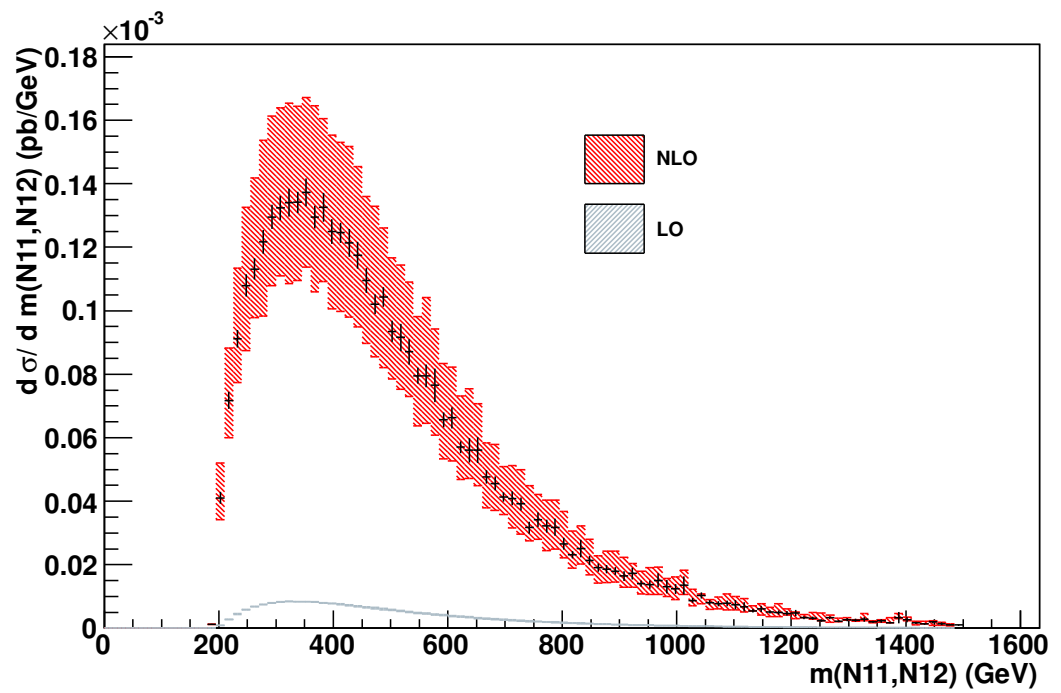


Figure 5.6: Comparison of the NLO and LO $m_{\chi_1^0 \chi_1^0}$ distributions for the process $pp \rightarrow \chi_1^0 \chi_1^0$. The band gives the dependence of the result on $\mu = \mu_F = \mu_R$ between $\mu_0/2$ and $2\mu_0$. We choose $\mu_0 = m_Z$. The black line gives the bin error for the value at the central scale.

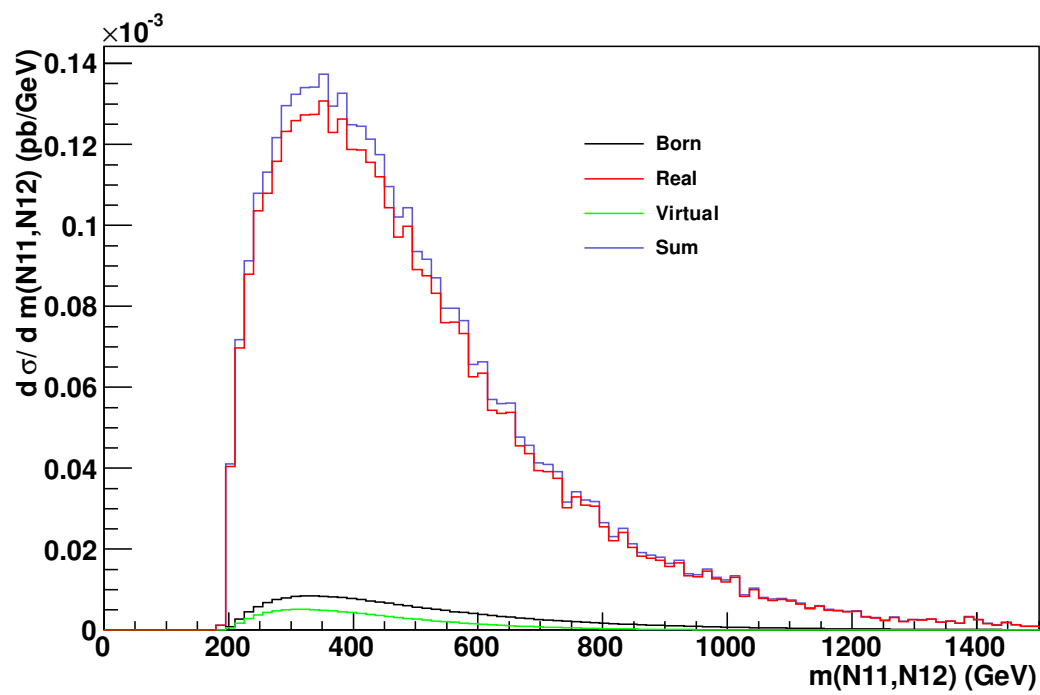


Figure 5.7: Contributions to the NLO $m_{\chi_1^0\chi_1^0}$ distributions for the process $pp \rightarrow \chi_1^0\chi_1^0$. We choose $\mu = \mu_F = \mu_R = \mu_0$ where $\mu_0 = m_Z$.

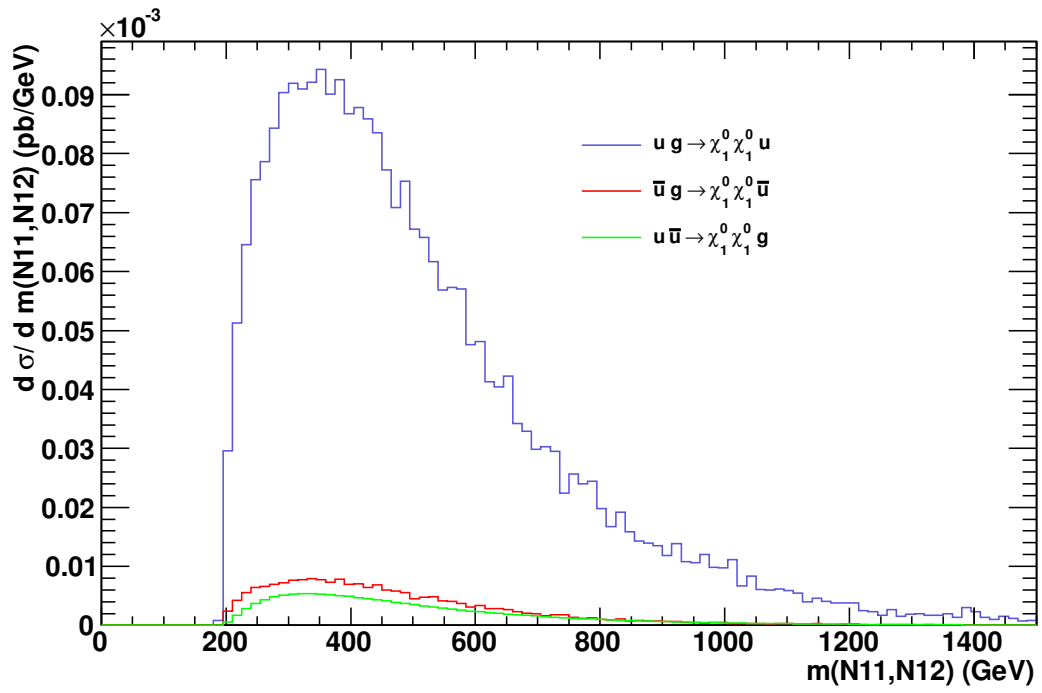


Figure 5.8: Contributions to the real emission differential cross section from the different channels relating to the u quark. This is including the effect of the parton distribution functions. We observe that the channel $ug \rightarrow \chi_1^0 \chi_1^0 u$ is significantly larger than the others.

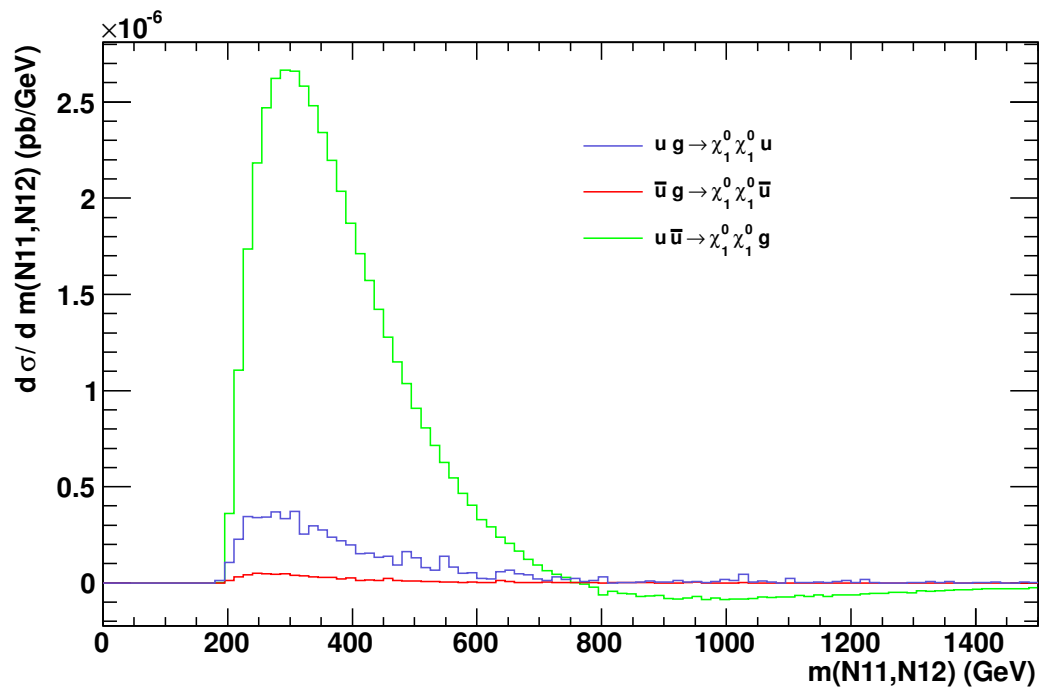


Figure 5.9: Contributions to the real emission differential cross section from the different channels relating to the u quark after the jet veto. This is including the effect of the parton distribution functions. One can see that the contribution of the dominant channels are greatly reduced when we impose the jet veto.

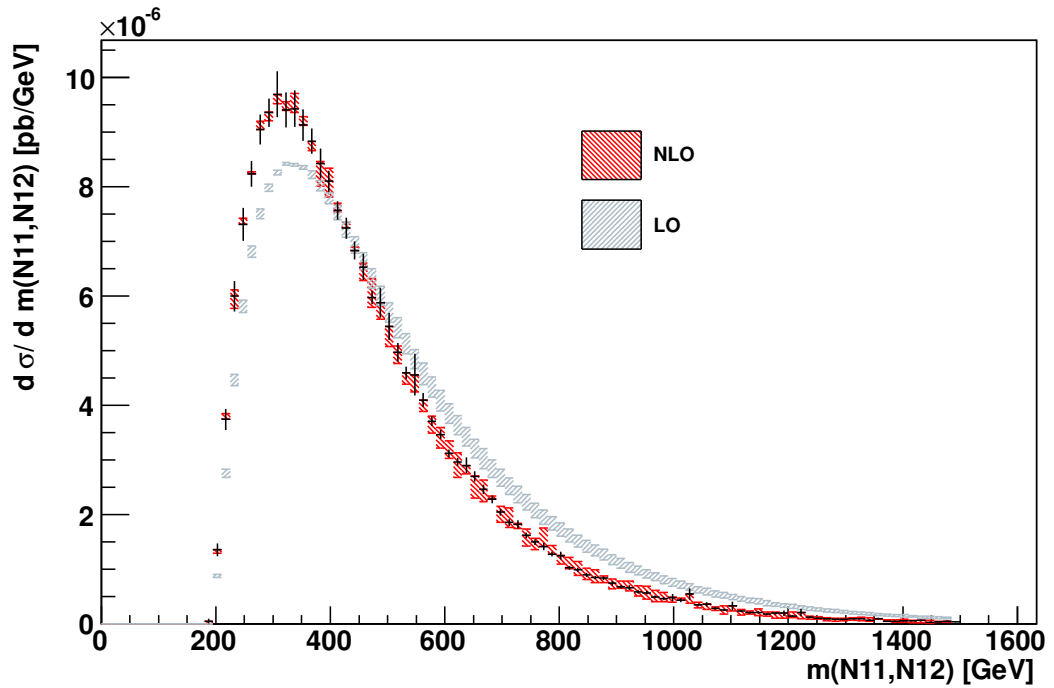


Figure 5.10: Comparison of the NLO and LO $m_{\chi_1^0 \chi_1^0}$ distributions for the process $pp \rightarrow \chi_1^0 \chi_1^0$ with a jet veto on jets with $p_T^{jet} > 20$ GeV and $\eta < 4.5$. The band gives the dependence of the result on $\mu = \mu_F = \mu_R$ between $\mu_0/2$ and $2\mu_0$. We choose $\mu_0 = m_Z$. The black line gives the bin error for the value at the central scale.

Chapter 6

Conclusions and Outlook

6.1 Conclusions

The Large Hadron Collider needs precise theoretical predictions; in perturbative QCD one must work at least to Next to Leading Order. These calculations are typically long, with many diagrams to be computed and are therefore error prone. Due to this we desire an automated approach to these calculations and in this thesis we have outlined the necessary components required to achieve this within the context of the Minimal Supersymmetric Standard Model.

We outlined the experimental status of searches for the Higgs boson and supersymmetry. The Higgs boson's allowed mass range is getting smaller as more data is collected at the LHC, and it is only a matter of time before a definite statement about its existence can be made. In contrast, the search for supersymmetry is looking pessimistic but such is the nature of the theory that these searches merely exclude the allowed parameter space. In fact, the value of exclusions for specific supersymmetry breaking scenarios is questionable; model independent searches allow one to look for generic signals of SUSY and then afterwards the actual nature of supersymmetry breaking can be examined.

We proceeded to describe the details of a NLO calculation. Initially, we looked at the color structure of an amplitude and how this can be reduced in an algorithmic way. Next, we discussed the spinor helicity formalism and how one can reduce any spinorial expression to one that includes spinor products that can be computed numerically. A key feature of our approach is that it can deal with diagrams with ill-defined fermion flow i.e. diagrams that include Majorana fermions. It is therefore applicable to theories beyond the Standard Model, specifically the MSSM.

This discussion led to another on regularisation scheme choice, where we described the freedom one has in dimensional regularisation. We focused on the cases of 't Hooft-Veltman and dimensional reduction: the difference between the two lying in the treatment of internal gauge bosons. This difference can lead to ϵ terms in the numerator algebra for diagrams where gluons are involved in 't Hooft-Veltman. Therefore, as we regularize our loop integral by extending the integration dimension to $n = 4 - 2\epsilon$ we are lead to finite differences between the

two schemes.

We also examined the treatment of the loop integrals. The reduction of a tensor integral, appearing in a virtual diagram, to a scalar integral basis can introduce artificial singularities at certain kinematic points encoded in the determinant of the Gram matrix. This can ruin any automated approach as we rely on the numerical cancellation of singularities between different pieces of the amplitude. We discussed an approach that allows one to stop the reduction process at an alternative basis of integrals that avoids this problem *if* the kinematic region is dangerous. If not, then we can proceed with the reduction to scalar integrals. This approach can handle massive or massless internal particles but the final integrals in the reduction basis for the massive internal case had to be implemented. For the triangle integrals we have a set of infrared divergent integrals that needed to be computed and tested. Our results for these integrals were presented in a compact representation. Also, the corresponding tensor integrals, and the form factor reduction was tested. The implementation of these diagrams was a crucial step to allow our methods to be applied to processes beyond the Standard Model, such as the MSSM.

Our final chapter focused on the application of our implementation to a physical process; that of neutralino pair production at the LHC. We presented the full NLO results for this process and examined the effect of a jet veto on the real radiation part. Our conclusion was that a jet-veto was necessary to suppress the contributions from the real radiation part that are of a different nature to the radiative corrections of the original process. With this suppression we observed that the NLO calculation has reduced scale uncertainty. This NLO calculation has allowed us to assess the estimate of the error in the leading order calculation and has resulted in a more precise prediction.

6.2 Outlook

Our intention for the virtual matrix element code is to make it public and open source. It is set to provide a key component of an all encompassing framework for the full NLO calculation following the Binoth Les Houches accord [84]. This allows the interaction of the different components of the NLO calculations (the real emission, subtraction terms, virtual and renormalization). With the LHC now collecting data the time to complete precise calculations for Standard Model and beyond the Standard Model processes must be shortened and an agreement between all areas of the community can only facilitate this.

The next step for the application of these tools to the neutralino pair production result is to investigate the process with an additional jet in the final state. We have already seen that we have large enhancements at NLO for this channel and this process also provides a much clearer signal of missing energy plus jet. Also, we are interested in examining the decay chain of $\chi_1^0 \chi_2^0$ where the second neutralino then decays to another neutralino plus a lepton. Again, because of the lepton in the final state, this is experimentally much more interesting than just a missing energy signal.

Appendix A

Feynman Rules

A.1 Supersymmetric QCD

In this section we describe the supersymmetric extension to Quantum Chromodynamics (SUSY-QCD) [85]. Here we write down the SUSY-QCD Lagrangian. The bare Lagrangian is

$$\mathcal{L} = \mathcal{L}_0 + \mathcal{L}_{\text{ghost}} + \mathcal{L}_{\text{soft}} + \mathcal{L}_{\text{gauge fix}} \quad (\text{A.1})$$

where

$$\mathcal{L}_0 = -\frac{1}{4}(F_{\mu\nu}^a)^2 + \frac{1}{2}\bar{g}_a i\gamma^\mu (D_\mu)^{ab} \tilde{g}_b + \bar{q} i\gamma^\mu D_\mu q \quad (\text{A.2})$$

$$+ |D_\mu \tilde{q}_L|^2 + |D_\mu \tilde{q}_R|^2 - \frac{g^2}{2} \left(\tilde{q}_L^\dagger T^a q_L - \tilde{q}_R^\dagger T^a q_R \right)^2 \quad (\text{A.3})$$

$$- \sqrt{2}g \left(\tilde{q}_L^\dagger \tilde{g} P_L q + \bar{q} P_R \tilde{g} \tilde{q}_L - \tilde{q}_R^\dagger \tilde{g} P_R q - \bar{q} P_L \tilde{g} \tilde{q}_R \right) \quad (\text{A.4})$$

$$- m\bar{q}q - m^2 (|\tilde{q}_L|^2 + |\tilde{q}_R|^2) \quad (\text{A.5})$$

$$\mathcal{L}_{\text{gauge fix}} = -\frac{1}{2\xi} (\partial_\mu G_a^\mu)^2 \quad (\text{A.6})$$

$$\mathcal{L}_{\text{ghost}} = -\bar{u}^a \partial_\mu (D^\mu)^{ab} u_b. \quad (\text{A.7})$$

We have the definitions

$$F_a^{\mu\nu} = \partial^\mu G_a^\nu - \partial^\nu G_a^\mu - gf_{abc} G_b^\mu G_c^\nu \quad (\text{A.8})$$

and for the covariant derivative acting on fields in the fundamental representation:

$$D^\mu = \partial^\mu + igT^a G^{\mu a} \quad (\text{A.9})$$

and likewise for fields in the adjoint representation

$$D^{\mu,ab} = \partial^\mu \delta^{ab} + g f^{abc} G^{\mu c}. \quad (\text{A.10})$$

The Feynman rules for this theory are presented in Figure A.2, Figure A.3 and Figure A.4. SUSY also mixes interactions of the weak gauge fields with the gluons. These interactions are presented in Figure A.5.

A.2 Neutralino Sector

In this section we present the Feynman rules for the neutralino sector [17]. The rule for the squark-squark-neutralino interaction is related to the quark-Z and quark-photon interactions. Here, because we take the massless quark approximation, we omit any Higgsino contribution, as all these coupling vanish in the massless quark limit. For the quark-Z boson interaction we write the Feynman rule as

$$i\gamma^\mu [g_L \Pi_- + g_R \Pi_+] \quad (\text{A.11})$$

giving our constants as

$$g_L^f = -\frac{e}{s_w c_w} (T_f^3 - Q_f s_w^2) \quad (\text{A.12})$$

$$g_R^f = \frac{e}{s_w c_w} (Q_f s_w^2). \quad (\text{A.13})$$

The Feynman rules for (charge flow from quark to squark) is

$$i \left[A_L^f \Pi_- + A_R^f \Pi_+ \right]. \quad (\text{A.14})$$

where the constants are

$$A_L^f = -\sqrt{2} S_{KL} \frac{e}{s_w c_w} \left[T_f^3 N_{i2} c_w + N_{i1} s_w (Q_f - T_3^f) \right] \quad (\text{A.15})$$

$$A_R^f = \sqrt{2} S_{KR} \frac{e}{s_w c_w} [N_{i1} Q_f s_w] \quad (\text{A.16})$$

(for neutralino family i , squark family K and fermion flavour f). For the charge conjugated vertex (flow opposite to above: squark to quark) we have

$$i \left[A_R^{f*} \Pi_- + A_L^{f*} \Pi_+ \right]. \quad (\text{A.17})$$

In this final mixed Neutralino state the supersymmetric relation to the original coupling is lost. We can retrieve the original form if we shift the mixing matrices from the wino bino mixing matrices to the photino and zino matrices. We use the the mixing relations (2.100) to obtain

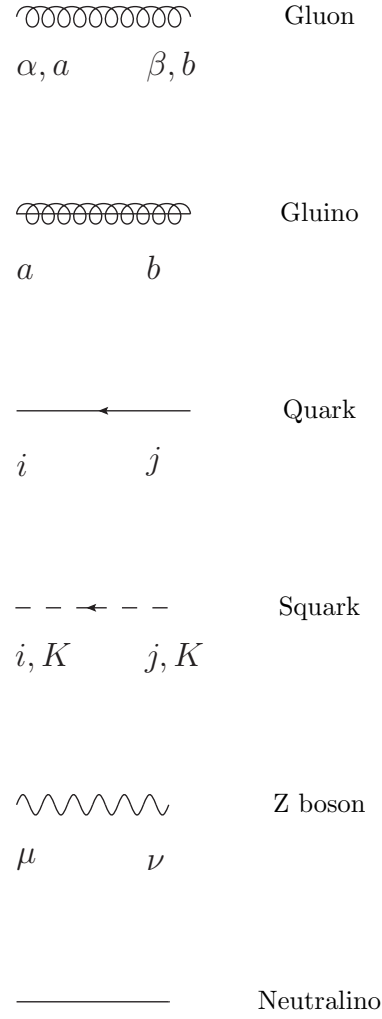


Figure A.1: Diagrammatic representation of particles. The indices are as follows: a, b stand for color indices in the adjoint representation and lowercase i, j represent color indices of the fundamental representation. Any Greek letters stand for the usual Lorentz indices. K, M represent the squark mass eigenstates which runs over 1 and 2 when we have squark mixing. Otherwise, an explicit L or R is present to indicate the squark interaction eigenstate.

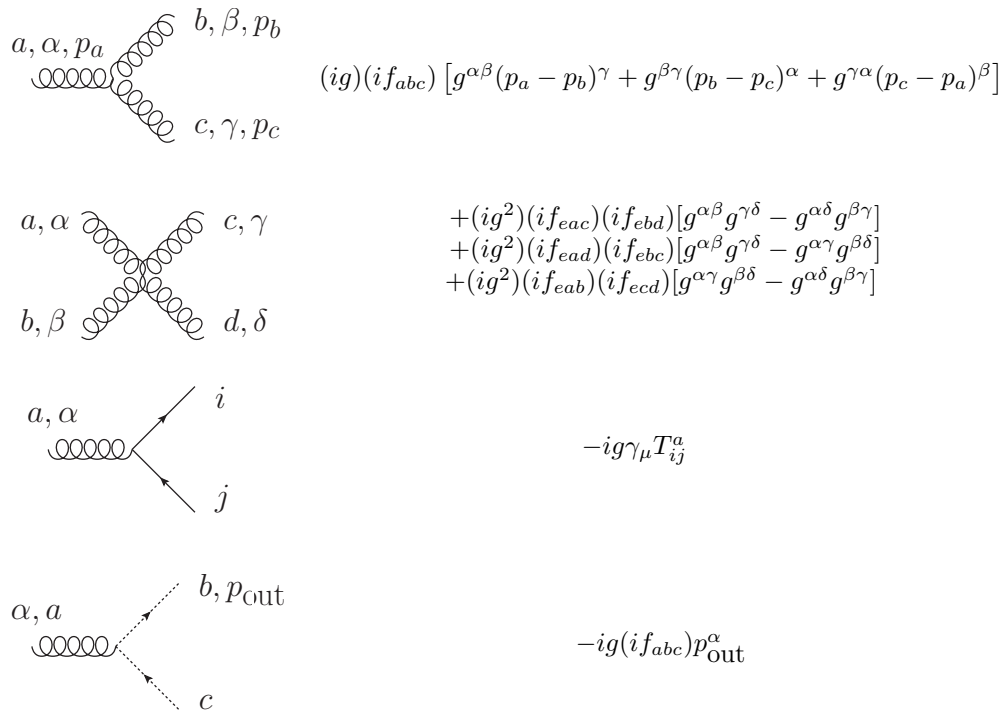


Figure A.2: QCD feynman rules.

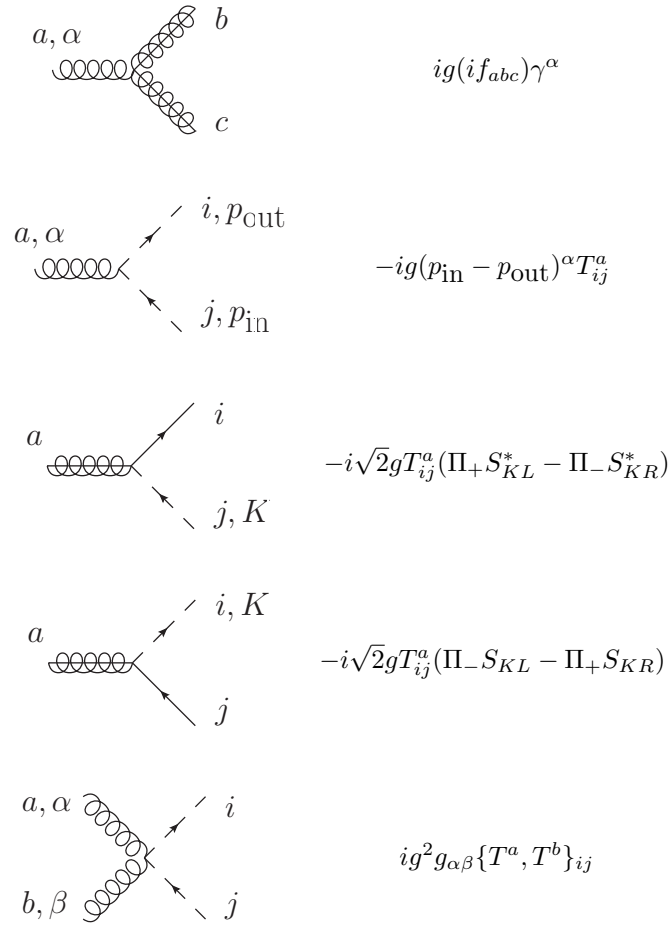


Figure A.3: Supersymmetric QCD feynman rules

$$\begin{array}{c}
 \begin{array}{ccc}
 L, k \searrow & & / L, i \\
 & \times & \\
 L, l \nearrow & & \searrow L, j
 \end{array} & -ig^2 [T_{ij}^a T_{kl}^a + T_{il}^a T_{kj}^a] \\
 \\
 \begin{array}{ccc}
 R, k \searrow & & / L, i \\
 & \times & \\
 R, l \nearrow & & \searrow L, j
 \end{array} & +ig^2 [T_{ij}^a T_{lk}^a] \\
 \\
 \begin{array}{ccc}
 R, k \searrow & & / R, i \\
 & \times & \\
 R, l \nearrow & & \searrow R, j
 \end{array} & -ig^2 [T_{ij}^a T_{kl}^a + T_{il}^a T_{kj}^a]
 \end{array}$$

Figure A.4: Four scalar interactions in Supersymmetric QCD.

$$\begin{array}{c}
 \begin{array}{ccc}
 g, \alpha, a & & / K, j \\
 \text{gluon} & & \\
 \gamma, \beta & & \searrow M, i
 \end{array} & 2ig_s T_{ij}^a \delta_{km} (eQ_f) \\
 \\
 \begin{array}{ccc}
 g, \alpha, a & & / K, j \\
 \text{gluon} & & \\
 Z, \beta & & \searrow M, i
 \end{array} & 2ig_s T_{ij}^a \frac{e}{c_w s_w} (T_f^3 S_{kL}^* S_{mL} - Q_f s_w^2 \delta_{km})
 \end{array}$$

Figure A.5: Squark-Gauge boson-gluon vertices with squark mixing. We get off diagonal contributions in the Z boson vertex.

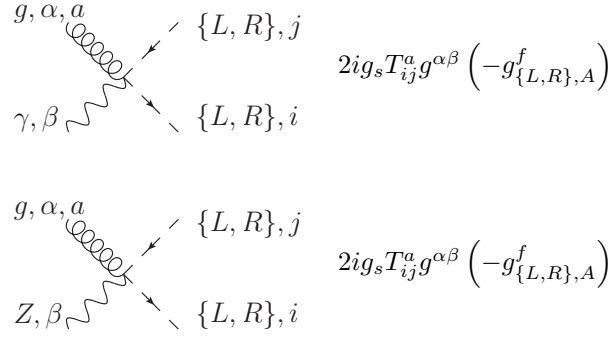


Figure A.6: Squark-Gauge boson gluon vertices without squark mixing.

the following equivalent expressions:

$$A_L^f = \sqrt{2} S_{KL} \left(N_{i1}^* g_L^A + N_{i2}^* g_L^Z \right). \quad (\text{A.18})$$

and

$$A_R^f = -\sqrt{2} S_{KR} \left(g_R^A N_{i1}' + g_R^Z N_{i2}' \right). \quad (\text{A.19})$$

In this basis we can see clearly the relation between the Standard Model coupling and the SUSY coupling. The full Feynman rules are presented in Figure A.7. We need the following two couplings also:

$$g_{\chi\chi Z,L} = -i \frac{e}{2c_w s_w} (N_{i3}^* N_{j3}^* - N_{i4}^* N_{j4}^*) \quad (\text{A.20})$$

$$g_{\chi\chi Z,R} = i \frac{e}{2c_w s_w} (N_{i3}^* N_{j3} - N_{i4}^* N_{j4}). \quad (\text{A.21})$$

They are proportional to the higgsino mixing matrices. This is because we arrive at this vertex through a SUSY transformation from the Higgs-Z vertex. That is, the coupling must be Higgsino only. Because we make the approximation of massless quarks we omit the discussion of the Higgs-squark-squark couplings as these vanish in this approximation.

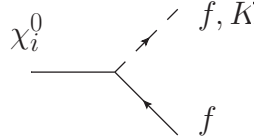
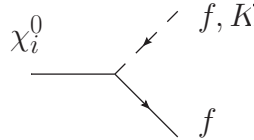
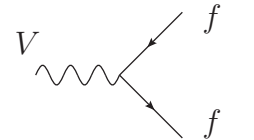
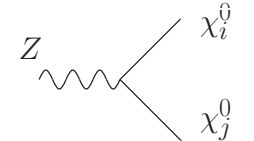
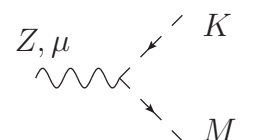
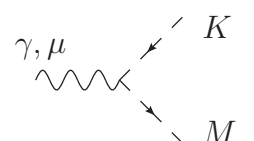
	$i \left[A_L^f \Pi_- + A_R^f \Pi_+ \right]$
	$i \left[A_R^{f*} \Pi_- + A_L^{f*} \Pi_+ \right]$
	$i \gamma^\mu \left[g_{L,V}^f \Pi_- + g_{R,V}^f \Pi_+ \right]$
	$\gamma^\mu \left[g_{\chi\chi Z, L} \Pi_- + g_{\chi\chi Z, R} \Pi_+ \right]$
	$i \left[g_{L,Z}^f S_{KL}^* S_{ML} + g_{R,Z}^f S_{KR}^* S_{MR} \right] (p_K - p_M)^\mu$
	$i \delta_{KM} (-e Q_f) (p_K - p_M)^\mu$

Figure A.7: Neutralino Feynman Rules in wino bino basis. The constants are found in the main text. We have dropped the color indices as all these interactions are diagonal in color space. The indices we have are f for the flavour of the quark/squark and K for the generation of the squark. The complex conjugate has an effect on the mixing matrices present in the couplings. All momenta are incoming.

Appendix B

Breaking SUSY by choice of Regularisation Scheme

B.1 Verifying the invariance of the SUSY Yang Mills Lagrangian

This is a non-trivial exercise in spinor algebra. We set the auxiliary fields to zero to make it easier. Then we compute the variation of the two parts of the Lagrangian separately. The Lagrangian is

$$\mathcal{L} = \underbrace{-\frac{1}{4}G_{\mu\nu}^a G^{\mu\nu a}}_{\mathcal{L}_1} + \underbrace{\frac{i}{2}\bar{\lambda}^a \not{D}\lambda^a}_{\mathcal{L}_2}. \quad (\text{B.1})$$

where we have:

$$D_\mu^{ab} = \delta^{ab}\partial_\mu - gf^{abc}W_\mu^c \quad (\text{B.2})$$

$$G_{\mu\nu}^a = \partial_\mu W_\nu^a - \partial_\nu W_\mu^a + gf^{abc}W_\mu^b W_\nu^c. \quad (\text{B.3})$$

Now we show that the above Lagrangian is invariant under the following supersymmetric transformations:

$$\delta W_\mu^a = i\bar{\epsilon}\gamma_\mu\lambda^a \quad (\text{B.4})$$

$$\delta\lambda^a = \frac{1}{2}G_{\mu\nu}^a\gamma^\mu\gamma^\nu.$$

B.1.1 \mathcal{L}_1

The gauge field kinetic term's variation gives

$$\delta\mathcal{L}_1 = -\frac{1}{2}G_{\mu\nu}^a(\delta G^{\mu\nu a}) \quad (\text{B.5})$$

$$= -\frac{1}{2}G_{\mu\nu}^a(2\partial^\mu\delta W^{\nu a} + 2gf^{abc}\delta W^{\mu b}W^{\nu c}) \quad (\text{B.6})$$

$$= -i(\bar{\epsilon}\gamma^\nu\partial^\mu\lambda^a)G_{\mu\nu}^a - igG_{\mu\nu}^af^{abc}(\bar{\epsilon}\gamma^\mu\lambda^b)W^{\nu c} \quad (\text{B.7})$$

where we have used the anti-symmetry of $G^{\mu\nu}$ to simplify the expression, before plugging in the SUSY transformations.

B.1.2 \mathcal{L}_2

We now look at the variation of the Majorana term. The quickest way to get to our result is to show that

$$\delta\mathcal{L}_2 = \frac{i}{2}\left[(\delta\bar{\lambda}^a)\not{D}^{ab}\lambda^b + \bar{\lambda}^a(\delta\not{D}^{ab})\lambda^b + \bar{\lambda}^a\not{D}^{ab}(\delta\lambda^b)\right] \quad (\text{B.8})$$

$$= \frac{i}{2}\left[\underbrace{2(\delta\bar{\lambda}^a)\not{D}^{ab}\lambda^b}_{\delta\mathcal{L}_{2a}} + \underbrace{\bar{\lambda}^a(\delta\not{D}^{ab})\lambda^b}_{\delta\mathcal{L}_{2b}}\right] \quad (\text{B.9})$$

We consider each part in turn.

B.1.2.1 \mathcal{L}_{2a}

This piece gives the cancellation with the piece from $\delta\mathcal{L}_1$. The first term gives

$$\underbrace{2(\delta\bar{\lambda}^a)\not{D}\lambda}_{\delta\mathcal{L}_{2a}} = \frac{2}{2}\bar{\epsilon}\gamma^\nu\gamma^\mu\gamma^\rho(\partial_\rho\lambda^a - gf^{abc}\lambda^bW_\rho^c)G_{\mu\nu}^a. \quad (\text{B.10})$$

Using the following identity for the gamma matrices:

$$\gamma^\alpha\gamma^\beta\gamma^\gamma = \hat{g}^{\alpha\beta}\hat{\gamma}^\gamma - \hat{g}^{\beta\gamma}\hat{\gamma}^\alpha + \hat{g}^{\gamma\alpha}\hat{\gamma}^\beta - i\gamma_5\gamma_\delta\epsilon^{\alpha\beta\gamma\delta} + \bar{g}^{\alpha\beta}\hat{\gamma}^\gamma - \bar{g}^{\beta\gamma}\hat{\gamma}^\alpha + \bar{g}^{\gamma\alpha}\hat{\gamma}^\beta. \quad (\text{B.11})$$

we can begin rewriting our expression. We have

$$\underbrace{2(\delta\bar{\lambda}^a)\not{D}\lambda}_{\delta\mathcal{L}_{2a}} = \bar{\epsilon}(g^{\nu\mu}\gamma^\rho - \gamma^\mu g^{\nu\rho} + \gamma^\nu g^{\mu\rho} - i\gamma_5\gamma_\delta\epsilon^{\nu\mu\rho\delta})(\partial_\rho\lambda^a - gf^{abc}\lambda^bW_\rho^c)G_{\mu\nu}^a. \quad (\text{B.12})$$

The first term vanishes due to the symmetric $g^{\mu\nu}$ hitting the anti-symmetric field strength tensor. The final term also vanishes although this is far less obvious: we can rewrite it as

$$-i\bar{\epsilon}\gamma_5\gamma_\delta\epsilon^{\nu\mu\rho\delta}(\partial_\rho\lambda^a - if^{abc}\lambda^bW_\rho^c)G_{\mu\nu}^a \quad (\text{B.13})$$

$$= -i\bar{\epsilon}\gamma_5\gamma_\delta\lambda^a[-\lambda^a(\delta^{ab}\partial_\rho - if^{abc}W_\rho^c)]G_{\mu\nu}^b \quad (\text{B.14})$$

where we have used the usual integration by parts trick on the first term and on the second we have used the antisymmetry of the tensor f . Now this is equal to

$$-2i\bar{\epsilon}\gamma_5\gamma_\delta\lambda^a D_\rho^{ab}\tilde{G}^{b\rho\delta} \quad (\text{B.15})$$

where the dual field strength tensor is

$$\tilde{G}^{\mu\nu} = \frac{1}{2}\epsilon^{\mu\nu\alpha\beta}F_{\alpha\beta}. \quad (\text{B.16})$$

A general result of Yang Mills theory is that the dual strength tensor has the equation of motion (from the Bianchi identity)

$$D^\nu\tilde{F}_{\mu\nu} = 0 \quad (\text{B.17})$$

therefore our final term here is zero. This only leaves the second and third terms. Our final result is

$$\delta\mathcal{L}_{2a} = 2\bar{\epsilon}\gamma^\nu(\partial^\mu\lambda^a)G_{\mu\nu}^a + 2gf^{abc}(\bar{\epsilon}\gamma^\mu\lambda^b)W^{\nu c}G_{\mu\nu}^a \quad (\text{B.18})$$

upon using the anti-symmetry properties of the field strength tensor. Recalling, that we took out a factor of $i/2$ we see that this term alone cancels with that coming from $\delta\mathcal{L}_1$. This leaves us with the inspection of $\delta\mathcal{L}_{2b}$.

B.1.2.2 \mathcal{L}_{2b}

Now we examine the part \mathcal{L}_{2b} . We see that this is equal to

$$\bar{\lambda}^a(\delta\mathcal{D}^{ab})\lambda^b - gf^{abc}\bar{\lambda}^a\gamma^\mu\lambda^b\delta W_\mu^c = -igf^{abc}(\bar{\lambda}^a\gamma^\mu\lambda^b)(\bar{\epsilon}\gamma_\mu\lambda^c) \quad (\text{B.19})$$

This part is exactly zero, but to show this one has to use Fierz identities that only hold in 4 dimensions. We rewrite the expression in terms of Weyl spinors to get (we drop color indices)

$$\bar{\epsilon}\gamma^\mu\lambda\bar{\lambda}\gamma_\mu\lambda = \begin{pmatrix} \chi_\epsilon^\alpha & \bar{\psi}_{\epsilon\dot{\alpha}} \end{pmatrix} \begin{pmatrix} 0 & \sigma^\mu \\ \bar{\sigma}^\mu & 0 \end{pmatrix} \begin{pmatrix} \psi_\alpha \\ \bar{\psi}^{\dot{\alpha}} \end{pmatrix} \begin{pmatrix} \psi^\beta & \bar{\psi}_{\dot{\beta}} \end{pmatrix} \begin{pmatrix} 0 & \sigma^\mu \\ \bar{\sigma}^\mu & 0 \end{pmatrix} \begin{pmatrix} \psi_\beta \\ \bar{\psi}^{\dot{\beta}} \end{pmatrix} \quad (\text{B.20})$$

$$= (\bar{\sigma}^\mu)^{\dot{\alpha}\alpha}(\bar{\sigma}^\mu)^{\dot{\beta}\beta} \left[\bar{\psi}_{\epsilon\dot{\alpha}}\bar{\psi}^{\dot{\beta}}\psi_\alpha\psi^\beta - \bar{\psi}_{\epsilon\dot{\alpha}}\bar{\psi}^{\dot{\beta}}\psi_\alpha\psi^\beta - \chi_\epsilon^\beta\psi_\alpha\bar{\psi}^{\dot{\beta}}\bar{\psi}_{\dot{\beta}} + \chi_\epsilon^\beta\psi_\alpha\bar{\psi}^{\dot{\beta}}\bar{\psi}_{\dot{\alpha}} \right] \quad (\text{B.21})$$

$$= 2 \left[(\bar{\psi}^\epsilon\bar{\psi})(\psi\psi) - (\bar{\psi}^\epsilon\bar{\psi})(\psi\psi) - (\bar{\chi}_\epsilon\bar{\psi})(\psi\psi) + (\bar{\chi}_\epsilon\bar{\psi})(\psi\psi) \right] \quad (\text{B.22})$$

which is non-zero because the fields ψ have color indices. However, it is symmetric in at least two of three of these color indices and it comes with the anti-symmetric tensor. Therefore this is zero. In order to achieve this result we have used the Fierz identity which only holds in 4 dimensions. We expect to run into problems when we extend to dimensions that are not 4.

The term $f^{abc}\bar{\lambda}^a\gamma^\mu\lambda^b\delta W_\mu^c$ and its non-zero value away from $n = 4$ is known as the Siegel ambiguity [86, 62, 87]. This exact non-zero variation of the Lagrangian can lead to a discrepancy

in the couplings that were equal at tree level. A simple example is that of the quark-gluon coupling g_s and the quark-gluino-squark coupling. The equality between the two is not preserved when we use dimensional regularisation. To obtain equality at the one-loop level we have to include finite counter terms in the renormalization constants.

B.2 Finite Scheme Dependent Differences

In this section we look at examples of how the scheme dependent finite difference comes about by comparing dimensional regularisation and dimensional reduction. We look at two contributions to the squark self-energy: the one coming from the gluon contribution and the one from the gluino contribution.

B.2.1 Squark Self Energy

B.2.1.1 Gluon contribution

Consider the gluon loop contribution to the squark self energy. We have the following expression (for simplicity we drop the color indices, any factors of i and the couplings)

$$\Gamma = \int \frac{d^n k}{i\pi^{\frac{n}{2}}} \frac{1}{(k+p)^2 - m_q^2} (k-2p)_\alpha (k-2p)_\beta \frac{-g_{\alpha\beta}}{k^2} \quad (\text{B.23})$$

In dimensional regularisation everything (apart from the external momentum p) is continued to n dimensions. In dimensional reduction, only the internal momentum k is. Therefore we have

$$\Gamma_{\text{DRED}} = \int \frac{d^n k}{i\pi^{\frac{n}{2}}} \left[-\frac{i}{(k+p)^2 - m_q^2} (k-2p)^\alpha (k-2p)^\beta \right] \frac{\hat{g}_{\alpha\beta}}{k^2} \quad (\text{B.24})$$

$$\Gamma_{\text{DREG}} = \int \frac{d^n k}{i\pi^{\frac{n}{2}}} \left[-\frac{i}{(k+p)^2 - m_q^2} (k-2p)^\alpha (k-2p)^\beta \right] \frac{\hat{g}_{\alpha\beta} + \bar{g}_{\alpha\beta}}{k^2}. \quad (\text{B.25})$$

We see that the difference is proportional to the term $\hat{g}^{\alpha\beta}$ coming from the gluon propagator. The tensor decomposition of the integral will give a term proportional to $g^{\alpha\beta} = \hat{g}^{\alpha\beta} + \bar{g}^{\alpha\beta}$ for both cases. Therefore if we write Δ as the difference between the **DREG** and the **DRED** result we have

$$\Delta = \Gamma_{\text{DREG}} - \Gamma_{\text{DRED}} = - \int \frac{d^n k}{i\pi^{\frac{n}{2}}} \frac{\bar{k}^2}{(k+p)^2 - m_q^2 k^2}. \quad (\text{B.26})$$

as $\bar{k} \cdot \hat{p} = 0$. We have shown that we can relate this \bar{k} integral to a higher dimensional one, and our result for this part is

$$\int \frac{d^n k}{i\pi^{\frac{n}{2}}} \frac{\bar{k}^2}{(k+p)^2 - m_q^2 k^2} = +\epsilon I_N^{n+2}(p^2; m_q^2, 0) \quad (\text{B.27})$$

where the higher dimensional integral is

$$I_N^{n+2}(s; m^2, 0) = -\frac{\Gamma(1+\epsilon)}{\epsilon} \left(-\frac{s}{6} + \frac{m^2}{2} \right). \quad (\text{B.28})$$

Therefore our finite difference is

$$\Delta = -\Gamma(1+\epsilon) \left(\frac{s}{6} - \frac{m^2}{2} \right) \quad (\text{B.29})$$

B.2.1.2 Squark Gluino Loop

A careful examination of this diagram shows that there are no extra finite terms: this should be expected there is no gluon involved. However, for illustrative purposes we look at it in detail. The graph looks like (again we ignore the color factor and factors of i)

$$\Gamma = \int \frac{d^n k}{i\pi^{\frac{n}{2}}} \frac{\text{tr}\{\Pi_+(\not{k} + m_{\tilde{g}})\Pi_-(\not{k} + \not{p})\}}{[k^2 - m_{\tilde{g}}^2][(k+p)^2]}. \quad (\text{B.30})$$

We split $k = \hat{k} + \bar{k}$ for the internal momentum, in both dimensional regularisation and dimensional reduction. The term of interest (as it could possibly lead to a finite difference) contains

$$\text{tr}\{\Pi_+\not{k}\Pi_-\not{k}\} = \text{tr}\left\{\Pi_+(\not{\hat{k}} + \not{\bar{k}})\Pi_-(\not{\hat{k}} + \not{\bar{k}})\right\} \quad (\text{B.31})$$

$$= \text{tr}\left\{\Pi_+\hat{k}\hat{k}\right\} \quad (\text{B.32})$$

as in the **HV** scheme we have $\Pi_+\hat{k} = \hat{k}\Pi_+$. Therefore the trace is reduced to a four dimensional trace. This occurs in both dimensional regularisation and dimensional reduction and we have no extra ϵ pieces. Therefore the finite difference between the two schemes is zero.

Appendix C

Loop Integrals

C.1 Derivation of loop integral formula

As explained in Section 4 in virtual calculations one has to perform an integral over the unresolved momentum running in the loop. One can cast this integral into a general form and arrive at a formula that relates the momentum integral in Minkowski space to a function of kinematic variables and a possible integral over the Feynman parameters. Here we carry out the procedure for the general N -point, n dimensional scalar case. To begin, we define the general integral as:

$$I_N^n = \int \frac{d^n k}{i\pi^{\frac{n}{2}}} \frac{1}{\prod_{j=1}^N (q_j^2 - m_j^2 + i\delta)} \quad (\text{C.1})$$

$$= \Gamma(N) \int_0^\infty \prod_{i=1}^N dz_i \delta(1 - \sum_{l=1}^N z_l) \int \frac{d^n k}{i\pi^{\frac{n}{2}}} \left[\sum_{k=1}^N z_k (q_k^2 - m_k^2 + i\delta) \right]^{-N} \quad (\text{C.2})$$

using standard Feynman parameterisation. The denominator is quadratic in the loop momentum k . Our aim is to symmetrize the k integral. To this end, we rewrite the denominator as follows:

$$\sum_{k=1}^N z_k (q_k^2 - m_k^2) + i\delta = \sum_{k=1}^N z_k [(k + r_k)^2 - m_k^2] + i\delta \quad (\text{C.3})$$

$$= \sum_{k=1}^N z_k [k^2 + 2r_k \cdot k + r_k^2 - m_k^2] + i\delta \quad (\text{C.4})$$

$$= k^2 + 2k \cdot Q + \sum_{k=1}^N z_k (r_k^2 - m_k^2) + i\delta \quad (\text{C.5})$$

$$(\text{C.6})$$

where $Q^\mu = \sum_{k=1}^N z_k r_k$. We change variables here, letting $k \rightarrow k + Q \implies k = l - Q$, then

$$\begin{aligned} k^2 + 2k \cdot Q &= l^2 + Q^2 - 2l \cdot Q + 2l \cdot Q - 2Q^2 \\ &= l^2 - Q^2 \end{aligned}$$

so our denominator is now:

$$l^2 - Q^2 + \sum_{k=1}^N z_k (r_k^2 - m_k^2) + i\delta = l^2 - R^2 + i\delta \quad (\text{C.7})$$

where

$$R^2 = Q^2 - \sum_{i=1}^N z_i (r_i^2 - m_i^2) \quad (\text{C.8})$$

$$= \sum_{i,j=1}^N z_i z_j r_i \cdot r_j - \sum_{i,j=1}^N z_i (r_i^2 - m_i^2) z_j \quad (\text{C.9})$$

$$= \sum_{i,j=1}^N z_i z_j r_i \cdot r_j - \frac{1}{2} \sum_{i=1}^N z_i (r_i^2 - m_i^2) \sum_{j=1}^N z_j - \frac{1}{2} \sum_{j=1}^N z_j (r_j^2 - m_j^2) \sum_{i=1}^N z_i \quad (\text{C.10})$$

$$= -\frac{1}{2} \sum_{i,j=1}^N z_i z_j (r_i^2 + r_j^2 - 2r_i \cdot r_j - m_i^2 - m_j^2) \quad (\text{C.11})$$

$$= -\frac{1}{2} \sum_{i,j=1}^N z_i z_j S_{ij} \quad (\text{C.12})$$

$$= -\frac{1}{2} \vec{z} \cdot \mathbf{S} \cdot \vec{z}. \quad (\text{C.13})$$

We have used the definition of the kinematic or *Cayley matrix* $S_{ij} = (r_i - r_j)^2 - m_i^2 - m_j^2$. This encodes all the kinematics of the loop. We can now re-write our integral in the symmetric form:

$$I_N^R = \Gamma(N) \int_0^\infty \prod_{i=1}^N dz_i \delta(1 - \sum_{l=1}^N z_l) \int \frac{d^n l}{i\pi^{\frac{n}{2}}} [l^2 - R^2 + i\delta]^{-N} \quad (\text{C.14})$$

$$= \Gamma(N) \int_0^\infty \prod_{i=1}^N dz_i \delta(1 - \sum_{l=1}^N z_l) \int \frac{d^n l}{i\pi^{\frac{n}{2}}} \left[l^2 + \frac{1}{2} z \cdot S \cdot z + i\delta \right]^{-N}. \quad (\text{C.15})$$

We are now in a position to carry out the k integral. We carry out the complex integral in the l_0 plane. In Euclidean space the poles occur at:

$$l_0^2 = R^2 + |\vec{l}|^2 - i\delta \quad (\text{C.16})$$

we solve this, as δ is small:

$$\sqrt{x - ib} = \sqrt{x} \left(1 - \frac{ib}{x} \right) \quad (\text{C.17})$$

$$= \sqrt{x} \left(1 - \frac{1}{2} \frac{ib}{x} \right) \sim \sqrt{x} - i\delta \quad (\text{C.18})$$

giving

$$l^{0,\pm} \simeq \pm \sqrt{R^2 + |\vec{l}|^2} \mp i\delta. \quad (\text{C.19})$$

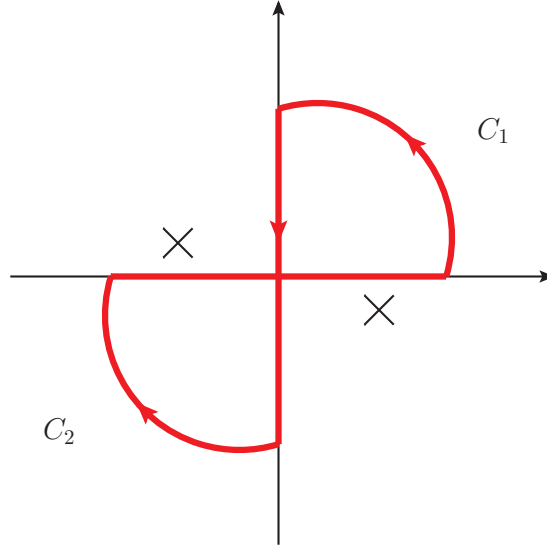


Figure C.1: The location of poles and the contour integral in the l_0 plane as described in (C.20).

In the complex l^0 plane we see that the poles are shifted away from the real axis: for the positive real part they are pushed into the fourth quadrant and for the negative real part they are pushed up into the second quadrant. This is shown in Figure C.1. The Wick rotation is carried out as follows: we analytically continue the variable l^0 to the complex plane and close the integration contour at infinity in the first and third quadrants. This integral has to vanish as it contains no poles. Therefore we have

$$\oint_C f(l_0^2 - |\vec{l}|^2) \equiv 0 \quad (\text{C.20})$$

$$= \int_{-R}^R dl_0 f(l_0^2 - |\vec{l}|^2) + \int_{+R}^{-R} dl_0 f(l_0^2 - |\vec{l}|^2) + \int_{C_1} f(l_0^2 - |\vec{l}|^2) + \int_{C_2} f(l_0^2 - |\vec{l}|^2). \quad (\text{C.21})$$

We can parameterise the curved part as:

$$\int_{C_1} dl_0 f(l_0^2 - |\vec{l}|^2) = iR \int_0^{\frac{\pi}{2}} d\theta e^{i\theta} f(R^2 - |\vec{l}|^2) \quad (\text{C.22})$$

$$(\text{C.23})$$

giving

$$\left| \int_{C_1} dl_0 f(R^2 - |\vec{l}|^2) \right| = R \left| f(R^2 - |\vec{l}|^2) \right| \left| i \int_0^{\frac{\pi}{2}} d\theta e^{i\theta} \right| \quad (\text{C.24})$$

$$\leq R |f(R^2 - |\vec{l}|^2)| \quad (\text{C.25})$$

(actually the integral is $i \int_0^{\pi/2} e^{i\theta} = -1 + e^{i\pi/2}$). In practice the function f is of the form $\sim (k^2)^{-n}$ so for $n \geq 1$, and in the limit $R \rightarrow \infty$ then the curved contribution to the integral is zero i.e. (C.24) becomes

$$\left| \int_{C_1} dl_0 f(R^2 - |\vec{l}|^2) \right| \leq R^{1-2k} \xrightarrow{R \rightarrow \infty} 0. \quad (\text{C.26})$$

Therefore (C.20) gives us

$$\int_{-\infty}^{\infty} dl_0 f(l_0^2 - |\vec{l}|^2) = - \int_{+\infty}^{-\infty} dl_0 f(l_0^2 - |\vec{l}|^2) \quad (\text{C.27})$$

and we let $l^0 \rightarrow il_4$ such that $l^2 \rightarrow -l_E^2 = -l_4^2 - |\vec{l}|^2$. giving

$$\int_{-\infty}^{\infty} dl_0 f(l_0^2 - |\vec{l}|^2) = - \int_{+\infty}^{-\infty} dl_0 f(l_0^2 - |\vec{l}|^2) = i \int_{-\infty}^{\infty} dl_4 f(-l_E^2). \quad (\text{C.28})$$

This completes the Wick rotation. After this step our integral takes the form:

$$I_N^n = i(-1)^N \Gamma(N) \int_0^\infty \prod_{i=1}^N dz_i \delta(1 - \sum_{l=1}^N z_l) \int \frac{d^n l_E}{i\pi^{\frac{n}{2}}} [l_E^2 + R^2 - i\delta]^{-N} \quad (\text{C.29})$$

We finish off the momentum space integral by introducing polar-coordinates. We use:

$$\int_{-\infty}^{+\infty} d^n l_E = \int_0^\infty dr r^{n-1} \int d\Omega_{n-1} \quad (\text{C.30})$$

where

$$r = \sqrt{l_E^2}, \quad \int d\Omega_{n-1} = V(n) = \frac{2\pi^{\frac{n}{2}}}{\Gamma(\frac{n}{2})} \quad (\text{C.31})$$

where $V(n)$ is the volume of the n -dimensional unit sphere. Thus,

$$I_N^n = 2(-1)^N \frac{\Gamma(N)}{\Gamma(n/2)} \int_0^\infty \prod_{i=1}^N dz_i \delta(1 - \sum_{l=1}^N z_l) \int_0^\infty dr r^{n-1} [r^2 + R^2 - i\delta]^{-N}. \quad (\text{C.32})$$

The $i\pi^{n/2}$ in the definition of our integral has been cancelled by the i coming from the Wick rotation and the $\pi^{n/2}$ coming from the angular integration in the Euclidean momentum space.

We complete the r integral by substituting $r^2 = x$, giving,:

$$\int_0^\infty dr^{n-1} \frac{1}{[r^2 + R^2 - i\delta]^N} = \frac{1}{2} \int_0^\infty dx x^{\frac{n}{2}-1} \frac{1}{[x + R^2 - i\delta]^N} \quad (\text{C.33})$$

$$= [R^2 - i\delta]^{1-N-1+\frac{n}{2}} \frac{1}{2} \int_0^\infty \frac{y^{\frac{n}{2}-1}}{(1+y)^N} \quad (\text{C.34})$$

$$= \frac{1}{2} [R^2 - i\delta]^{\frac{n}{2}-N} B\left(\frac{n}{2}, N - \frac{n}{2}\right) \quad (\text{C.35})$$

$$= \frac{1}{2} [R^2 - i\delta]^{\frac{n}{2}-N} \frac{\Gamma(\frac{n}{2}) \Gamma(N - \frac{n}{2})}{\Gamma(N)} \quad (\text{C.36})$$

where we have used the definition of the beta function:

$$B(a, b) = \int_0^\infty dz \frac{z^{a-1}}{(1+z)^{a+b}} = \int_0^1 dy y^{a-1} (1-y)^{b-1} = \frac{\Gamma(a)\Gamma(b)}{\Gamma(a+b)}. \quad (\text{C.37})$$

The result for the loop integral is therefore:

$$I_N^n = (-1)^N \Gamma(N - n/2) \int_0^\infty \prod_{i=1}^N dz_i \delta(1 - \sum_{l=1}^N z_l) [R^2 - i\delta]^{\frac{n}{2}-N} \quad (\text{C.38})$$

C.1.0.3 General Formula

We can now write down a formula for the general integral:

$$\int \frac{d^n l}{i\pi^{\frac{n}{2}}} \frac{(l^2)^r}{(l^2 - R^2 + i\delta)^N} = (-1)^{N+r} \frac{\Gamma(r + \frac{n}{2}) \Gamma(N - r - \frac{n}{2})}{\Gamma(\frac{n}{2}) \Gamma(N)} [R^2 - i\delta]^{r-N+\frac{n}{2}}. \quad (\text{C.39})$$

So the wick rotation had been performed (the left hand side is in Minkowski space) and also a shift in k , $k^\mu \rightarrow k^\mu + Q^\mu = k^\mu + \sum_{i=1}^N z_i r_i^\mu$ to get the quadratic form in the numerator.

C.2 Derivation in dimension splitting

After performing the dimension splitting as described in section 3.7 we arrive at integrals of the form

$$I_N^{n, \alpha; \mu_1 \dots \mu_r}(a_1, \dots, a_r; S) = \int \frac{d^n k}{i\pi^{\frac{n}{2}}} \frac{(\bar{k}^2)^\alpha \hat{q}_{a_1}^{\mu_1} \dots \hat{q}_{a_r}^{\mu_r}}{\prod_{j=1}^N (q_j^2 - m_j^2 + i\delta)} \quad (\text{C.40})$$

where, as before, we distinguish the vectors living in the 4 dimensional sub space by a hat and those in the $(n - 4)$ space by a bar. Writing out the q vectors explicitly this becomes:

$$I_N^{n,\alpha;\mu_1\dots\mu_r}(a_1,\dots,a_r;S) = \int \frac{d^n k}{i\pi^{\frac{n}{2}}} \frac{(\bar{k}^2)^\alpha \prod_{\nu=1}^r (\hat{k} + \hat{r}_{a_\nu})^{\mu_\nu}}{\prod_{j=1}^N [(k + r_j)^2 - m_j^2 + i\delta]} \quad (\text{C.41})$$

We apply the Feynman parameter formula

$$I_N^{n,\alpha;\mu_1\dots\mu_r}(a_1,\dots,a_r;S) = \Gamma(N) \int_0^\infty \prod_{j=1}^N dz_j \delta(1 - \sum_{i=1}^N z_i) \quad (\text{C.42})$$

$$\int \frac{d^4 \hat{k}}{i\pi^2} \frac{d^{n-4} \bar{k}}{\pi^{\frac{n}{2}-2}} \frac{(\bar{k}^2)^\alpha \prod_{\nu=1}^r (\hat{k} + \hat{r}_{a_\nu})^{\mu_\nu}}{\left[\sum_{k=1}^N z_k (q_k^2 - m_k^2 + i\delta) \right]^N} \quad (\text{C.43})$$

before we shift the integration momentum by $k \rightarrow l = k + Q$. Here $Q = \sum_{k=1}^N z_k r_k$ and here Q is a four dimensional object (it is made up of $r_i = \hat{r}_i$ as these are simply combinations of the external momenta. Therefore this shift does not affect the \bar{k} -integral in the $(n - 4)$ subspace. Using $k = l - Q$ we obtain for the numerator:

$$\hat{k}^\mu + \hat{r}_a^\mu \rightarrow \hat{l}^\mu - \sum_{k=1}^N z_k \hat{r}_k + \hat{r}_a = \hat{l} - \sum_{k=1}^N z_k (\hat{r}_k - \hat{r}_a)^\mu, \quad (\text{C.44})$$

and the denominator changes as:

$$\sum_{k=1}^N z_k [(q_k^2 - m_k^2) + i\delta] = \sum_{k=1}^N \bar{q}_j^2 + \sum_{j=1}^N z_k (\hat{q}_k^2 - m_k^2) + i\delta = \bar{k}^2 + \hat{l}^2 - R^2 + i\delta \quad (\text{C.45})$$

as $\bar{q}_j = \bar{k}$ and where $R^2 = \frac{1}{2} z \cdot S \cdot s$ as before. It is important to note that we have defined $\bar{k}^2 = -|\bar{k}|^2$ i.e. it is negative. This is so that we have, above, $k^2 = \hat{k}_0^2 - |\vec{k}|^2 - |\bar{k}|^2 = \hat{k}^2 + \bar{k}^2$. Therefore we arrive at the form:

$$I_N^{n,\alpha;\mu_1\dots\mu_r}(a_1,\dots,a_r;S) = \Gamma(N) \int_0^\infty \prod_{j=1}^N dz_j \delta(1 - \sum_{i=1}^N z_i) \quad (\text{C.46})$$

$$\int \frac{d^4 \hat{l}}{i\pi^2} \frac{d^{n-4} \bar{k}}{\pi^{\frac{n}{2}-2}} \frac{(\bar{k}^2)^\alpha \prod_{\nu=1}^r \left[\hat{l}^{\mu_\nu} - \sum_{k=1}^N z_k (\hat{r}_k - \hat{r}_{a_\nu})^{\mu_\nu} \right]}{\left[\bar{k}^2 + \hat{l}^2 + \frac{1}{2} z \cdot S \cdot z i\delta \right]^N}. \quad (\text{C.47})$$

The above integral is symmetric in \hat{l} and therefore the tensor structure is always an even number of powers in \hat{l} . In fact, we can rewrite this as a sum of terms $(\hat{l}^2)^n$ where n is some positive

integer. Our integral is therefore split into a sum of integrals with the form

$$I_N^{d,\alpha,l}(l_1, \dots, l_r; S) = \Gamma(N) \int_0^\infty \prod_{j=1}^N dz_j \delta(1 - \sum_{i=1}^N z_i) \int \frac{d^4 \hat{l}}{i\pi^2} \frac{d^{n-4} \bar{k}}{\pi^{\frac{n}{2}-2}} \frac{(\bar{k}^2)^\alpha (k^2)^l \prod_{\nu=1}^r z_\nu^{l_\nu}}{\left[k^2 + \hat{l}^2 + \frac{1}{2} z \cdot S \cdot z + i\delta \right]^N}. \quad (\text{C.48})$$

Therefore we start from (C.48) and obtain, after Wick rotation,

$$I_N^{n,\alpha,l}(l_1, \dots, l_r; S) = i\Gamma(N) (-1)^{l+\alpha-N} \int_0^\infty \prod_{j=1}^N dz_j \delta(1 - \sum_{i=1}^N z_i) \quad (\text{C.49})$$

$$\int \frac{d^4 \hat{l}_E}{i\pi^2} \frac{d^{n-4} \bar{k}}{\pi^{\frac{n}{2}-2}} \frac{|\bar{k}^2|^\alpha (\hat{l}_E^2)^l \prod_{\nu=1}^r z_\nu^{l_\nu}}{\left[|\bar{k}|^2 + \hat{l}_E^2 - \frac{1}{2} z \cdot S \cdot z - i\delta \right]^N} \quad (\text{C.50})$$

where we recall we have defined $\bar{k}^2 = -|\bar{k}|^2$. We take a minus from the denominator, and from \hat{l}_E and \bar{k} . We wish to carry out the momentum integral. As the two integrals are now in same sign metrics we can carry out the angular integral i.e.

$$\int d^4 \hat{l}_E = \int_0^\infty dr r^3 \int d\Omega_3 \quad (\text{C.51})$$

$$\int d^{n-4} \bar{k} = \int_0^\infty dq q^{n-5} \int d\Omega_{n-5} \quad (\text{C.52})$$

$$(\text{C.53})$$

where

$$r = \sqrt{\hat{l}_E^2}, \quad q = \sqrt{|\bar{k}|^2} \quad (\text{C.54})$$

and

$$\Omega_n = \frac{2\pi^{\frac{n}{2}}}{\Gamma(\frac{n}{2})}. \quad (\text{C.55})$$

With this change of variables we have:

$$I_N^{n,\alpha,l}(l_1, \dots, l_r; S) = \Gamma(N) (-1)^{l+\alpha-N} \int_0^\infty \prod_{j=1}^N dz_j \delta(1 - \sum_{i=1}^N z_i) \quad (\text{C.56})$$

$$\frac{i2\pi^2}{i\pi^2} \frac{2\pi^{\frac{n}{2}-2}}{\pi^{\frac{n}{2}-2}} \frac{1}{\Gamma(\frac{n}{2}-2)} \int_0^\infty dr r^3 \int_0^\infty dq q^{n-5} \frac{r^{2l} q^{2\alpha} \prod_{\nu=1}^r z_\nu^{l_\nu}}{\left[r^2 + q^2 - \frac{1}{2} z \cdot S \cdot z - i\delta \right]^N} \quad (\text{C.57})$$

We extract the integral of interest:

$$I = \int_0^\infty dr r^3 \int_0^\infty dq q^{n-5} \frac{r^{2l} q^{2\alpha} \prod_{\nu=1}^N z_\nu^{l_\nu}}{[r^2 + q^2 + A]^N} \quad (\text{C.58})$$

where $A = -1/2z \cdot S \cdot z$. We rewrite this in terms of β functions. Firstly we consider the q integral. We make a change of variables:

$$q = s^{\frac{1}{2}}(r^2 + A)^{\frac{1}{2}} \quad (\text{C.59})$$

$$dq = \frac{1}{2} s^{-\frac{1}{2}} ds (r^2 + A)^{\frac{1}{2}} \quad (\text{C.60})$$

gives us

$$I = \int_0^\infty dr \frac{r^{3+2l}}{2} (r^2 + A)^{\frac{n}{2}-2+\alpha-N} \int_0^\infty ds \frac{s^{n2-3+\alpha}}{(1+s)^N} \quad (\text{C.61})$$

$$= \int_0^\infty dr \frac{r^{3+2l}}{2} (r^2 + A)^{\frac{n}{2}-2+\alpha-N} B\left(\frac{n}{2} - 2 + \alpha, N - \frac{n}{2} + 2 - \alpha\right). \quad (\text{C.62})$$

We now carry out the r integral by using the following change of variables:

$$r = t^{\frac{1}{2}} A^{\frac{1}{2}} \quad (\text{C.63})$$

$$dr = \frac{1}{2} t^{-\frac{1}{2}} dt A^{\frac{1}{2}} \quad (\text{C.64})$$

which gives us

$$I = \frac{1}{4} B\left(\frac{n}{2} - 2 + \alpha, N - \frac{n}{2} + 2 - \alpha\right) A^{n/2+\alpha-N+l} \int_0^\infty dt \frac{t^{1+l}}{(1+t)^{2+N-\alpha-\frac{n}{2}}} \quad (\text{C.65})$$

$$= B\left(\frac{n}{2} - 2 + \alpha, N - \frac{n}{2} + 2 - \alpha\right) B(2+l, 2+N-\alpha-\frac{n}{2}-2-l) A^{\frac{n}{2}+\alpha-N+l}. \quad (\text{C.66})$$

This formula becomes:

$$I = \frac{1}{4} \left(-\frac{1}{2}z \cdot S \cdot z\right)^{\frac{n}{2}+\alpha-N+l} \frac{\Gamma(\frac{n}{2} - 2 + \alpha)\Gamma(N - \frac{n}{2} + 2 - \alpha)}{\Gamma(N)} \frac{\Gamma(l+2)\Gamma(N - \alpha - \frac{n}{2} - l)}{\Gamma(N + 2 - \alpha - \frac{n}{2})} \quad (\text{C.67})$$

$$= \frac{1}{4} \left(-\frac{1}{2}z \cdot S \cdot z\right)^{\frac{n}{2}+\alpha-N+l} \frac{\Gamma(N - \alpha - \frac{n}{2} - l)\Gamma(\frac{n}{2} - 2 + \alpha)\Gamma(l+2)}{\Gamma(N)} \quad (\text{C.68})$$

therefore our final result looks likes:

$$I_N^{n,\alpha,l}(l_1, \dots, l_r; S) = (-1)^{N+\alpha+l} \frac{\Gamma(N - \alpha - \frac{n}{2} - l)\Gamma(\frac{n}{2} - 2 + \alpha)\Gamma(l+2)}{\Gamma(\frac{n}{2} - 2)} \quad (\text{C.69})$$

$$\int_0^\infty \prod_{j=1}^N dz_j \delta\left(1 - \sum_{i=1}^N z_i\right) \frac{\prod_{\nu=1}^N z_\nu^{l_\nu}}{\left(-\frac{1}{2}z \cdot S \cdot z\right)^{N-l-\alpha-\frac{n}{2}}}. \quad (\text{C.70})$$

The conclusion of this calculation is that we can rewrite our result as

$$I_N^{n,\alpha,l}(l_1, \dots, l_r; S) = (-1)^{\alpha+l} \frac{\Gamma(\frac{n}{2} - 2 + \alpha)\Gamma(l+2)}{\Gamma(\frac{n}{2} - 2)} I_N^{n+2\alpha+2l}(l_1, \dots, l_N; S) \quad (\text{C.71})$$

where

$$I_N^n(l_1, \dots, l_N; S) = (-1)^N \Gamma(N - \frac{n}{2}) \int_0^\infty \prod_{j=1}^N dz_j \delta(1 - \sum_{i=1}^N z_i) \frac{\prod_{\nu=1}^N z_\nu^{l_\nu}}{(-\frac{1}{2}z \cdot S \cdot z)^{N - \frac{n}{2}}}. \quad (\text{C.72})$$

That is the integral has is rewritten as a higher dimensional integral. We note here that $\Gamma(\frac{n}{2} - 2)$ is of order ϵ . Therefore to give a contribution the integral must be divergent (for $\alpha > 0$). And because it is higher dimensional this divergence will always be of UV origin.

A nice consistency check is the following: if we split our integral into two as above then

$$\int \frac{d^n k}{i\pi^{\frac{n}{2}}} \frac{k^2}{\sum_{j=1}^N (q_j^2 - m_j^2) + i\delta} = \int \frac{d^n k}{i\pi^{\frac{n}{2}}} \frac{\hat{k}^2 + \bar{k}^2}{\sum_{j=1}^N (q_j^2 - m_j^2) + i\delta} \quad (\text{C.73})$$

$$= I_N^{n,0,1} + I_N^{n,1,0} \quad (\text{C.74})$$

$$= (-2 + \epsilon) I_N^{n+2} \quad (\text{C.75})$$

and from (4.21) we have

$$\int \frac{d^n k}{i\pi^{\frac{n}{2}}} \frac{k^2}{\sum_{j=1}^N (q_j^2 - m_j^2) + i\delta} = g_{\mu\nu} I_N^{n,\mu\nu} \quad (\text{C.76})$$

$$= g^{\mu\nu} \left[-\frac{1}{2} g^{\mu\nu} I_N^{n+2} \right] \quad (\text{C.77})$$

$$= (-2 + \epsilon) I_N^{n+2}. \quad (\text{C.78})$$

Appendix D

Miscellaneous comments

D.1 Loop Integral conventions

Here we make some comments on the Section 4.2.

D.1.1 The Integral $\int_0^1 dz \frac{1}{z^{1+2\epsilon}}$

The following integral appears in our calculations. The limits of the integral must be considered carefully.

$$\int_0^1 dz \frac{1}{z^{1+2\epsilon}} = \int_0^1 dz \frac{d}{dz} \left(\frac{z^{-2\epsilon}}{-2\epsilon} \right) = - \frac{1}{2\epsilon} z^{-2\epsilon} \Big|_0^1 = - \frac{1}{2\epsilon} e^{-2\epsilon \log z} \Big|_0^1 = - \frac{1}{2\epsilon}. \quad (\text{D.1})$$

The upper limit is clearly 1 (one can Taylor expand in epsilon). The lower limit is zero as ϵ is negative. This result is simply a special case of the function (D.8).

D.1.2 Combining complex logarithms

When dealing with complex logarithms we can arrive at problems when manipulating them in the usual way. The definition of the complex logarithm is $\log(z) = r + i\theta$. We remove any ambiguity in the definition of the polar angle by introducing a branch cut along the negative real axis. There is an obvious problem when we want to combine logarithms like $\log z + \log w = \log(zw)$ as there is a danger that we may cross the branch cut. We can introduce an additional function η such that

$$\log(wz) = \log(z) + \log(w) + \eta(w, z) \quad (\text{D.2})$$

to take care when this occurs. Alternatively we can stick to the following rules:

$$\log z + \log w = \log(zw) \quad (\text{D.3})$$

if z, w have imaginary parts of different sign and

$$\log z - \log w = \log\left(\frac{z}{w}\right) \quad (\text{D.4})$$

if both have imaginary parts of the same sign.

D.1.3 Notes on the integral $I_3^n(m_1^2, s_2, 0, m_1^2, 0, 0)$

For this integral we wish to take the limit of the integral $I_3^n(s_1, s_2, 0, m_1^2, 0, 0)$ taking the first leg on shell. Following the same procedure as that for the original integral we arrive at a result that contains the terms $\log(-i\delta)$. Naively we have the integral

$$\begin{aligned} \int_0^1 \int_0^1 du dz \frac{z}{\bar{z}^{1+\epsilon} f(u, z)^{1+\epsilon}} &= \int_0^1 \int_0^1 du dz \frac{1}{\bar{z}^{1+\epsilon}} \left(\frac{z}{f(u, z)^{1+\epsilon}} - \frac{1}{f(u, 1)^{1+\epsilon}} \right) \\ &+ \int_0^1 \int_0^1 du dz \frac{1}{\bar{z}^{1+\epsilon}} \left(\frac{1}{f(u, 1)^{1+\epsilon}} \right) \end{aligned}$$

and then we expand the final integral in ϵ

$$\frac{1}{f(u, 1)^{1+\epsilon}} = \frac{1}{f(u, 1)} \left[1 - \epsilon \log f(u, 1) + \frac{\epsilon^2}{2} \log^2 f(u, 1) + \mathcal{O}(\epsilon^3) \right]. \quad (\text{D.5})$$

For our original integral this is valid as $f(u, z) = (-s_2 u - s_1 \bar{u})z + m_1^2 - i\delta$ so $f(u, 1)$ is well defined. Taking the limit $s_1 \rightarrow m_1^2$ we arrive at $f(u, z) = -s_2 u + m_1^2((1-z) + zu)$ which clearly diverges as $z \rightarrow 1$ and $u \rightarrow 0$. Therefore $f(u, 1)$ is ill defined over our integration region and we cannot expand this function. This is an example of an overlapping divergence where simple subtraction is actually not allowed. We conclude that putting this leg on shell changes the pole structure of the integral. This overlapping singularity problem can be resolved by re-parameterizing the Feynman integral. For this example this is possible by writing $x_1 = z\bar{u}$, $x_2 = zu$ and $x_3 = \bar{z}$. Using this parametrisation the u and z integration factorises.

D.1.4 Functions arising in results

Here I present the definitions of some special functions arising in the following integrals.

$$\text{Li}_2(z) = - \int_0^z dt \frac{\log(1-t)}{t} \quad (\text{D.6})$$

and

$$\Gamma(z) = \int_0^\infty t^{z-1} e^{-t} dt. \quad (\text{D.7})$$

In the derivation of these results we also use the Euler-Beta function defined as

$$B(x, y) = \int_0^1 t^{x-1} (1-t)^{y-1} dt = \frac{\Gamma(x)\Gamma(y)}{\Gamma(x+y)} \quad (\text{D.8})$$

and we use the property $\Gamma(1+x) = x\Gamma(x)$.

D.1.5 Dilogarithm Identities

The following dilogarithm identities are used:

$$\begin{aligned}\text{Li}_2(z) + \text{Li}_2(1-z) &= \frac{\pi^2}{6} - \log z \log(1-z) \\ \text{Li}_2(z) + \text{Li}_2\left(\frac{1}{z}\right) &= -\frac{\pi^2}{6} - \frac{1}{2} \log^2(-z), |z| > 0\end{aligned}$$

D.1.6 r_Γ

We define

$$r_\Gamma = \frac{\Gamma(1+\epsilon)\Gamma(1-\epsilon)^2}{\Gamma(1-2\epsilon)}. \quad (\text{D.9})$$

Several conventions exist for the representation of loop integrals. We can write

$$\frac{1}{\Gamma(1-\epsilon)} = r_\Gamma + \mathcal{O}(\epsilon^3) \quad (\text{D.10})$$

$$= \left(1 - \frac{\pi^2}{6}\epsilon^2\right) \Gamma(1+\epsilon) + \mathcal{O}(\epsilon^3). \quad (\text{D.11})$$

transforming (3.124) to

$$f_1(s) = \Gamma(1+\epsilon) \frac{C_F \alpha_s}{4\pi} \left(\frac{4\pi\mu^2}{s}\right)^\epsilon \left(-\frac{2}{\epsilon^2} - \frac{3}{\epsilon} + \frac{4\pi^2}{3} - 8\right). \quad (\text{D.12})$$

D.1.7 s

Our scalar functions are made up of logarithms. We can extract the logarithmic contributions by multiplying by

$$\left(\frac{-s-i\delta}{-s-i\delta}\right)^\epsilon \quad (\text{D.13})$$

and expanding the numerator. The denominator gives (in the limit $\delta \rightarrow 0$)

$$(-s-i\delta)^{-\epsilon} = (s)^{-\epsilon} e^{-i\pi\epsilon} \quad (\text{D.14})$$

$$= (s)^{-\epsilon} \left[1 - i\pi\epsilon - \frac{\pi^2}{2}\epsilon^2 + \mathcal{O}(\epsilon^2)\right]. \quad (\text{D.15})$$

Appendix E

Outline of Code

E.1 Generation of the Virtual matrix elements

In this section we briefly outline the code we used in our calculation of the virtual matrix elements. We work towards an automated approach. The code is part of Golem-2.0 [88, 89, 80, 81, 90] and full technical details will be found upon its public release. There are five distinct tasks that need to be performed in the code (as outlined in Figure E.1) that are linked together using a Python script [91]. These five components are:

- Generation of all diagrams, for the process specified by the user, by Qgraf [82].
- The translation of the diagrams to the computer algebra system Form [92] that is processed such that all loop diagrams are written in the form factor representation.
- Numerator algebra performed by the Form library Spinney [1].
- The generation of source code for each diagram by Haggies [93].
- Fortran95 source code calls the Golem95 library [2] for the evaluation of the loop integrals.

The user needs to provide the process and helicities to be calculated and, optionally, any user defined model files. There must be three of these model files; one in a format for Qgraf, the second to be used by the Form program and another that contains the numerical values of the parameters. This is provided in a Python file and written to a Fortran95 module.

Once the source code has been generated what remains is for the user to provide a momenta configuration for a particular phase space point. Then the program will output three numbers A, B, C such that:

$$|\mathcal{M}_V|^2 = \frac{\alpha_s}{2\pi} \frac{(4\pi)^\epsilon}{\Gamma(1-\epsilon)} \left[\frac{A}{\epsilon^2} + \frac{B}{\epsilon} + C \right]. \quad (\text{E.1})$$

In our calculation the final matrix element module was embedded in the MadGraph/MadEvent framework [3] alongside the dipole subtraction terms [76] and the real emission terms. The phase space integral was performed using MadEvent routines.

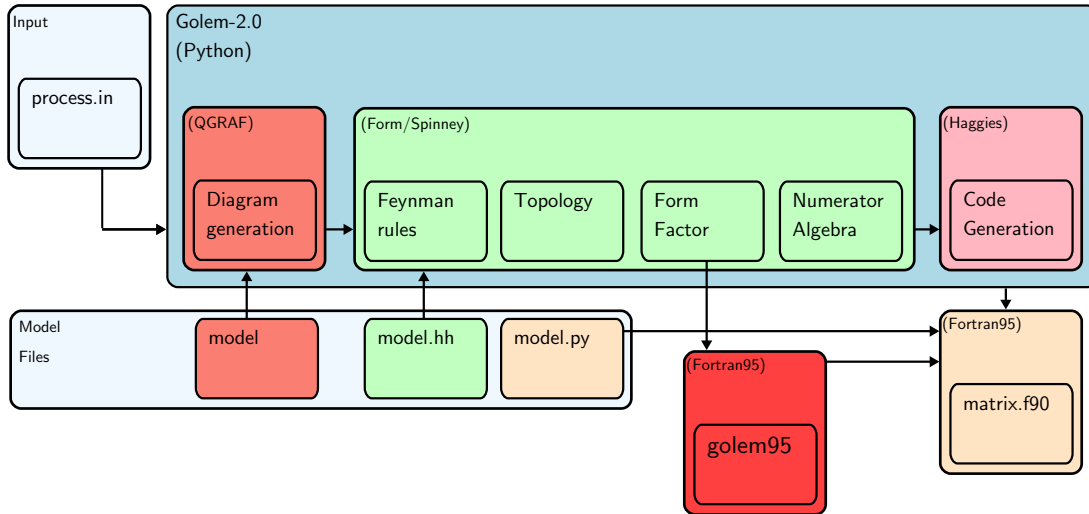


Figure E.1: Schematic diagram of the code.

E.2 Majorana fermion issues

E.2.1 On the Relative Sign of Feynman Graphs

The flipping rules have been tested in the above framework. where the diagrams are generated by Qgraf [82]. The relative sign calculated by Qgraf is incorrect when dealing with Majorana fermions. Here, we present a method to calculate it. Firstly we calculate $(-1)^P$ using the following code:

```

Function NCOrder;
Id fDUMMY1?{UbarSpa, UbarSpb}(vDUMMY1?) =
    NCOrder(vDUMMY1)*fDUMMY1(vDUMMY1);
Id fDUMMY1?{USpa, USpb}(vDUMMY1?) =
    fDUMMY1(vDUMMY1)*NCOrder(vDUMMY1);
#call tHooftAlgebra
#call SpCollect
ChainIn NCOrder;
AntiSymmetrize NCOrder;
Id NCOrder(? all) = 1;
    
```

We multiply our diagram by a non-commuting function of the external momenta which encodes the order of the spinors in the diagram. The arguments of this function are then brought into Form's natural ordering. The exchange of any two arguments gives a minus sign.

Secondly we must determine $(-1)^L$ with L being the number of close fermion loops. This is easily calculated in the following code:

$$\mathbf{Id} \text{ trL} = (-1) * \text{trL};$$

Every closed spinor chain, corresponding to a closed fermion loop, contributes a minus sign.

E.2.1.1 Fixing Fermion Chain Order

The method we have described relies on being able to fix the fermion chain order. This is achieved in the procedure `RemoveNCContainer`. In our code an incoming (outgoing) Majorana fermion will initially be treated as in incoming (outgoing) Dirac fermion (as opposed to an anti-fermion). When we join an incoming Majorana spinor with an incoming Dirac fermion or an outgoing Dirac anti-fermion, one spinor will need to be flipped. The same applies when an outgoing Majorana fermion is joined to an incoming anti-fermion or an outgoing fermion. As an example we have an expression:

$$\text{NCContainer}(\text{UbarSpa}(k1) * \text{Sm}(i1) * \text{ProjPlus} * \text{UbarSpa}(k2))$$

which is transformed using `RemoveNCContainer` to

$$\text{NCContainer}(\text{UbarSpa}(k1), \text{Sm}(i1), \text{ProjPlus}, \\ \text{SpFlip}(\text{UbarSpa}(k2)))$$

and then using (3.101) we have the fermion chain:

$$\text{UbarSpa}(k1) * \text{Sm}(i1) * \text{ProjPlus} * \text{USpb}(k2).$$

E.2.2 Majorana Exchange

Corresponding to the section 3.5.1.2 In our code, part of the output is:

$$\text{NCContainer}(\text{USpa}(k1) * \text{SpFlip}(\text{Sm}(\mu) * \text{ProjPlus}) * \text{Sm}(k4) \\ * \text{Sm}(\nu) * \text{ProjPlus} * \text{USpb}(k2)) * \text{inv}(\text{es23}).$$

Upon applying the `RemoveNCContainer` routine we obtain the result

$$- \text{UbarSpb}(k1) * \text{ProjPlus} * \text{Sm}(\mu) * \text{Sm}(k4) * \text{Sm}(\nu) \\ * \text{ProjMinus} * \text{USpa}(k2) * \text{inv}(\text{es23})$$

We have picked up a minus sign from the flipping of the γ^μ . What remains is to multiply by $(-1)^P$ as explained previously.

Appendix F

Numerical Results for Three Point Tensor Integrals

We use the notation of (4.23) and present the numerical results for the kinematic regions examined in Section 4.2.

Appendix A. Numerical Results for Three Point Tensor Integrals

	ϵ^{-2}		ϵ^{-1}		ϵ^0	
	Re	Im	Re	Im	Re	Im
$s_1 = 11.0 \quad s_2 = 7.0 \quad m_1^2 = 5.0$						
$I_3^n(1)$	0.000000000	0.000000000	0.000000000	0.000000000	0.090311368	-0.203999523
$I_3^n(2)$	0.000000000	0.000000000	-0.161979608	0.000000000	0.079370188	-0.709664941
$I_3^n(1, 1)$	0.000000000	0.000000000	0.000000000	0.000000000	-0.016337073	-0.084779023
$I_3^n(1, 2)$	0.000000000	0.000000000	0.000000000	0.000000000	0.055394004	-0.072856972
$I_3^n(1, 1, 1)$	0.000000000	0.000000000	0.000000000	0.000000000	-0.024566588	-0.036379743
$I_3^n(1, 1, 2)$	0.000000000	0.000000000	0.000000000	0.000000000	0.001385840	-0.027124241
$I_3^n(1, 2, 2)$	0.000000000	0.000000000	0.000000000	0.000000000	0.037613279	-0.034693796
$I_3^n(2, 2, 2)$	0.000000000	0.000000000	-0.093620785	0.000000000	-0.026737434	-0.349955155
I_3^{n+2}	0.000000000	0.000000000	-0.500000000	0.000000000	-0.555245614	-1.060797519
$I_3^{n+2}(1)$	0.000000000	0.000000000	-0.166666667	0.000000000	-0.102297860	-0.212300802
$I_3^{n+2}(2)$	0.000000000	0.000000000	-0.166666667	0.000000000	-0.259263646	-0.402170488
$s_1 = 7.0 \quad s_2 = 3.0 \quad m_1^2 = 5.0$						
$I_3^n(1)$	0.000000000	0.000000000	0.000000000	0.000000000	-0.218164460	-0.224399475
$I_3^n(2)$	0.000000000	0.000000000	0.250000000	0.392699082	-0.326263699	1.005158769
$I_3^n(1, 1)$	0.000000000	0.000000000	0.000000000	0.000000000	-0.077492484	-0.032057068
$I_3^n(1, 2)$	0.000000000	0.000000000	0.000000000	0.000000000	-0.098470383	-0.056099869
$I_3^n(1, 1, 1)$	0.000000000	0.000000000	0.000000000	0.000000000	-0.033853621	-0.006106108
$I_3^n(1, 1, 2)$	0.000000000	0.000000000	0.000000000	0.000000000	-0.021169072	-0.005342845
$I_3^n(1, 2, 2)$	0.000000000	0.000000000	0.000000000	0.000000000	-0.053855981	-0.018699956
$I_3^n(2, 2, 2)$	0.000000000	0.000000000	0.208333333	0.098174770	0.376231887	0.414914310
I_3^{n+2}	0.000000000	0.000000000	-0.500000000	0.000000000	-0.608015260	-0.224399475
$I_3^{n+2}(1)$	0.000000000	0.000000000	-0.166666667	0.000000000	-0.017962058	-0.021371379
$I_3^{n+2}(2)$	0.000000000	0.000000000	-0.166666667	0.000000000	-0.248135942	-0.037399913
$s_1 = 7.0 \quad s_2 = -3.0 \quad m_1^2 = 5.0$						
$I_3^n(1)$	0.000000000	0.000000000	0.000000000	0.000000000	-0.151514036	-0.089759790
$I_3^n(2)$	0.000000000	0.000000000	0.127725887	0.062831853	-0.046856314	0.160825403
$I_3^n(1, 1)$	0.000000000	0.000000000	0.000000000	0.000000000	-0.051804745	-0.012822827
$I_3^n(1, 2)$	0.000000000	0.000000000	0.000000000	0.000000000	-0.044039486	-0.008975979
$I_3^n(1, 1, 1)$	0.000000000	0.000000000	0.000000000	0.000000000	-0.023802599	-0.002442443
$I_3^n(1, 1, 2)$	0.000000000	0.000000000	0.000000000	0.000000000	-0.010365796	-0.000854855
$I_3^n(1, 2, 2)$	0.000000000	0.000000000	0.000000000	0.000000000	-0.018218507	-0.001196797
$I_3^n(2, 2, 2)$	0.000000000	0.000000000	0.048442369	0.002513274	0.026748182	0.010621806
I_3^{n+2}	0.000000000	0.000000000	-0.500000000	0.000000000	-0.220123574	-0.089759790
$I_3^{n+2}(1)$	0.000000000	0.000000000	-0.166666667	0.000000000	0.068522272	-0.008548551
$I_3^{n+2}(2)$	0.000000000	0.000000000	-0.166666667	0.000000000	-0.067047007	-0.005983986
$s_1 = 3.0 \quad s_2 = -3.0 \quad m_1^2 = 5.0$						
$I_3^n(1)$	0.000000000	0.000000000	0.000000000	0.000000000	-0.107080421	0.000000000
$I_3^n(2)$	0.000000000	0.000000000	0.089650313	0.000000000	-0.016895515	0.000000000
$I_3^n(1, 1)$	0.000000000	0.000000000	0.000000000	0.000000000	-0.034679585	0.000000000
$I_3^n(1, 2)$	0.000000000	0.000000000	0.000000000	0.000000000	-0.030300067	0.000000000
$I_3^n(1, 1, 1)$	0.000000000	0.000000000	0.000000000	0.000000000	-0.017101918	0.000000000

$I_3^n(1, 1, 2)$	0.000000000	0.000000000	0.000000000	0.000000000	-0.007666957	0.000000000
$I_3^n(1, 2, 2)$	0.000000000	0.000000000	0.000000000	0.000000000	-0.013844277	0.000000000
$I_3^n(2, 2, 2)$	0.000000000	0.000000000	0.037738924	0.000000000	0.006089093	0.000000000
I_3^{n+2}	0.000000000	0.000000000	-0.500000000	0.000000000	0.038470882	0.000000000
$I_3^{n+2}(1)$	0.000000000	0.000000000	-0.166666667	0.000000000	0.126178492	0.000000000
$I_3^{n+2}(2)$	0.000000000	0.000000000	-0.166666667	0.000000000	-0.017487304	0.000000000
$s_1 = -3.0 \quad s_2 = -5.0 \quad m_1^2 = 5.0$						
$I_3^n(1)$	0.000000000	0.000000000	0.000000000	0.000000000	-0.066475675	0.000000000
$I_3^n(2)$	0.000000000	0.000000000	0.053712897	0.000000000	-0.048642293	0.000000000
$I_3^n(1, 1)$	0.000000000	0.000000000	0.000000000	0.000000000	-0.024251840	0.000000000
$I_3^n(1, 2)$	0.000000000	0.000000000	0.000000000	0.000000000	-0.020475060	0.000000000
$I_3^n(1, 1, 1)$	0.000000000	0.000000000	0.000000000	0.000000000	-0.012826746	0.000000000
$I_3^n(1, 1, 2)$	0.000000000	0.000000000	0.000000000	0.000000000	-0.005566093	0.000000000
$I_3^n(1, 2, 2)$	0.000000000	0.000000000	0.000000000	0.000000000	-0.009782234	0.000000000
$I_3^n(2, 2, 2)$	0.000000000	0.000000000	0.026073025	0.000000000	-0.007329019	0.000000000
I_3^{n+2}	0.000000000	0.000000000	-0.500000000	0.000000000	0.263768836	0.000000000
$I_3^{n+2}(1)$	0.000000000	0.000000000	-0.166666667	0.000000000	0.183898234	0.000000000
$I_3^{n+2}(2)$	0.000000000	0.000000000	-0.166666667	0.000000000	0.045062034	0.000000000

Table F.1: Kinematic points for $I_3^n(s_1, s_2, 0, m_1^2, 0, 0)$.

	ϵ^{-2}		ϵ^{-1}		ϵ^0	
	Re	Im	Re	Im	Re	Im
$m_1^2 = 7.0 \quad s_2 = 5.0$						
$I_3^n(1)$	0.000000000	0.000000000	0.000000000	0.000000000	-0.130898676	-0.448798951
$I_3^n(2)$	0.000000000	0.000000000	-0.500000000	0.000000000	-0.980673100	-2.692793703
$I_3^n(1, 1)$	0.000000000	0.000000000	0.000000000	0.000000000	-0.090128382	-0.064114136
$I_3^n(1, 2)$	0.000000000	0.000000000	0.000000000	0.000000000	0.024679044	-0.160285339
$I_3^n(1, 1, 1)$	0.000000000	0.000000000	0.000000000	0.000000000	-0.040976835	-0.012212216
$I_3^n(1, 1, 2)$	0.000000000	0.000000000	0.000000000	0.000000000	-0.019108753	-0.030530541
$I_3^n(1, 2, 2)$	0.000000000	0.000000000	0.000000000	0.000000000	0.035561450	-0.076326352
$I_3^n(2, 2, 2)$	0.000000000	0.000000000	-0.166666667	0.000000000	-0.156682957	-0.714414656
I_3^{n+2}	0.000000000	0.000000000	-0.500000000	0.000000000	-0.826179720	-0.448798951
$I_3^{n+2}(1)$	0.000000000	0.000000000	-0.166666667	0.000000000	-0.069623714	-0.042742757
$I_3^{n+2}(2)$	0.000000000	0.000000000	-0.166666667	0.000000000	-0.370051655	-0.256456543
$m_1^2 = 3.0 \quad s_2 = 5.0$						
$I_3^n(1)$	0.000000000	0.000000000	0.000000000	0.000000000	-0.305430244	0.000000000
$I_3^n(2)$	0.000000000	0.000000000	0.500000000	0.000000000	1.417002020	0.000000000
$I_3^n(1, 1)$	0.000000000	0.000000000	0.000000000	0.000000000	-0.064856585	0.000000000
$I_3^n(1, 2)$	0.000000000	0.000000000	0.000000000	0.000000000	-0.087858537	0.000000000
$I_3^n(1, 1, 1)$	0.000000000	0.000000000	0.000000000	0.000000000	-0.026730407	0.000000000
$I_3^n(1, 1, 2)$	0.000000000	0.000000000	0.000000000	0.000000000	-0.016507317	0.000000000
$I_3^n(1, 2, 2)$	0.000000000	0.000000000	0.000000000	0.000000000	-0.042065041	0.000000000
$I_3^n(2, 2, 2)$	0.000000000	0.000000000	0.166666667	0.000000000	0.350749183	0.000000000
I_3^{n+2}	0.000000000	0.000000000	-0.500000000	0.000000000	-0.389850800	0.000000000
$I_3^{n+2}(1)$	0.000000000	0.000000000	-0.166666667	0.000000000	0.033699598	0.000000000
$I_3^{n+2}(2)$	0.000000000	0.000000000	-0.166666667	0.000000000	-0.182489020	0.000000000
$m_1^2 = -3.0 \quad s_2 = 5.0$						
$I_3^n(1)$	0.000000000	0.000000000	0.000000000	0.000000000	-0.156667876	0.000000000
$I_3^n(2)$	0.000000000	0.000000000	0.125000000	0.000000000	0.087987230	0.000000000
$I_3^n(1, 1)$	0.000000000	0.000000000	0.000000000	0.000000000	-0.042223835	0.000000000
$I_3^n(1, 2)$	0.000000000	0.000000000	0.000000000	0.000000000	-0.036110103	0.000000000
$I_3^n(1, 1, 1)$	0.000000000	0.000000000	0.000000000	0.000000000	-0.019509040	0.000000000
$I_3^n(1, 1, 2)$	0.000000000	0.000000000	0.000000000	0.000000000	-0.008640183	0.000000000
$I_3^n(1, 2, 2)$	0.000000000	0.000000000	0.000000000	0.000000000	-0.015433219	0.000000000
$I_3^n(2, 2, 2)$	0.000000000	0.000000000	0.041666667	0.000000000	0.013280142	0.000000000
I_3^{n+2}	0.000000000	0.000000000	-0.500000000	0.000000000	-0.068609538	0.000000000
$I_3^{n+2}(1)$	0.000000000	0.000000000	-0.166666667	0.000000000	0.103058768	0.000000000
$I_3^{n+2}(2)$	0.000000000	0.000000000	-0.166666667	0.000000000	-0.037687349	0.000000000

 Table F.2: Kinematic points for $I_3^n(m_1^2, s_2, 0, m_1^2, 0, 0)$.

	ϵ^{-2}		ϵ^{-1}		ϵ^0	
	Re	Im	Re	Im	Re	Im
$s_1 = 7.0 \quad m_1^2 = 5.0$						
$I_3^n(1)$	0.000000000	0.000000000	0.000000000	0.000000000	0.049358089	-0.320570679
$I_3^n(2)$	0.000000000	0.000000000	-0.250000000	0.000000000	-0.015015594	-1.186111512
$I_3^n(1, 1)$	0.000000000	0.000000000	0.000000000	0.000000000	-0.057326260	-0.091591623
$I_3^n(1, 2)$	0.000000000	0.000000000	0.000000000	0.000000000	0.053342174	-0.114489528
$I_3^n(1, 1, 1)$	0.000000000	0.000000000	0.000000000	0.000000000	-0.040188455	-0.026169035
$I_3^n(1, 1, 2)$	0.000000000	0.000000000	0.000000000	0.000000000	-0.008568903	-0.032711294
$I_3^n(1, 2, 2)$	0.000000000	0.000000000	0.000000000	0.000000000	0.041274051	-0.054518823
$I_3^n(2, 2, 2)$	0.000000000	0.000000000	-0.125000000	0.000000000	-0.065134423	-0.494921875
I_3^{n+2}	0.000000000	0.000000000	-0.500000000	0.000000000	-0.776821631	-0.769369629
$I_3^{n+2}(1)$	0.000000000	0.000000000	-0.166666667	0.000000000	-0.107841221	-0.103803839
$I_3^{n+2}(2)$	0.000000000	0.000000000	-0.166666667	0.000000000	-0.334490205	-0.332782895
$s_1 = 3.0 \quad m_1^2 = 5.0$						
$I_3^n(1)$	0.000000000	0.000000000	0.000000000	0.000000000	-0.175717073	0.000000000
$I_3^n(2)$	0.000000000	0.000000000	0.250000000	0.000000000	0.296359546	0.000000000
$I_3^n(1, 1)$	0.000000000	0.000000000	0.000000000	0.000000000	-0.049521951	0.000000000
$I_3^n(1, 2)$	0.000000000	0.000000000	0.000000000	0.000000000	-0.063097561	0.000000000
$I_3^n(1, 1, 1)$	0.000000000	0.000000000	0.000000000	0.000000000	-0.022540921	0.000000000
$I_3^n(1, 1, 2)$	0.000000000	0.000000000	0.000000000	0.000000000	-0.013490515	0.000000000
$I_3^n(1, 2, 2)$	0.000000000	0.000000000	0.000000000	0.000000000	-0.033071364	0.000000000
$I_3^n(2, 2, 2)$	0.000000000	0.000000000	0.125000000	0.000000000	0.204532077	0.000000000
I_3^{n+2}	0.000000000	0.000000000	-0.500000000	0.000000000	-0.214133727	0.000000000
$I_3^{n+2}(1)$	0.000000000	0.000000000	-0.166666667	0.000000000	0.066714232	0.000000000
$I_3^{n+2}(2)$	0.000000000	0.000000000	-0.166666667	0.000000000	-0.140423979	0.000000000
$s_1 = -3.0 \quad m_1^2 = 5.0$						
$I_3^n(1)$	0.000000000	0.000000000	0.000000000	0.000000000	-0.072220206	0.000000000
$I_3^n(2)$	0.000000000	0.000000000	0.062500000	0.000000000	-0.044896282	0.000000000
$I_3^n(1, 1)$	0.000000000	0.000000000	0.000000000	0.000000000	-0.025920549	0.000000000
$I_3^n(1, 2)$	0.000000000	0.000000000	0.000000000	0.000000000	-0.023149828	0.000000000
$I_3^n(1, 1, 1)$	0.000000000	0.000000000	0.000000000	0.000000000	-0.013565909	0.000000000
$I_3^n(1, 1, 2)$	0.000000000	0.000000000	0.000000000	0.000000000	-0.006177320	0.000000000
$I_3^n(1, 2, 2)$	0.000000000	0.000000000	0.000000000	0.000000000	-0.011315006	0.000000000
$I_3^n(2, 2, 2)$	0.000000000	0.000000000	0.031250000	0.000000000	-0.002386973	0.000000000
I_3^{n+2}	0.000000000	0.000000000	-0.500000000	0.000000000	0.220271286	0.000000000
$I_3^{n+2}(1)$	0.000000000	0.000000000	-0.166666667	0.000000000	0.172180233	0.000000000
$I_3^{n+2}(2)$	0.000000000	0.000000000	-0.166666667	0.000000000	0.024045526	0.000000000

Table F.3: Kinematic points for $I_3^n(s_1, s_1, 0, m_1^2, 0, 0)$.

Appendix A. Numerical Results for Three Point Tensor Integrals

	ϵ^{-2}		ϵ^{-1}		ϵ^0	
	Re	Im	Re	Im	Re	Im
$s_2 = 25.0 \quad m_1^2 = 9.0 \quad m_2^2 = 3.0$						
$I_3^n(1)$	0.000000000	0.000000000	0.000000000	0.000000000	-0.761889398	0.000000000
$I_3^n(2)$	0.000000000	0.000000000	0.000000000	0.000000000	-1.264643179	0.000000000
$I_3^n(1, 1)$	0.000000000	0.000000000	0.000000000	0.000000000	-0.161605287	0.000000000
$I_3^n(1, 2)$	0.000000000	0.000000000	0.000000000	0.000000000	-0.219339412	0.000000000
$I_3^n(1, 1, 1)$	0.000000000	0.000000000	0.000000000	0.000000000	-0.051298500	0.000000000
$I_3^n(1, 1, 2)$	0.000000000	0.000000000	0.000000000	0.000000000	-0.056438358	0.000000000
$I_3^n(1, 2, 2)$	0.000000000	0.000000000	0.000000000	0.000000000	-0.089787916	0.000000000
$I_3^n(2, 2, 2)$	0.000000000	0.000000000	0.000000000	0.000000000	-0.185533535	0.000000000
I_3^{n+2}	0.000000000	0.000000000	-0.500000000	0.000000000	-0.416905166	0.000000000
$I_3^{n+2}(1)$	0.000000000	0.000000000	-0.166666667	0.000000000	-0.011579149	0.000000000
$I_3^{n+2}(2)$	0.000000000	0.000000000	-0.166666667	0.000000000	-0.155246517	0.000000000
$s_2 = 10.0 \quad m_1^2 = 9.0 \quad m_2^2 = 3.0$						
$I_3^n(1)$	0.000000000	0.000000000	0.000000000	0.000000000	-0.108946412	0.000000000
$I_3^n(2)$	0.000000000	0.000000000	0.000000000	0.000000000	-0.161132575	0.000000000
$I_3^n(1, 1)$	0.000000000	0.000000000	0.000000000	0.000000000	-0.031277434	0.000000000
$I_3^n(1, 2)$	0.000000000	0.000000000	0.000000000	0.000000000	-0.023195772	0.000000000
$I_3^n(1, 1, 1)$	0.000000000	0.000000000	0.000000000	0.000000000	-0.014112675	0.000000000
$I_3^n(1, 1, 2)$	0.000000000	0.000000000	0.000000000	0.000000000	-0.006738948	0.000000000
$I_3^n(1, 2, 2)$	0.000000000	0.000000000	0.000000000	0.000000000	-0.008724900	0.000000000
$I_3^n(2, 2, 2)$	0.000000000	0.000000000	0.000000000	0.000000000	-0.029522111	0.000000000
I_3^{n+2}	0.000000000	0.000000000	-0.500000000	0.000000000	0.190956426	0.000000000
$I_3^{n+2}(1)$	0.000000000	0.000000000	-0.166666667	0.000000000	0.155669485	0.000000000
$I_3^{n+2}(2)$	0.000000000	0.000000000	-0.166666667	0.000000000	0.082745911	0.000000000
$s_2 = 1.0 \quad m_1^2 = 9.0 \quad m_2^2 = 3.0$						
$I_3^n(1)$	0.000000000	0.000000000	0.000000000	0.000000000	-0.077344936	0.000000000
$I_3^n(2)$	0.000000000	0.000000000	0.000000000	0.000000000	-0.111439547	0.000000000
$I_3^n(1, 1)$	0.000000000	0.000000000	0.000000000	0.000000000	-0.023460935	0.000000000
$I_3^n(1, 2)$	0.000000000	0.000000000	0.000000000	0.000000000	-0.015211534	0.000000000
$I_3^n(1, 1, 1)$	0.000000000	0.000000000	0.000000000	0.000000000	-0.011118615	0.000000000
$I_3^n(1, 1, 2)$	0.000000000	0.000000000	0.000000000	0.000000000	-0.004522008	0.000000000
$I_3^n(1, 2, 2)$	0.000000000	0.000000000	0.000000000	0.000000000	-0.005619015	0.000000000
$I_3^n(2, 2, 2)$	0.000000000	0.000000000	0.000000000	0.000000000	-0.021386478	0.000000000
I_3^{n+2}	0.000000000	0.000000000	-0.500000000	0.000000000	0.358328079	0.000000000
$I_3^{n+2}(1)$	0.000000000	0.000000000	-0.166666667	0.000000000	0.204872812	0.000000000
$I_3^{n+2}(2)$	0.000000000	0.000000000	-0.166666667	0.000000000	0.145123685	0.000000000
$s_2 = -5.0 \quad m_1^2 = 9.0 \quad m_2^2 = 3.0$						
$I_3^n(1)$	0.000000000	0.000000000	0.000000000	0.000000000	-0.065950630	0.000000000
$I_3^n(2)$	0.000000000	0.000000000	0.000000000	0.000000000	-0.093878333	0.000000000
$I_3^n(1, 1)$	0.000000000	0.000000000	0.000000000	0.000000000	-0.020494382	0.000000000
$I_3^n(1, 2)$	0.000000000	0.000000000	0.000000000	0.000000000	-0.012480933	0.000000000
$I_3^n(1, 1, 1)$	0.000000000	0.000000000	0.000000000	0.000000000	-0.009915220	0.000000000

$I_3^n(1, 1, 2)$	0.000000000	0.000000000	0.000000000	0.000000000	-0.003747701	0.000000000
$I_3^n(1, 2, 2)$	0.000000000	0.000000000	0.000000000	0.000000000	-0.004572921	0.000000000
$I_3^n(2, 2, 2)$	0.000000000	0.000000000	0.000000000	0.000000000	-0.018399235	0.000000000
I_3^{n+2}	0.000000000	0.000000000	-0.500000000	0.000000000	0.440827645	0.000000000
$I_3^{n+2}(1)$	0.000000000	0.000000000	-0.166666667	0.000000000	0.229523018	0.000000000
$I_3^{n+2}(2)$	0.000000000	0.000000000	-0.166666667	0.000000000	0.175473190	0.000000000

Table F.4: Kinematic points for $I_3^n(m_1^2, s_2, m_2^2, m_1^2, m_2^2, 0)$.

	ϵ^{-2}		ϵ^{-1}		ϵ^0	
	Re	Im	Re	Im	Re	Im
$s_1 = 25.0 \quad m_1^2 = 5.0$						
$I_3^n(1)$	0.000000000	0.000000000	0.000000000	0.000000000	0.086081788	-0.280992589
$I_3^n(2)$	0.000000000	0.000000000	0.000000000	0.000000000	0.086081788	-0.280992589
$I_3^n(1, 1)$	0.000000000	0.000000000	0.000000000	0.000000000	0.005824536	-0.084297777
$I_3^n(1, 2)$	0.000000000	0.000000000	0.000000000	0.000000000	0.037216358	-0.056198518
$I_3^n(1, 1, 1)$	0.000000000	0.000000000	0.000000000	0.000000000	-0.008522428	-0.037465679
$I_3^n(1, 1, 2)$	0.000000000	0.000000000	0.000000000	0.000000000	0.012405453	-0.018732839
$I_3^n(1, 2, 2)$	0.000000000	0.000000000	0.000000000	0.000000000	0.012405453	-0.018732839
$I_3^n(2, 2, 2)$	0.000000000	0.000000000	0.000000000	0.000000000	-0.008522428	-0.037465679
I_3^{n+2}	0.000000000	0.000000000	-0.500000000	0.000000000	-0.480076573	-0.702481473
$I_3^{n+2}(1)$	0.000000000	0.000000000	-0.166666667	0.000000000	-0.104469969	-0.234160491
$I_3^{n+2}(2)$	0.000000000	0.000000000	-0.166666667	0.000000000	-0.104469969	-0.234160491
$s_1 = 10.0 \quad m_1^2 = 5.0$						
$I_3^n(1)$	0.000000000	0.000000000	0.000000000	0.000000000	-0.196604666	0.000000000
$I_3^n(2)$	0.000000000	0.000000000	0.000000000	0.000000000	-0.196604666	0.000000000
$I_3^n(1, 1)$	0.000000000	0.000000000	0.000000000	0.000000000	-0.061146692	0.000000000
$I_3^n(1, 2)$	0.000000000	0.000000000	0.000000000	0.000000000	-0.037155641	0.000000000
$I_3^n(1, 1, 1)$	0.000000000	0.000000000	0.000000000	0.000000000	-0.028379248	0.000000000
$I_3^n(1, 1, 2)$	0.000000000	0.000000000	0.000000000	0.000000000	-0.012385214	0.000000000
$I_3^n(1, 2, 2)$	0.000000000	0.000000000	0.000000000	0.000000000	-0.012385214	0.000000000
$I_3^n(2, 2, 2)$	0.000000000	0.000000000	0.000000000	0.000000000	-0.028379248	0.000000000
I_3^{n+2}	0.000000000	0.000000000	-0.500000000	0.000000000	-0.007164713	0.000000000
$I_3^{n+2}(1)$	0.000000000	0.000000000	-0.166666667	0.000000000	0.053167318	0.000000000
$I_3^{n+2}(2)$	0.000000000	0.000000000	-0.166666667	0.000000000	0.053167318	0.000000000
$s_1 = 1.0 \quad m_1^2 = 5.0$						
$I_3^n(1)$	0.000000000	0.000000000	0.000000000	0.000000000	-0.086081788	0.000000000
$I_3^n(2)$	0.000000000	0.000000000	0.000000000	0.000000000	-0.086081788	0.000000000
$I_3^n(1, 1)$	0.000000000	0.000000000	0.000000000	0.000000000	-0.029122682	0.000000000
$I_3^n(1, 2)$	0.000000000	0.000000000	0.000000000	0.000000000	-0.013918212	0.000000000
$I_3^n(1, 1, 1)$	0.000000000	0.000000000	0.000000000	0.000000000	-0.014775718	0.000000000
$I_3^n(1, 1, 2)$	0.000000000	0.000000000	0.000000000	0.000000000	-0.004639404	0.000000000
$I_3^n(1, 2, 2)$	0.000000000	0.000000000	0.000000000	0.000000000	-0.004639404	0.000000000
$I_3^n(2, 2, 2)$	0.000000000	0.000000000	0.000000000	0.000000000	-0.014775718	0.000000000
I_3^{n+2}	0.000000000	0.000000000	-0.500000000	0.000000000	0.380741308	0.000000000
$I_3^{n+2}(1)$	0.000000000	0.000000000	-0.166666667	0.000000000	0.182469325	0.000000000
$I_3^{n+2}(2)$	0.000000000	0.000000000	-0.166666667	0.000000000	0.182469325	0.000000000

 Table F.5: Kinematic points for $I_3^n(m_1^2, s_2, m_1^2, m_1^2, m_1^2, 0)$.

Bibliography

- [1] G. Cullen, M. Koch-Janusz, and T. Reiter, “spinney: A Form Library for Helicity Spinors,” *Comput. Phys. Commun.* **182** (2011) 2368–2387, [arXiv:1008.0803 \[hep-ph\]](#).
- [2] G. Cullen *et al.*, “Golem95C: A library for one-loop integrals with complex masses,” *Comput. Phys. Commun.* **182** (2011) 2276–2284, [arXiv:1101.5595 \[hep-ph\]](#).
- [3] J. Alwall *et al.*, “MadGraph/MadEvent v4: The New Web Generation,” *JHEP* **09** (2007) 028, [arXiv:0706.2334 \[hep-ph\]](#).
- [4] H. Fritzsch and M. Gell-Mann, “Current algebra: Quarks and what else?,” *eConf C720906V2* (1972) 135–165, [arXiv:hep-ph/0208010](#).
- [5] D. J. Gross and F. Wilczek, “Ultraviolet Behaviour Of Non-Abelian Gauge Theories,” *Phys. Rev. Lett.* **30** (1973) 1343–1346.
- [6] H. D. Politzer, “Reliable Perturbative Results for Strong Interaction?,” *Phys. Rev. Lett.* **30** (1973) 1346–1349.
- [7] S. L. Glashow, “Partial Symmetries of Weak Interactions,” *Nucl. Phys.* **22** (1961) 579–588.
- [8] A. Salam, “Weak and Electromagnetic Interactions,” *Svartholm: Elementary Particle Theory, Proceedings Of The Nobel Symposium Held 1968, Lerum, Sweden, Stockholm* (1968) 367–377.
- [9] S. Weinberg, “A Model of Leptons,” *Phys. Rev. Lett.* **19** (1967) 1264–1266.
- [10] G. ’t Hooft, “Renormalization of Massless Yang-Mills Fields,” *Nucl. Phys.* **B33** (1971) 173–199.
- [11] G. ’t Hooft and M. J. G. Veltman, “Regularization and Renormalization of Gauge Fields,” *Nucl. Phys.* **B44** (1972) 189–213.
- [12] M. Schmaltz and D. Tucker-Smith, “Little Higgs Review,” *Ann. Rev. Nucl. Part. Sci.* **55** (2005) 229–270, [arXiv:hep-ph/0502182](#).
- [13] L. Susskind, “Dynamics of Spontaneous Symmetry Breaking in the Weinberg- Salam Theory,” *Phys. Rev.* **D20** (1979) 2619–2625.
- [14] S. Chang, R. Dermisek, J. F. Gunion, and N. Weiner, “Nonstandard Higgs Boson Decays,” *Ann. Rev. Nucl. Part. Sci.* **58** (2008) 75–98, [arXiv:0801.4554 \[hep-ph\]](#).
- [15] J. R. Andersen *et al.*, “Discovering Technicolor,” [arXiv:1104.1255 \[hep-ph\]](#).
- [16] B. Holdom, “Technicolor,” *Phys. Lett.* **B150** (1985) 301.
- [17] J. F. Gunion and H. E. Haber, “Higgs Bosons in Supersymmetric Models. 1,” *Nucl. Phys.* **B272** (1986) 1.
- [18] R. K. Ellis, W. J. Stirling, and B. R. Webber, “QCD and collider physics,” *Camb. Monogr. Part. Phys. Nucl. Phys. Cosmol.* **8** (1996) 1–435.
- [19] T. Binoth, “Introduction to the Standard Model: Lecture Notes,” 2006.
- [20] A. Ceccucci, Z. Ligeti, and Y. Sakai, “The CKM Quark Mixing Matrix,” 2010.
- [21] S. Dawson, “Introduction to electroweak symmetry breaking,” [arXiv:hep-ph/9901280](#).
- [22] J. F. Gunion, H. E. Haber, G. L. Kane, and S. Dawson, “The Higgs Hunter’s Guide,” *Front. Phys.* **80** (2000) 1–448.
- [23] K. Riesselmann, “Limitations of a Standard Model Higgs boson,” [arXiv:hep-ph/9711456](#).

- [24] B. W. Lee, C. Quigg, and H. B. Thacker, “The Strength of Weak Interactions at Very High-Energies and the Higgs Boson Mass,” *Phys. Rev. Lett.* **38** (1977) 883–885.
- [25] ALEPH *et al.*, “Precision Electroweak Measurements and Constraints on the Standard Model,” [arXiv:1012.2367 \[hep-ex\]](#).
- [26] A. Nisati *et al.*, “Higgs Searches in ATLAS,” Presented at the The XXV International Symposium on Lepton Photon Interactions at High Energies in Mumbai, August, 2011.
- [27] V. Sharma *et al.*, “Higgs Searches at CMS,” Presented at the The XXV International Symposium on Lepton Photon Interactions at High Energies in Mumbai, August, 2011.
- [28] Y. A. Golfand and E. P. Likhtman, “Extension of the Algebra of Poincare Group Generators and Violation of p Invariance,” *JETP Lett.* **13** (1971) 323–326.
- [29] D. V. Volkov and V. P. Akulov, “Is the Neutrino a Goldstone Particle?,” *Phys. Lett.* **B46** (1973) 109–110.
- [30] J. Wess and B. Zumino, “Supergauge Transformations in Four-Dimensions,” *Nucl. Phys.* **B70** (1974) 39–50.
- [31] P. Ramond, “Dual Theory for Free Fermions,” *Phys.Rev.* **D3** (1971) 2415–2418.
- [32] A. Neveu and J. H. Schwarz, “Factorizable dual model of pions,” *Nucl. Phys.* **B31** (1971) 86–112.
- [33] J.-L. Gervais and B. Sakita, “Field theory interpretation of supergauges in dual models,” *Nucl. Phys.* **B34** (1971) 632–639.
- [34] A. Signer, “Abc of SUSY,” *J. Phys.* **G36** (2009) 073002, [arXiv:0905.4630 \[hep-ph\]](#).
- [35] S. P. Martin, “A Supersymmetry Primer,” [arXiv:hep-ph/9709356](#).
- [36] A. Djouadi, “The Anatomy of electro-weak symmetry breaking. II. The Higgs bosons in the minimal supersymmetric model,” *Phys. Rept.* **459** (2008) 1–241, [arXiv:hep-ph/0503173](#).
- [37] S. L. Glashow and S. Weinberg, “Natural Conservation Laws for Neutral Currents,” *Phys. Rev.* **D15** (1977) 1958.
- [38] S. Heinemeyer, “MSSM Higgs physics at higher orders,” *Int. J. Mod. Phys.* **A21** (2006) 2659–2772, [arXiv:hep-ph/0407244](#).
- [39] T. Hahn and C. Schappacher, “The implementation of the minimal supersymmetric standard model in FeynArts and FormCalc,” *Comput. Phys. Commun.* **143** (2002) 54–68, [arXiv:hep-ph/0105349](#).
- [40] H. Baer and X. Tata, “Weak scale supersymmetry: From superfields to scattering events,” Cambridge, UK: Univ. Pr. (2006) 537 p.
- [41] B. C. Allanach *et al.*, “The Snowmass points and slopes: Benchmarks for SUSY searches,” *Eur. Phys. J.* **C25** (2002) 113–123, [arXiv:hep-ph/0202233](#).
- [42] P. Nath *et al.*, “The Hunt for New Physics at the Large Hadron Collider,” *Nucl. Phys. Proc. Suppl.* **200-202** (2010) 185–417, [arXiv:1001.2693 \[hep-ph\]](#).
- [43] M. D’Onofrio, G. De Lorenzo, and M. Martinez, “Search for the Gluino and Squark Production in Multijets Plus Missing Final E_T States,” 2010.
- [44] ATLAS Collaboration, J. B. G. da Costa *et al.*, “Search for squarks and gluinos using final states with jets and missing transverse momentum with the ATLAS detector in $\sqrt{s} = 7$ TeV proton-proton collisions,” *Phys. Lett.* **B701** (2011) 186–203, [arXiv:1102.5290 \[hep-ex\]](#).
- [45] CMS Collaboration, V. Khachatryan *et al.*, “Search for Supersymmetry in pp Collisions at 7 TeV in Events with Jets and Missing Transverse Energy,” *Phys. Lett.* **B698** (2011) 196–218, [arXiv:1101.1628 \[hep-ex\]](#).
- [46] O. Buchmueller *et al.*, “Implications of Initial LHC Searches for Supersymmetry,” *Eur. Phys. J.* **C71** (2011) 1634, [arXiv:1102.4585 \[hep-ph\]](#).
- [47] R. Pittau, “Recent news and results in the computation of NLO processes with new techniques,” [arXiv:1105.0278 \[hep-ph\]](#).
- [48] F. Bloch and A. Nordsieck, “Note on the Radiation Field of the electron,” *Phys. Rev.* **52** (1937) 54–59.

- [49] T. Kinoshita, “Mass singularities of Feynman amplitudes,” *J. Math. Phys.* **3** (1962) 650–677.
- [50] T. D. Lee and M. Nauenberg, “Degenerate Systems and Mass Singularities,” *Phys. Rev.* **133** (1964) B1549–B1562.
- [51] S. Catani and M. H. Seymour, “A general algorithm for calculating jet cross sections in NLO QCD,” *Nucl. Phys.* **B485** (1997) 291–419, [arXiv:hep-ph/9605323](#).
- [52] P. Cvitanovic, “Group theory: Birdtracks, Lie’s and exceptional groups,” . Princeton, USA: Univ. Pr. (2008) 273 p.
- [53] F. Maltoni, K. Paul, T. Stelzer, and S. Willenbrock, “Color-flow decomposition of QCD amplitudes,” *Phys. Rev.* **D67** (2003) 014026, [arXiv:hep-ph/0209271](#).
- [54] Z. Xu, D.-H. Zhang, and L. Chang, “Helicity Amplitudes for Multiple Bremsstrahlung in Massless Nonabelian Gauge Theories,” *Nucl. Phys.* **B291** (1987) 392.
- [55] L. J. Dixon, “Calculating scattering amplitudes efficiently,” [arXiv:hep-ph/9601359](#).
- [56] M. Bohm, A. Denner, and H. Joos, “Gauge theories of the strong and electroweak interaction,” . Stuttgart, Germany: Teubner (2001) 784 p.
- [57] H. E. Haber and G. L. Kane, “The Search for Supersymmetry: Probing Physics Beyond the Standard Model,” *Phys. Rept.* **117** (1985) 75–263.
- [58] A. Denner, H. Eck, O. Hahn, and J. Kublbeck, “Feynman rules for fermion number violating interactions,” *Nucl. Phys.* **B387** (1992) 467–484.
- [59] T. Hahn, “Generating Feynman diagrams and amplitudes with FeynArts 3,” *Comput. Phys. Commun.* **140** (2001) 418–431, [arXiv:hep-ph/0012260](#).
- [60] D. R. T. Jones and J. P. Leveille, “Dimensional Regularization and the Two Loop Axial Anomaly in Abelian, Nonabelian and Supersymmetric Gauge Theories,” *Nucl. Phys.* **B206** (1982) 473.
- [61] T. Reiter, “Automated Evaluation of One-Loop Six-Point Processes for the LHC,” [arXiv:0903.0947 \[hep-ph\]](#).
- [62] I. Jack and D. R. T. Jones, “Regularisation of supersymmetric theories,” [arXiv:hep-ph/9707278](#).
- [63] W. B. Kilgore, “Regularization Schemes and Higher Order Corrections,” *Phys. Rev.* **D83** (2011) 114005, [arXiv:1102.5353 \[hep-ph\]](#).
- [64] K. G. Chetyrkin and F. V. Tkachov, “Integration by parts: The algorithm to calculate β functions in 4 loops,” *Nuclear Physics B* **192** no. 1, (1981) 159 – 204.
- [65] G. Passarino and M. J. G. Veltman, “One Loop Corrections for $e^+ e^-$ Annihilation Into $\mu^+ \mu^-$ in the Weinberg Model,” *Nucl. Phys.* **B160** (1979) 151.
- [66] J. M. Campbell, E. W. N. Glover, and D. J. Miller, 2, “The One-loop QCD Corrections for γ^* to $q\bar{q}g$,” *Phys. Lett.* **B409** (1997) 503–508, [arXiv:hep-ph/9706297](#).
- [67] T. Binoth, J. P. Guillet, G. Heinrich, E. Pilon, and C. Schubert, “An algebraic / numerical formalism for one-loop multi-leg amplitudes,” *JHEP* **10** (2005) 015, [arXiv:hep-ph/0504267](#).
- [68] T. Binoth, J. P. Guillet, G. Heinrich, E. Pilon, and T. Reiter, “Golem95: a numerical program to calculate one-loop tensor integrals with up to six external legs,” *Comput. Phys. Commun.* **180** (2009) 2317–2330, [arXiv:0810.0992 \[hep-ph\]](#).
- [69] Landau, L.D, “On analytic properties of vertex parts in quantum field theory,” *Nuclear Physics* **13** no. 1, (1959) 181 – 192.
- [70] R. J. Eden, P. V. Landshoff, and D. I. Olive, *The analytic S-matrix*. 1966.
- [71] R. K. Ellis and G. Zanderighi, “Scalar one-loop integrals for QCD,” *JHEP* **02** (2008) 002, [arXiv:0712.1851 \[hep-ph\]](#).
- [72] W. Hollik, E. Kraus, and D. Stockinger, “Renormalization and symmetry conditions in supersymmetric QED,” *Eur. Phys. J.* **C11** (1999) 365–381, [arXiv:hep-ph/9907393](#).
- [73] S. P. Martin and M. T. Vaughn, “Regularization dependence of running couplings in softly broken supersymmetry,” *Phys. Lett.* **B318** (1993) 331–337, [arXiv:hep-ph/9308222](#).

- [74] W. Beenakker *et al.*, “The Production of charginos / neutralinos and sleptons at hadron colliders,” *Phys. Rev. Lett.* **83** (1999) 3780–3783, [arXiv:hep-ph/9906298](#).
- [75] W. Öller, H. Eberl, and W. Majerotto, “Precise predictions for chargino and neutralino pair production in e^+e^- annihilation,” *Phys. Rev. D* **71** no. 11, (Jun, 2005) 115002.
- [76] R. Frederix, T. Gehrmann, and N. Greiner, “Integrated dipoles with MadDipole in the MadGraph framework,” *JHEP* **06** (2010) 086, [arXiv:1004.2905 \[hep-ph\]](#).
- [77] Z. Nagy, “Next-to-leading order calculation of three jet observables in hadron hadron collision,” *Phys. Rev.* **D68** (2003) 094002, [arXiv:hep-ph/0307268](#).
- [78] A. D. Martin, W. J. Stirling, R. S. Thorne, and G. Watt, “Parton distributions for the LHC,” *Eur. Phys. J.* **C63** (2009) 189–285, [arXiv:0901.0002 \[hep-ph\]](#).
- [79] B. Feigl, H. Rzehak, and D. Zeppenfeld, “SUSY Background to Neutral MSSM Higgs Boson Searches,” [arXiv:1108.1110 \[hep-ph\]](#).
- [80] G. Heinrich, G. Ossola, T. Reiter, and F. Tramontano, “Tensorial Reconstruction at the Integrand Level,” *JHEP* **10** (2010) 105, [arXiv:1008.2441 \[hep-ph\]](#).
- [81] P. Mastrolia, G. Ossola, T. Reiter, and F. Tramontano, “Scattering Amplitudes from Unitarity-based Reduction Algorithm at the Integrand-level,” *JHEP* **08** (2010) 080, [arXiv:1006.0710 \[hep-ph\]](#).
- [82] Nogueira, P., “Automatic Feynman graph generation,” *J. Comput. Phys.* **105** (1993) 279–289.
- [83] N. D. Christensen and C. Duhr, “FeynRules - Feynman rules made easy,” *Comput. Phys. Commun.* **180** (2009) 1614–1641, [arXiv:0806.4194 \[hep-ph\]](#).
- [84] T. Binoth *et al.*, “A proposal for a standard interface between Monte Carlo tools and one-loop programs,” *Comput. Phys. Commun.* **181** (2010) 1612–1622, [arXiv:1001.1307 \[hep-ph\]](#).
- [85] W. Hollik and D. Stockinger, “Regularization and supersymmetry-restoring counterterms in supersymmetric QCD,” *Eur. Phys. J.* **C20** (2001) 105–119, [arXiv:hep-ph/0103009](#).
- [86] W. Siegel, “Supersymmetric Dimensional Regularization via Dimensional Reduction,” *Phys. Lett.* **B84** (1979) 193.
- [87] D. M. Capper, D. R. T. Jones, and P. van Nieuwenhuizen, “Regularization by Dimensional Reduction of Supersymmetric and Nonsupersymmetric Gauge Theories,” *Nucl. Phys.* **B167** (1980) 479.
- [88] G. Cullen *et al.*, “Recent Progress in the Golem Project,” *Nucl. Phys. Proc. Suppl.* **205-206** (2010) 67–73, [arXiv:1007.3580 \[hep-ph\]](#).
- [89] T. Reiter *et al.*, “Modern Feynman Diagrammatic One-Loop Calculations,” [arXiv:1011.6632 \[hep-ph\]](#).
- [90] G. Cullen, N. Greiner, G. Heinrich, G. Luisoni, P. Mastrolia, G. Ossola, T. Reiter, and F. Tramontano (in preparation).
- [91] van Rossum, G., “Python Tutorial,” tech. rep., Centrum voor Wiskunde en Informatica (CWI), Amsterdam, 1995.
- [92] J. A. M. Vermaseren, “New features of FORM,” [arXiv:math-ph/0010025](#).
- [93] T. Reiter, “Optimising Code Generation with haggies,” *Comput. Phys. Commun.* **181** (2010) 1301–1331, [arXiv:0907.3714 \[hep-ph\]](#).